



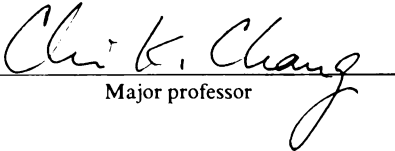
3 1293 00896 3211

This is to certify that the
dissertation entitled
INTERACTION OF INTERMOLECULAR CARBOXYLIC ACID
WITH HEME-O₂ COMPLEX

presented by
Gladys Maria Aviles

has been accepted towards fulfillment
of the requirements for

Ph.D. degree in Chemistry


Major professor

Date 14/Feb/91

**LIBRARY
Michigan State
University**

**PLACE IN RETURN BOX to remove this checkout from your record.
TO AVOID FINES return on or before date due.**

DATE DUE	DATE DUE	DATE DUE
_____	_____	_____
_____	_____	_____
_____	_____	_____
_____	_____	_____
_____	_____	_____
_____	_____	_____
_____	_____	_____

MSU Is An Affirmative Action/Equal Opportunity Institution

c:\crl\datedue.pm3-p.

INTERACTION OF INTERMOLECULAR CARBOXYLIC ACID
WITH HEME-O₂ COMPLEX

By

Gladys Maria Aviles

A DISSERTATION

Submitted to
Michigan State University
in partial fulfillment of the requirements
for the degree of

DOCTOR OF PHILOSOPHY

Department of Chemistry

1991



814-2148

ABSTRACT

INTERACTION OF INTERMOLECULAR CARBOXYLIC ACID
WITH HEME-O₂ COMPLEX

by

Gladys Maria Aviles

The study of how hydrogen-bonding affects the oxygen binding, activation and reduction in hemoproteins has been the concern of many researchers for the last 10 years. Although studies have shown that H-bonding increases metal dioxygen affinity there is no clear evidence on the influence of H-bonding on O₂ activation and reduction. In the first part of our work we present the study of the decomposition of Co(II) naphthoic acid porphyrin in the presence of oxygen. In this porphyrin the proton on the carboxylic acid is essential for the decomposition to occur. Our findings show that similar to heme degradation an oxaporphyrin species is one of the major products. Based on the results of our study we propose a mechanism similar to the one followed in heme degradation.

In an effort to provide a better understanding of the influence of H-bonding in O₂ activation and reduction we prepared a series of anthracene Kemp acid porphyrins. In this model series the conformation of the H-bonding should minimize the intramolecular attack on the porphyrin ring to avoid self-decomposition, thus allowing further studies on the reaction of H-bonded heme-O₂ species. O₂ binding studies of the anthracene Kemp acid porphyrin indicate that



the proton of this porphyrin is able to interact with and enhance the binding constant of the Co-O₂ complex.

In addition, we also studied the H-bonding effects on heme coordinated cyanide and CO. ¹⁵N NMR of the dicyano Fe(III) anthroic acid, acrylic acid, naphthoic acid and anthracene Kemp acid porphyrins showed that even though the distance between the proton in the anthracene Kemp acid porphyrin is not ideal for the best Co-O₂ interaction, it is close enough to have a strong interaction with the nitrogen of the CN ligand. From these results we expect that the proton of the anthracene Kemp acid porphyrin will also interact more efficiently with CO in carbonyl hemes, and therefore may influence the Fe-CO formation constant.

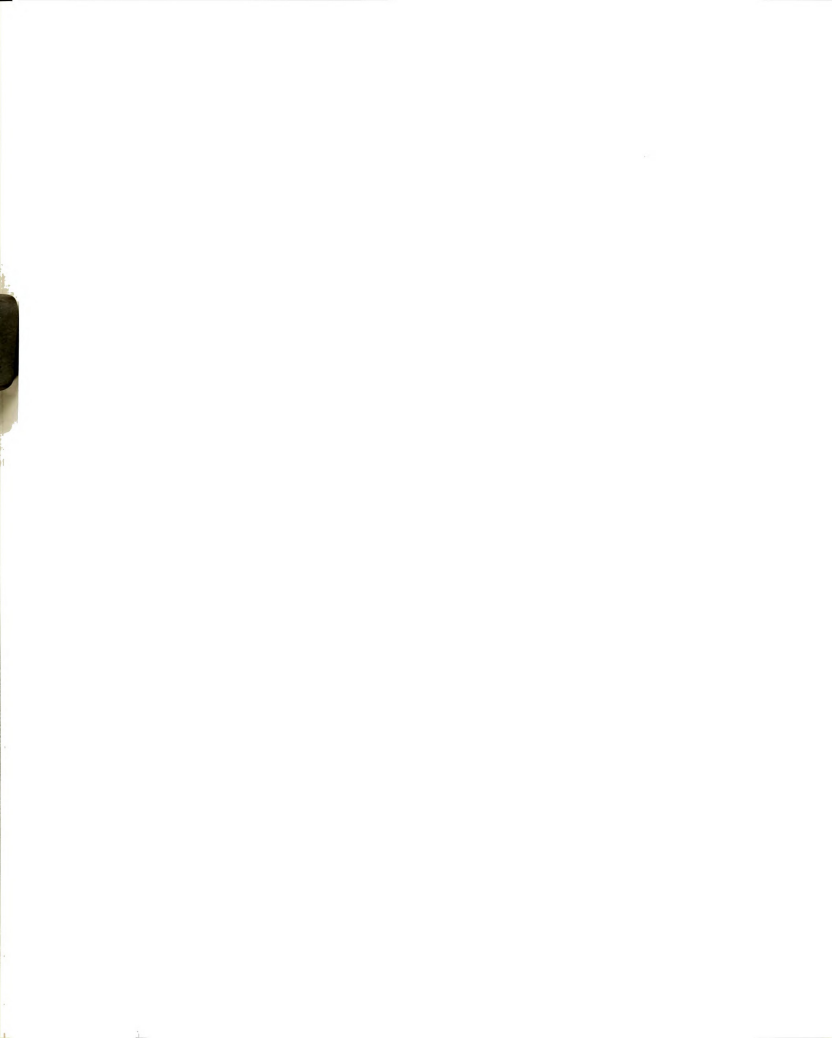
Finally, we studied the influence of geometric distortions in the ¹⁵N NMR of a series of Fe^{III}-CN strapped porphyrins. It can be clearly demonstrated that small changes in the geometric distortion of the cyanomet complex produces a large upfield shift in the C¹⁵N signal position, making this nucleus a good "reporter group." Differences in the steric effects within the heme pocket may play a major role in dictating the functionality of hemoproteins.



Copyright by
GLADYS M. AVILES
1991



To Mom and Dad...



ACKNOWLEDGMENTS

First, I would like to thank God. He gave me the ability to complete this work, and the wonderful people who made the journey so much easier.

Mom and Dad, to you I give very special thanks. You were always there whenever I needed a friend. You always supported and encouraged me; you always had faith in me. Once again, thank you Mom and Dad.

I also want to thank all my friends, especially Mayda, Mildred and Barb. Together we shared tears and laughter.

I would like to thank Dr. Chang for guiding me through my work and for his patience whenever I was "pulling my hair." And last, but not least, special thanks to all of the members of my group for their helpful discussions and friendship.

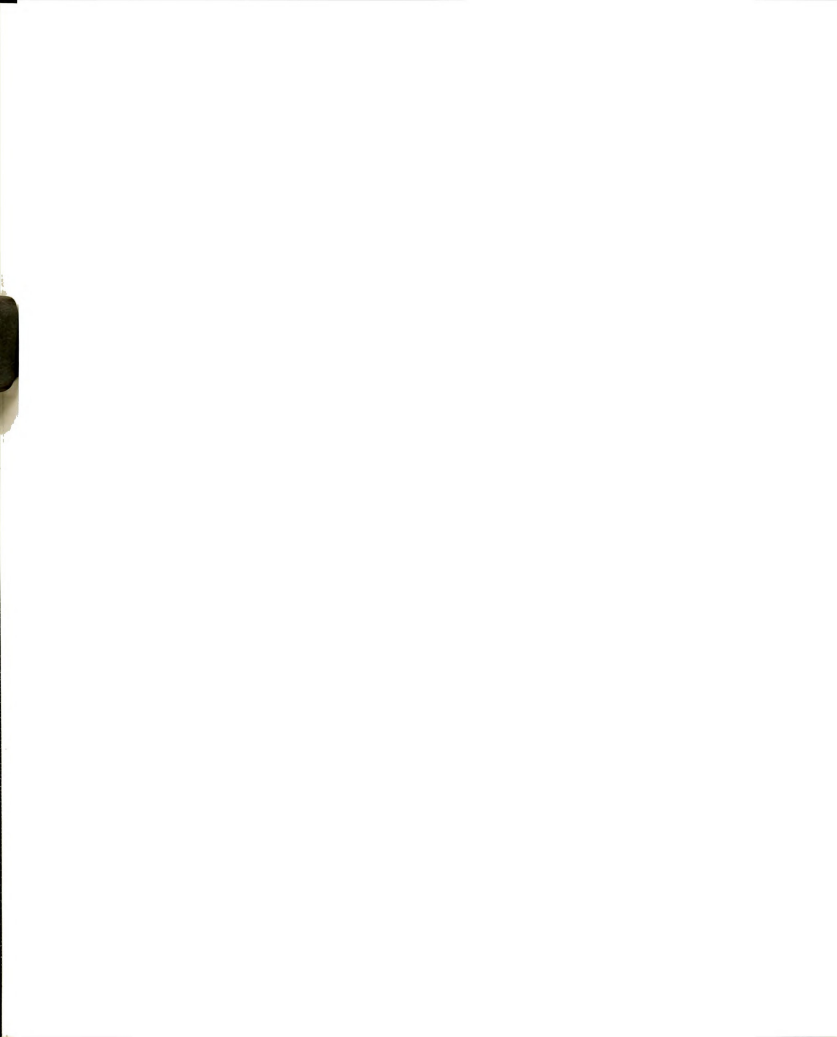
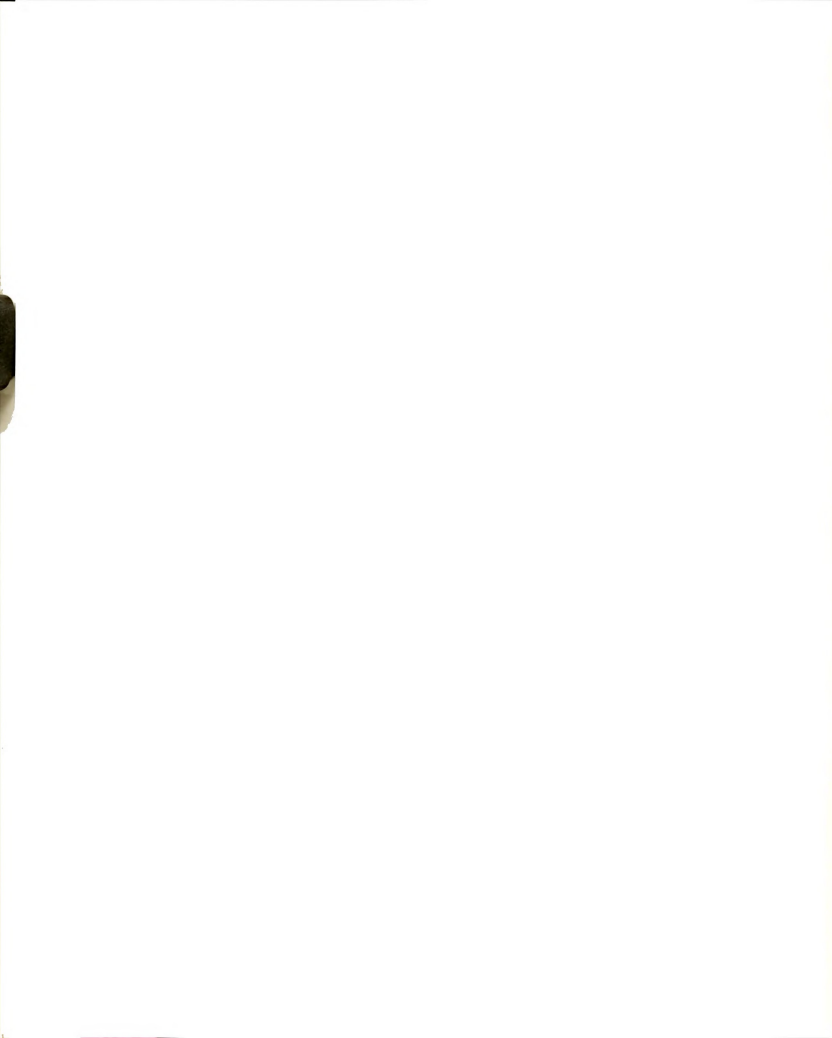


TABLE OF CONTENTS

Introduction	1
LIST OF REFERENCES	18
Decomposition of Co(II) Naphthoic Acid Porphyrin . . .	20
Introduction	20
Results	26
Final Decomposition Products	26
Formation of Intermediate	31
Discussion	38
Oxidation of Heme	38
Oxidation of Hemoproteins	43
Co ^{II} Naphthoic Acid Porphyrin	45
Experimental	50
5-(8-Carboxyl-1-naphthyl)-2,8,13,17-tetraethyl- 3,7,12,18-tetramethylporphyrin cobalt(II) (1)	50
2,8,13,17-Tetraethyl-3,7,12,18-tetramethyl-5- oxaporphyrin cobalt(II) (2)	51
1,8-Naphthalic anhydride from decomposition (3) .	52
Commercial 1,8-Naphthalic anhydride	52
3,8,12,17-Tetraethyl-2,7,13,18-tetramethyl- 1,19(21H,24H)-dione (Etio biliverdin) (4) . .	52
Decomposition Intermediate	53
Method used in the G.C. Study	53
1,8-Naphthaldehydic Acid	54
LIST OF REFERENCES	55
Synthesis of Novel Porphyrins and their Study of O ₂	
Binding to CO(II) and ¹⁵ N-NMR of Iron-bond C ¹⁵ N ⁻ . . .	58
Introduction	58
Results and Discussion	61
Synthesis of the Anthracene Acrylic Acid Porphyrins	61
Synthesis of Kemp Isomer Porphyrins	61
Synthesis of the Anthracene Kemp Acid Porphyrins Series	67
O ₂ Binding to Co ^{II} Kemp Isomer and Kemp Porphyrins	70
H-Bonding Effects on Heme Coordinated Cyanide . .	73
Experimental	76
5-(8-(trans-2-Ethoxycarbonylethenyl)-1-anthryl)- 2,8,13,17-tetraethyl-3,7,12,18- tetramethylporphine (2)	76

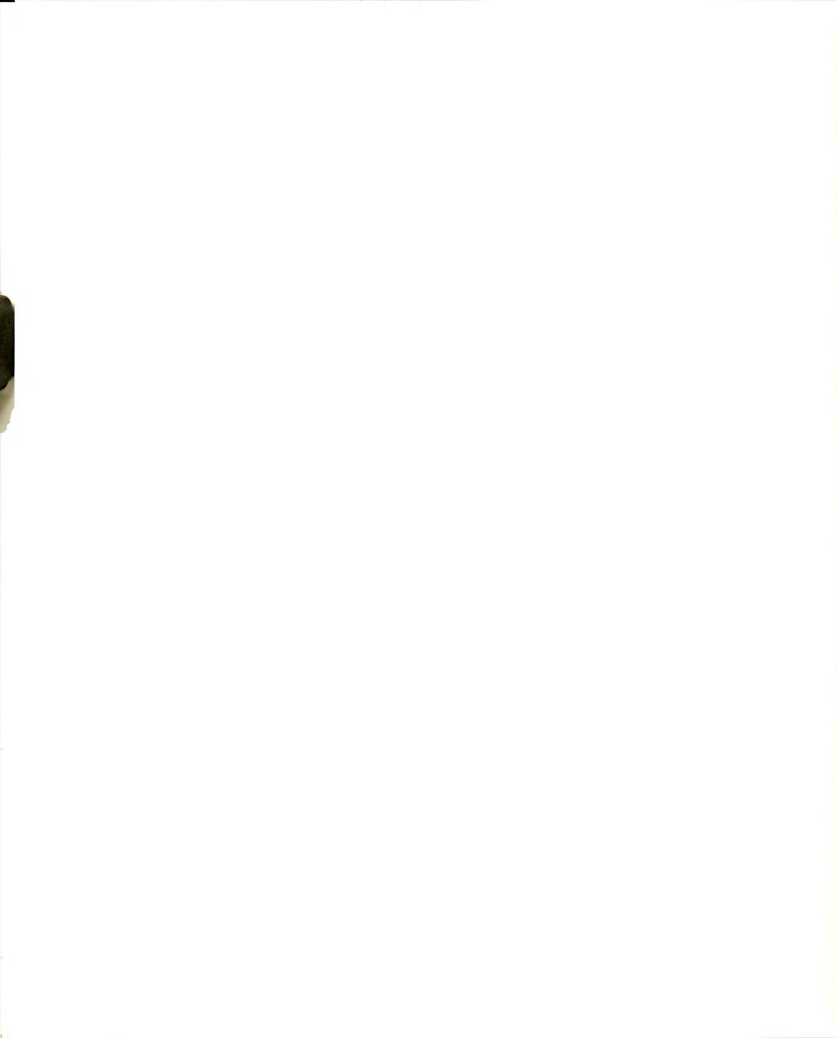


5-(8(trans-2-Hydroxycarbonylethenyl)-1-anthryl)- 2,8,13,17-tetraethyl-3,7,12,18- tetramethylporphine (3)	78
Naphthalene Kemp acid isomer porphyrin (6)	79
Anthracene Kemp acid isomer porphyrin (8)	80
5-(8-(Azidomethyl)-1-anthryl)-2,8,13,17-tetraethyl- 3,7,12,18-tetramethylporphine (9)	81
5-(8-(Aminomethyl)-1-anthryl)-2,8,13,17-tetraethyl- 3,7,12,18-tetramethylporphine (10)	82
5-(8-Kemp acid-1-anthryl)-2,8,13,17-tetraethyl- 3,7,12,18-tetramethylporphine (12)	83
5-(8-Kemp methylester-1-anthryl)-2,8,13,17- tetraethyl-3,7,12,18-tetramethylporphine (13)	84
5-(8-Kemp amide-1-anthryl)-2,8,13,17-tetraethyl- 3,7,12,18-tetramethylporphine (14)	85
5-(8-Kemp diol-1-anthryl)-2,8,13,17-tetraethyl- 3,7,12,18-tetramethylporphine (15)	85
Cobalt Insertion	86
Iron Insertion	87
Dioxygen binding to Co(II) porphyrins	88
¹⁵ N NMR of Dicyano Iron (III) Porphyrin Models	89
LIST OF REFERENCES	99
¹⁵ N Nuclear Magnetic Resonance Studies of Iron-Bond C ¹⁵ N ⁻ in Ferric Low-Spin Cyanide Complexes of Various Strapped Hemins. Importance of C ¹⁵ N ⁻ as a Reporter Molecule.	101
Introduction	101
Experimental	107
Dicyano Iron (III) Porphyrin Models	107
Mixed Imidazole Cyano-Iron (III) Porphyrin Complexes	107
Measurements	108
Theory	108
Results and Discussion	110
Dicyano Complex	110
Mixed Fe(III) Strap Complex	115
Biological Relevance	116
LIST OF REFERENCES	118
APPENDIX	121
2,7,13,18-tetraethyl-1,3,8,12,17,19-hexamethyl-10- phenyltetrahydrocorrin cobalt (II) perchlorate (4)	121
1,8-Bis[10-(2,7,13,18-tetraethyl-1,3,8,12,17,19- hexamethyl)-tetraelehydrocorrin] anthracene, cobalt(II) perchlorate. (7)	123



LIST OF TABLES

Table 3-1. Results of O ₂ Binding to Cobalt Porphyrins	70
Table 3-2. ¹⁵ N Chemical Shift for Fe ^{III} Porphyrin Models	75
Table 4-1. ¹⁵ N Chemical Shifts For Proteins and Protoporphyrin	103
Table 4-2. ¹⁵ N Chemical Shift for Strapped Porphyrins	113



LIST OF FIGURES

Figure 1-1. Secondary and tertiary structures characteristic of the hemoglobins. Helical segments are denoted <u>A</u> to <u>H</u> ; nonhelical ones <u>NA</u> , <u>AB</u> to <u>GH</u> , and <u>HC</u> . Residues along segments are numbered in sequence. The diagram shows the proximal His F8, the distal His E7, and the distal Val E11, and Tyr HC2 which play an important part in the allosteric mechanism. (Acc. Chem. Res. (1987), 20 , 310)	4
Figure 1-2. "Basket-handle" Porphyrins	5
Figure 1-3. Naphthalene Porphyrin Model Compounds . .	7
Figure 1-4. Schematic representation of the cytochrome c peroxidase-catalyzed heterolytic cleavage of the RO1-O2H bond. (Adapted from <u>J. Biol. Chem.</u> , 1980).	9
Figure 1-5. Schematic view of the "push-pull" mechanism for O-O bond cleavage of cytochrome c peroxidase (from Dawson, J.; <u>Science</u> , 1988). . . .	11
Figure 1-6. Proposed Catalytic Cycle for Oxygen Reduction by Cytochrome Oxidase (from Robert Kean's Dissertation, 1987)	13
Figure 1-7. Anthracene Diporphyrins	15
Figure 1-8. Decomposition of Co ^{II} Naphthoic Acid Porphyrin	15
Figure 2-1. Final decomposition products of Co(II) naphthoic acid porphyrin and heme IX	22
Figure 2-2. Heme catabolism main biocatabolic pathway	23
Figure 2-3. Mechanism followed in in vitro heme degradation	25
Figure 2-4. Visible absorption spectrum for Co ^{II} oxaporphyrin and verdohemochrome	28

Figure 2-5. Mass spectrum for Co ^{II} oxaporphyrin	28
Figure 2-6. Proton NMR and e/I mass spectra of the yellow decomposition product	29
Figure 2-7. Gas chromatogram of: (a) 1,8-naphthalic anhydride; (b) 1,8-naphthaldehydic acid; (c) decomposition product	30
Figure 2-8. Co ^{II} Naphthoic acid porphyrin final decomposition products	32
Figure 2-9. Physical data of Etio biliverdin obtained from decomposition: (a) e/I MS; (b) ¹ H NMR; (c) UV-Vis	33
Figure 2-10. UV-Vis spectra of intermediate species and N-alkyl Co ^{II} TPP	34
Figure 2-11. FD mass spectra of decomposition intermediate species	36
Figure 2-12. Mass spectra of decomposition products obtained when: (a) Methanol added under Argon; (b) Methanol added and O ₂ bubbled through	37
Figure 2-13. Oxophlorin π -radical formation	39
Figure 2-14. Formation of biliverdin from meso hydroxy porphyrin	40
Figure 2-15. Intramolecular electron transfer of meso hydroxylate porphyrin and formation of oxaporphyrin	41
Figure 2-16. Suggested mechanism in the formation of Fe ^{II} oxaporphyrin from Fe ^{II} oxophlorin	42
Figure 2-17. Possible mechanism involved in the oxidation of hemoproteins to biliverdin	46
Figure 2-18. Oxaporphyrin formation from Co ^{II} naphthoic acid porphyrin and protoheme IX	46
Figure 2-19. Suggested analogous pathway to heme degradation followed by the Co ^{II} naphthoic acid porphyrin decomposition	47
Figure 2-20. Proposed mechanism followed in the decomposition of Co ^{II} naphthoic acid porphyrin	49
Figure 3-1. Structures of the series of anthracene acrylic and anthracene Kemp porphyrins	59



Figure 3-2. Co-O ₂ complex of naphthalene Kemp isomer and anthracene Kemp acid porphyrins	73
Figure 3-3. ¹⁵ N-NMR spectra of the dicyano Fe ^{III} complex of anthroic acid, acrylic acid, naphthoic acid and anthracene Kemp acid porphyrins	77
Figure 3-4. Spectrophotometric titration of Co anthracene Kemp isomer porphyrin	90
Figure 3-5. ¹ H-NMR spectrum of anthracene acrylic ester porphyrin (2)	91
Figure 3-6. ¹ H-NMR spectrum of anthracene acrylic acid porphyrin (3)	92
Figure 3-7. ¹ H-NMR spectrum of naphthalene Kemp isomer porphyrin (6)	93
Figure 3-8. ¹ H-NMR spectrum of anthracene Kemp isomer porphyrin (8)	94
Figure 3-9. ¹ H-NMR spectrum of anthracene azido porphyrin (9)	95
Figure 3-10. ¹ H-NMR spectrum of anthracene amino porphyrin (10)	96
Figure 3-11. ¹ H-NMR spectrum of anthracene Kemp acid porphyrin (12)	97
Figure 3-12. ¹ H-NMR spectrum of anthracene Kemp ester porphyrin (13)	98
Figure 4-1. Chemical Structures of Cofacial Diporphyrins and Strapped Hemes	105
Figure 4-2. Chemical Structure of Heme 5	105
Figure 4-3. Chemical structure of OEP, FeSP and strapped hemes	111
Figure 4-4. ¹⁵ N-NMR spectra of the dicyano unstrapped and strapped hemes	112
Figure A1. UV-Vis and MS of phenyl tetra-dehydrocorrin (4)	124
Figure A2. Mass spectra of anthracene ditetradehydrocorrin	126

Chapter 1

Introduction

Hemoproteins, are proteins that in addition to their amino acid sequence, contain a heme (iron porphyrin) as their prosthetic group. Their ability to either reversibly bind oxygen, catalyze oxidation of organic compounds, decompose hydrogen peroxide or transport electrons, is remarkable.¹⁻³ Examples of the extremely broad range of their functions are:

Hemoglobin The first protein crystallized (1849) is responsible for the oxygen, carbon dioxide and proton transport.¹

Myoglobin Is found in muscle where it stores oxygen transferred from hemoglobin and liberates it to the mitochondria for oxidative¹ phosphorylation of adenosine diphosphate.

Cyt.P-450 A monooxygenase, incorporates one of the two oxygens of O₂ into a broad variety of substrates with the concomitant reduction of the other oxygen atom (by two electrons) to water.² It plays a key role in the oxidative metabolism of exogenous compounds such as drugs and other environmental products allowing their elimination from living organisms.

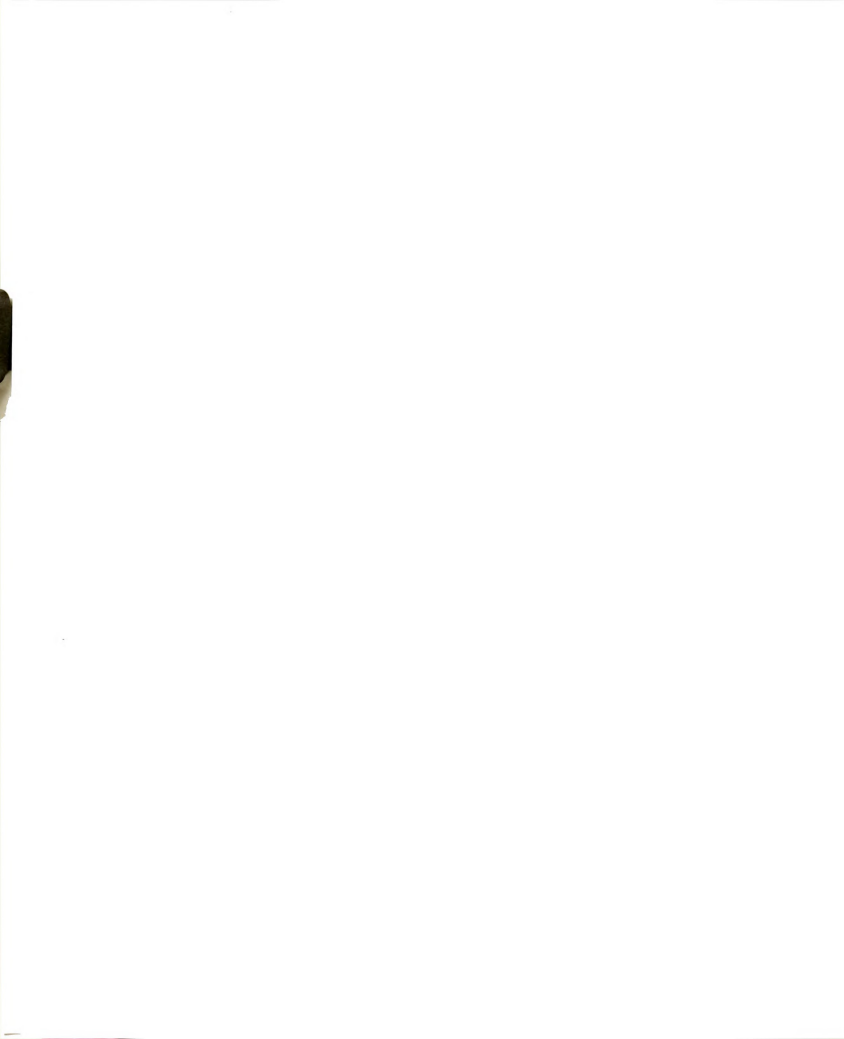


Peroxidases Among the peroxidases are cyt. c peroxidase (CCP) and horseradish peroxidase (HRP). They catalyze oxidation reactions in which H_2O_2 or substituted peroxides serve as the oxidizing agent.³ In so doing the peroxidases also protect the cell against these dangerously reactive compounds.

Cytochrome c Oxidase Catalyzes the reduction of dioxygen to water. The free energy generated in this process becomes available as ATP. It is estimated that 90% of the energy for heart muscle contraction is provided through aerobic metabolism via cytochrome c oxidase.

Although all of these hemoproteins have iron porphyrin prosthetic group, they have very different functions. By variations in the protein environment, this seemingly common catalytic center carries out a wide variety of chemical processes. Differences in the protein environment such as: hydrophobicity of the heme pocket, basicity and polarity of the proximal and distal ligands, size opening of the heme pocket and ability of the distal ligand to form hydrogen-bonding with the sixth ligand (O_2 , H_2O_2 or $ROOH$) of the heme iron play a major role in the protein function.

The study of how hydrogen-bonding affects the oxygen binding, activation and reduction in hemoproteins has been the concern of many researchers for the last 10 years. Direct evidence such as neutron diffraction studies of



oxymyoglobin (Figure 1-1) and oxyhemoglobin⁴ has left no doubt that heme-bound dioxygen has a tendency to form hydrogen-bond with proton donors. Using a cobalt salicylidenimine complex, Drago et.al.^{5a} observed a 400 fold increase in oxygen affinity when trifluoroethanol was present. In the oxygen binding study of the "basket-handle porphyrins" (BHP)^{5b} a tenfold increase in the oxygen binding equilibrium constant of the amide-BHP (2a) was observed when compared to the ether-BHP (2b). The change in the oxygen binding equilibrium constant is the exclusive result from a tenfold reduction of the oxygen dissociation rate in the amide-BHP. NMR spectra of the oxygenated complexes provided additional evidence for the hydrogen bond in the oxygenated amide-BHP (2a). The greater stability of the amide-BHP corresponds to a gain in free energy of 5.4 kJmol^{-1} which is certainly due, in part, to the interaction with the amide proton. In their model study Chang and Ward^{5c} have also demonstrated the importance of hydrogen bonding in oxygen binding. They observed up to a tenfold increase in the oxygen binding equilibrium constant when a proton donor capable of hydrogen bonding to the heme-bound O_2 is present.

In an effort to create an ideal environment for such hydrogen-bonding to occur, Chang and Kondylis^{5d} designed a porphyrin model in which an intramolecular proton donor is juxtaposed to the terminal oxygen atom of the coordinated



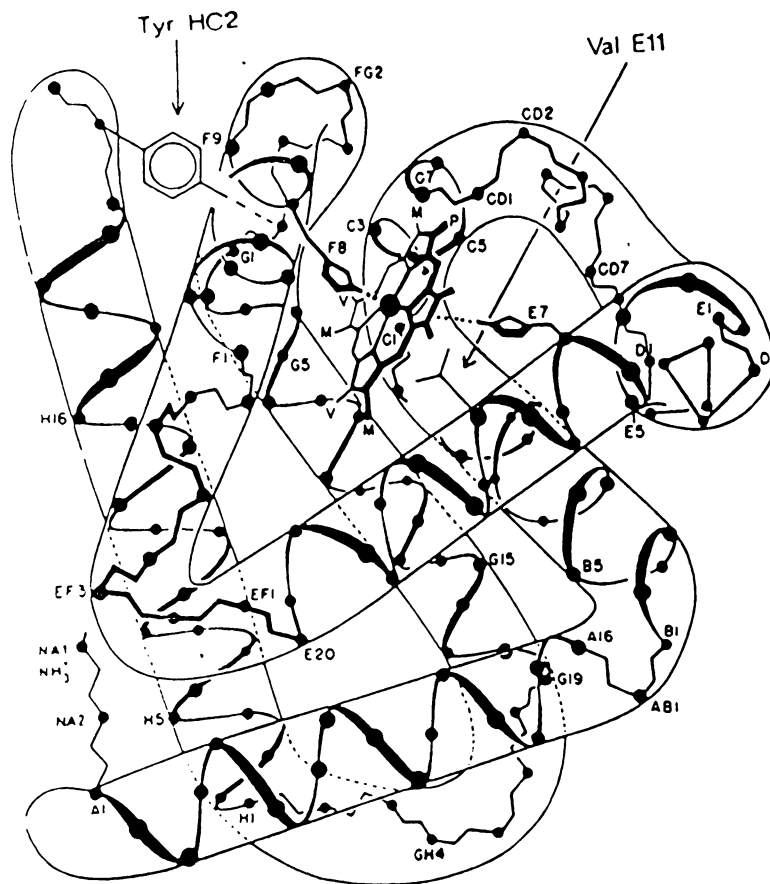
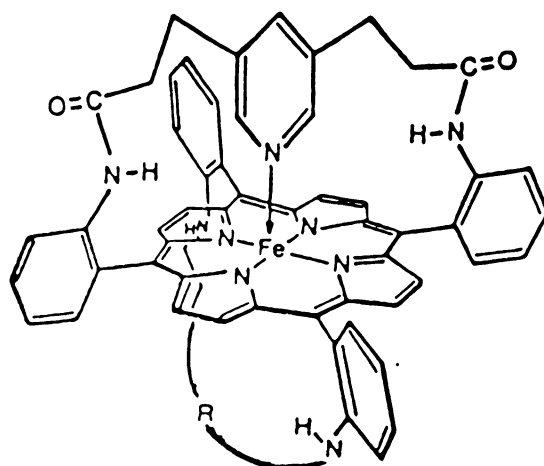
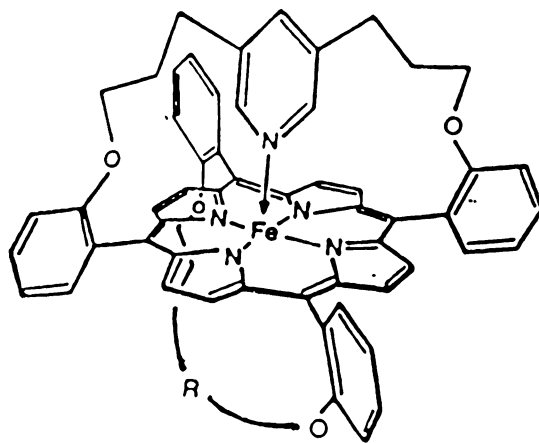


Figure 1-1. Secondary and tertiary structures characteristic of the hemoglobins. Helical segments are denoted A to H; nonhelical ones NA, AB to GH, and HC. Residues along segments are numbered in sequence. The diagram shows the proximal His F8, the distal His E7, and the distal Val E11, and Tyr HC2 which play an important part in the allosteric mechanism. (Acc. Chem. Res. (1987), 20, 310)



a. $R = \text{CO}(\text{CH}_2)_{10}\text{CO}$



b. $R = (\text{CH}_2)_{12}$

Figure 1-2. "Basket-handle" Porphyrins

dioxygen. A series of Co^{II} 1-naphthyl porphyrins substituted with amido, carboxy, and hydromethoxy at the 8-naphthyl position was prepared (Figure 1-3). In the oxygen binding study of these compounds it was observed that:

1. O₂ affinity increased by a 1500 fold on going from the Co^{II} naphthalene porphyrin (3a) to the Co^{II} naphthoic acid porphyrin (3d).
2. O₂ affinity increased as the hydrogen-bonding ability of the model compound increased.
3. A free energy gain between 3 Kcal/mol for (3d) and 1.1 Kcal/mol for (3b) with reference to (3a) was also observed.

These results clearly demonstrate that the presence of a protic group near the dioxygen binding site drastically increases the Co-O₂ formation constant by stabilizing the oxygen cobalt bond.

Of even more interest, is the importance of H-bonding in the activation and reduction of O₂, and in the cleavage of RO-OH. Nonenzymatic reduction of dioxygen to water by 4 electron reduction is a very difficult process. Although the reduction of dioxygen to water is thermodynamically favorable (~80 Kcal),⁶ the one electron step to the superoxide is thermodynamically highly disfavored (E = -0.33V).^{6c} Another property that contributes to the

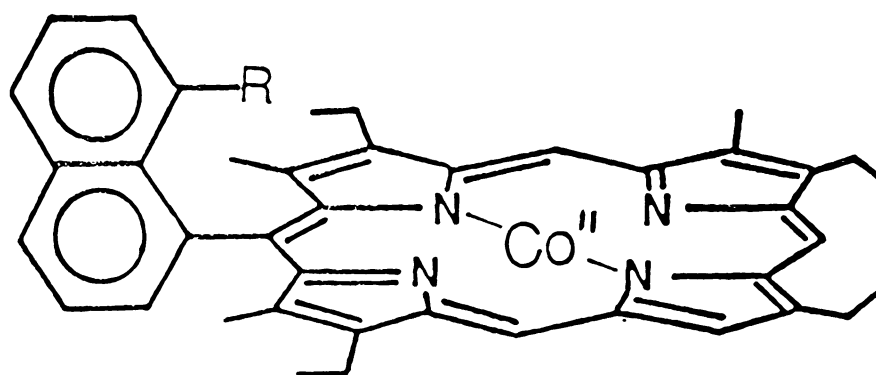


Figure 1-3.

Naphthalene Porphyrin Model Compounds

- 3a R = H
- 3b R = CH₂OH
- 3c R = CONH₂
- 3d R = CO₂H

slowness of its reactions is its electronic structure. The triplet ground state dictates that the reduction of dioxygen must involve spin reversal and therefore is spin forbidden and slow. The forbiddenness can be removed if dioxygen can interact with a paramagnetic center to participate in exchange coupling.

Cytochrome c peroxidase is an example in which hydrogen bonding is thought to promote heterolysis of peroxides by stabilizing a developing negative charge on the leaving group of the substrate. The crystal structure of cytochrome c peroxidase (CCP) has been determined.⁷ Similar to myoglobin in the Fe(III) state, CCP has a water ligand at the sixth coordination position which in turn is hydrogen-bonded to a distal histidine side chain. However distinct from myoglobin, CCP has a tryptophan and an arginine side chain close to the sixth coordination position (Figure 1-4). The Poulos mechanism⁸ based on the X-ray crystal structure of cytochrome c peroxidase utilizes the distal arginine and histidine hydrogen bonds with subsequent proton transfer to effect heterolytic hydroperoxide cleavage (Figure 1-4). The activity of CCP towards peroxides can be explained in the concept of "push-pull" effect. As has been discussed by Poulos,⁹ in CCP the proximal histidine hydrogen bonds more strongly to neighboring groups than in the globins. This makes the axial histidine a better electron donor (a better



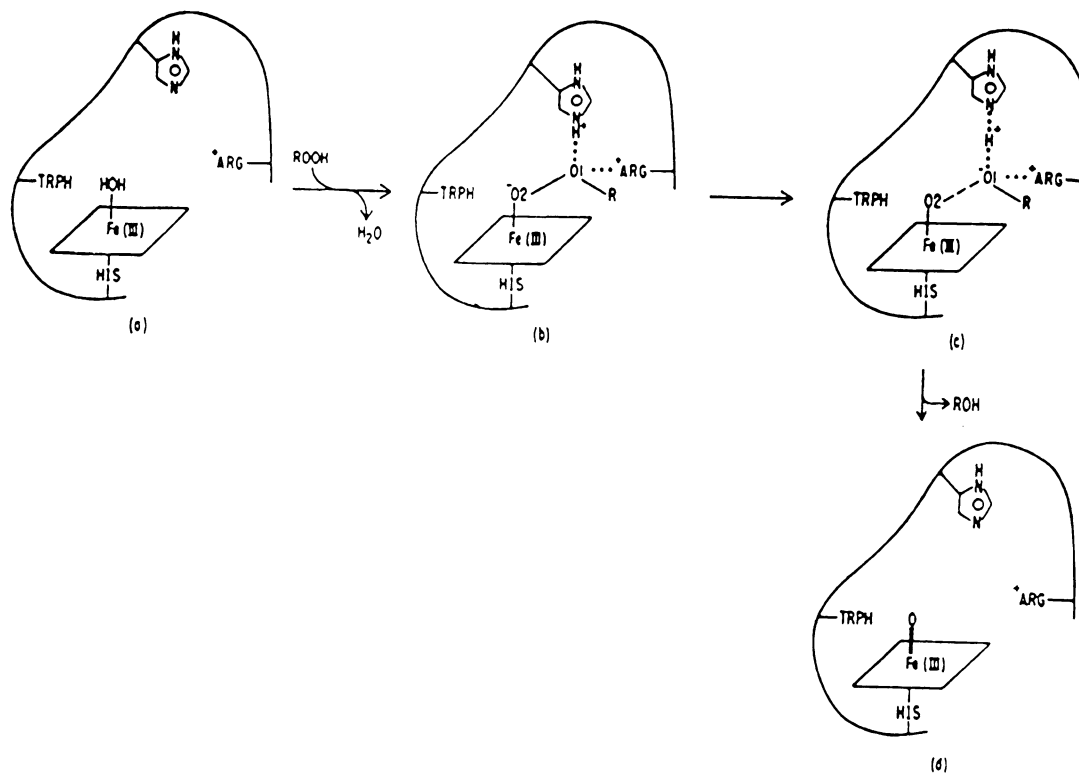


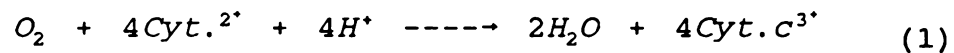
Figure 1-4. Schematic representation of the cytochrome c peroxidase-catalyzed heterolytic cleavage of the RO1-O2H bond. (Adapted from J. Biol. Chem., 1980).



"push") to the heme than in the globins and may also help stabilize higher oxidation states of the iron during catalysis. At the same time, the distal histidine serves as a proton donor and works together with a charged residue (arginine) to make the distal side substantially more polar than globins and to "pull" apart the O-O bond of the bound peroxide by stabilizing the separating charge (Figure 1-5).

The most biologically significant O-O bond fission is found in the reduction of dioxygen to water, catalyzed by cytochrome c oxidase, the terminal enzyme in the respiratory metabolism of all aerobic organisms.¹⁰

The catalytic activity of cytochrome c oxidase toward the reduction of oxygen is demonstrated by its ability to transfer reducing equivalents from ferro-cytochrome c to molecular oxygen (Equation 1). The electrons are provided by the reduced cytochrome c:



The free energy generated in the O₂ reduction ultimately becomes available as ATP. It is estimated that 90% of the energy for heart muscle contraction is provided through aerobic metabolism via cytochrome c oxidase.

It is well established that the active unit of the enzyme contains two heme groups (heme a and heme a₃), and two protein-bound copper ions (Cu_a and Cu_{a3}). Heme a is usually low spin and does not bind ligands. It serves as an



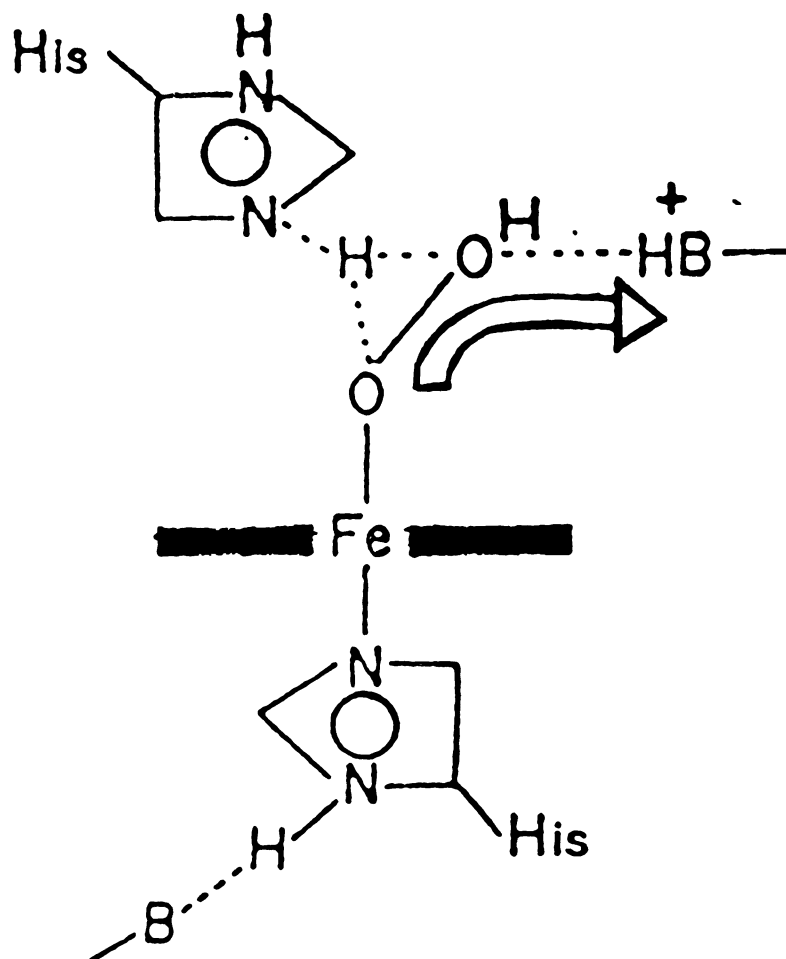


Figure 1-5. Schematic view of the "push-pull" mechanism for O-O bond cleavage of cytochrome c peroxidase (from Dawson, J.; Science, 1988).



electron shuttle, mediating the transfer of reducing equivalents from cytochrome c to the heme a_3 - O_2 complex.¹⁰ Heme a_3 is the binding site for various ligands such as O_2 and CO in the ferrous state and HCN, H_2S and HN_3 in the ferric state.¹¹ The most interesting feature of cytochrome c oxidase is that it permits the reduction of dioxygen to water via an efficient low energy pathway.

Although the structural relationship between iron and copper of the enzyme is far from established, the magnitude of the antiferromagnetic coupling observed ($-J > 200 \text{ cm}^{-1}$) for the oxidized enzyme suggests that heme a_3 and a copper ion are separated by no more than a few atoms. X-ray absorption fine structure (EXAFS) data indicates that there is a Fe-Cu separation of only 3-3.8 Å.¹² Many mechanistic approaches for the reduction of O_2 to water have been suggested, for example, Figure 1-6, adapted from reference 13, although, none of them have been fully documented and thus remain speculative.¹⁴

To understand the mechanism by which cytochrome c oxidase reduces oxygen to water, it is important to know the function of the copper and iron atoms, and how does the relation between them influence the reduction of the dioxygen molecule. Are heme a_3 and Cu_{a_3} equally important in the binding the transfer of electrons to O_2 ? Does the copper atom serve as a lewis acid, therefore, stabilizing the partially reduced O_2 ?



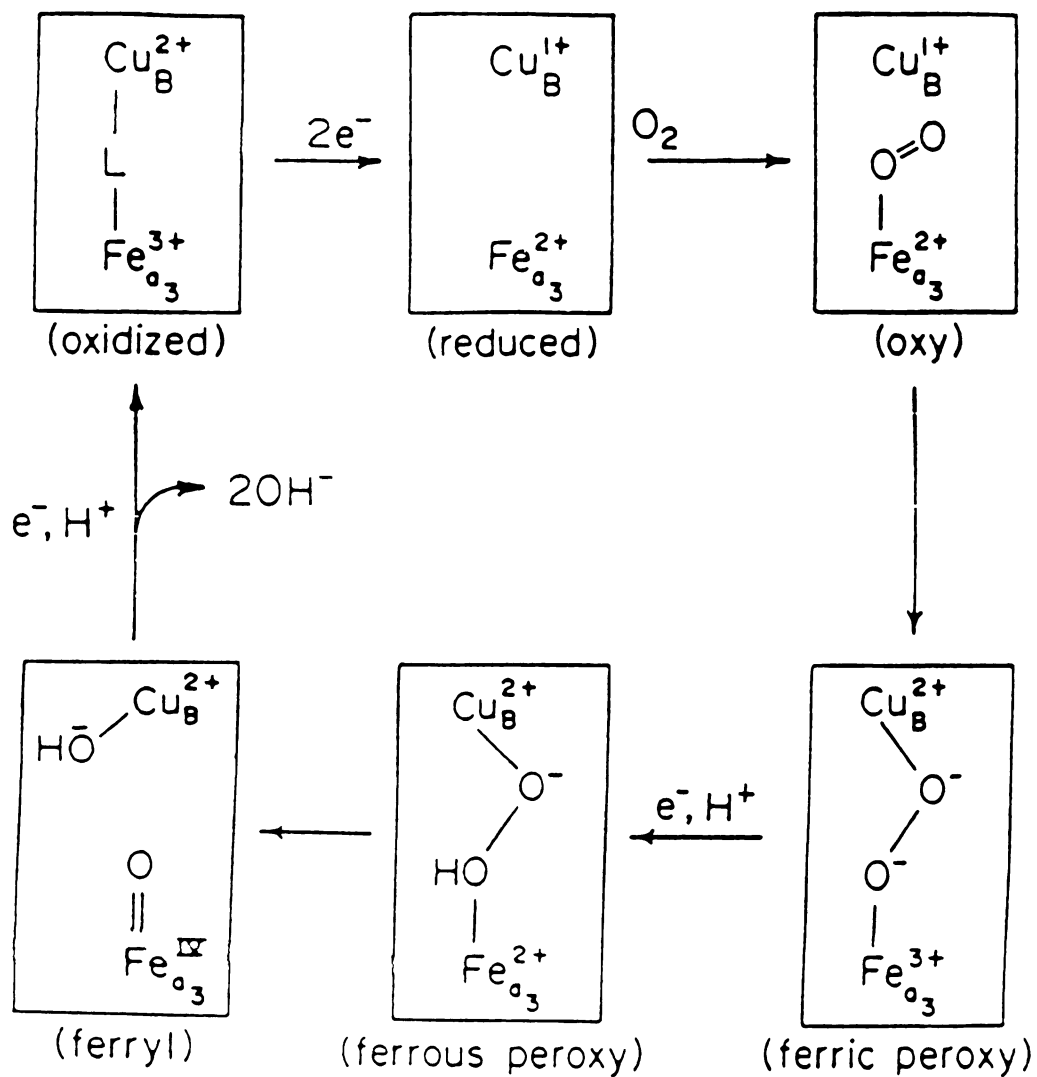


Figure 1-6. Proposed Catalytic Cycle for Oxygen Reduction by Cytochrome Oxidase (from Robert Kean's Dissertation, 1987).



A variety of metalloporphyrins¹⁵ have been tested for their catalytic effects on the electroreduction of dioxygen. Most monomeric metalloporphyrins catalyze only the 2-electron reduction to yield hydrogen peroxide. Surprisingly, the study of anthracene-bridged cobalt diporphyrins (Figure 1-7) showed that these cofacial dimers have the ability to catalyze the four electron reduction of dioxygen to water when adsorbed to graphite.¹⁶ This is true for both the dimetalated (7a) and monometalated (7b) derivatives. The unexpected high activity of (7b) toward the four-electron reduction of O₂ might arise from the proximity of the second porphyrin ring which would be protonated in acid (7c). It is conceivable that these protons, juxtaposed to the coordinated O₂ could prevent the premature dissociation of, as well as assist in proton transfer to the partially reduced O₂ coordinated to cobalt center in the second porphyrin ring. As already mentioned, kinetic measurements of oxygen binding to metal porphyrin complexes have shown that functional groups capable of hydrogen bonding make a significant contribution to the stability of the oxygen adduct of these complexes by decreasing the dissociation rate of the ligand binding. However, to demonstrate convincingly that hydrogen bonding promotes the oxygen reduction and activation in porphyrin models requires more elaborate studies.

Previously, Chang and Kondylis through the use of the Co(II) naphthoic acid porphyrin model, clearly demonstrated



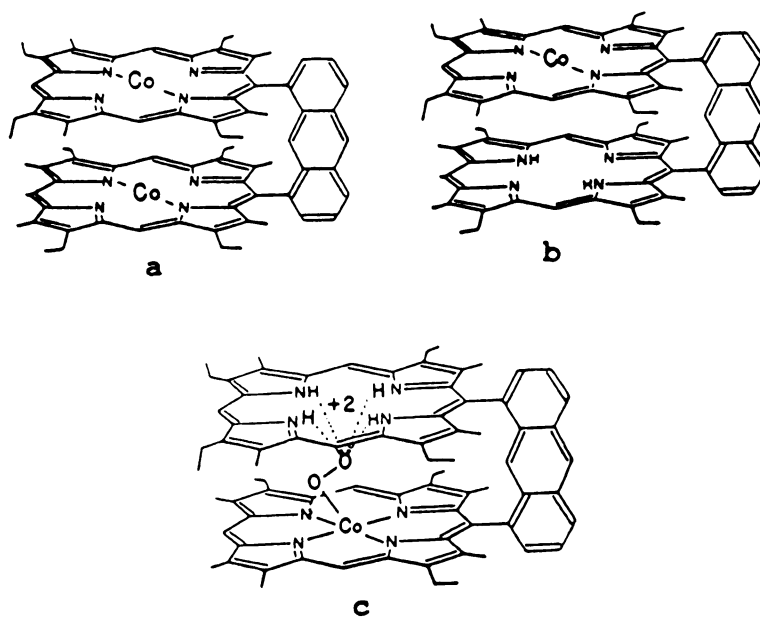
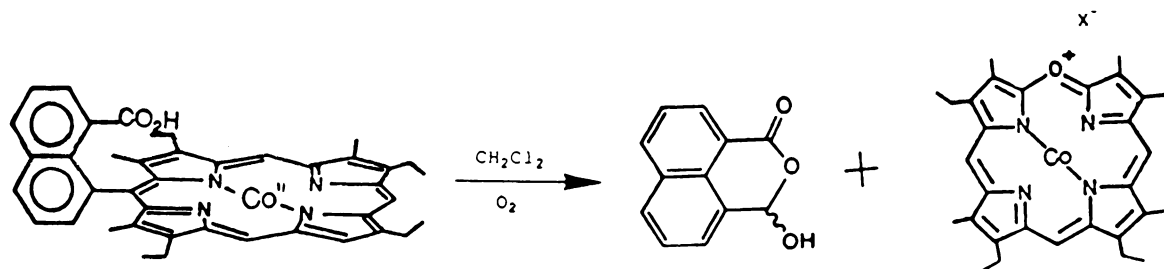


Figure 1-7. Anthracene Diporphyrins

Figure 1-8. Decomposition of Co^{II} Naphthoic Acid Porphyrin.



that the presence of H-bonding increases the Co-O₂ formation constant. The influence of H-bonding in the O₂ activation is not yet clear. Co(II) naphthoic acid porphyrin exhibits a very curious spontaneous self-decomposition in the presence of air, yielding oxaporphyrin and 1,8-naphthaldehydic acid (Figure 1-8) in neutral or acidic solutions. This behavior is not observed in any of the other Co(II)-naphthalene porphyrin derivatives studied. This is surprising since, tetracoordinated Co(II)-porphyrins are very stable at ambient temperatures when dissolved in non-coordinating solvents such as methylene chloride. The activation of dioxygen by Co(II)-porphyrins under such mild conditions and the destruction of the porphyrin ring, are completely unprecedented. This intriguing phenomenon was studied in more detail in an effort to elucidate the mechanism of decomposition. The results are presented in chapter 2.

In an effort to provide better understanding on the influence of H-bonding in O₂ activation and reduction we prepared a new series of model compounds: anthracene Kemp acid porphyrin for these studies. This system offers several advantages. First, an intramolecular proton is coming from the above to interact with the terminal oxygen atom of the coordinated dioxygen, and there is a very restricted freedom of motion between the proton source and O₂. Secondly, the conformation of the H-bonded dioxygen should minimize the intramolecular attack on the porphyrin



ring to avoid self decomposition, thus allowing further studies on the reaction of H-bonded heme-O₂ species. This goal has been accomplished. The syntheses of anthracene Kemp acid porphyrin and its derivatives are described in Chapter 3. The O₂ binding studies of these Co(II) anthracene Kemp porphyrins are presented in Chapter 3.



LIST OF REFERENCES

1. a. Anotonini, E. and Brunori, M. (1971) in Hemoglobin and Myoglobin and their Reactions with Ligand, North Holland Publishing Co. Amsterdam.
b. Griengerich, P.F.; McDonald, T.L. (1984) Acc. Chem. Res., **17**, 9-16.
c. The Porphyrins, Vol. VII part B, ed. David Dolphin, Academic Press Inc., N.Y. (1979), pp. 295-325.
d. Dickerson, R.E. and Geis, I., (1983) in Hemoglobin: Structure, Function Evolution and Pathology, Benjamin/Cummings Publishing, Menlo Park, CA.
2. a. Dawson, J.H. and Sono, M.; (1987), Chem. Rev., **87**, 1255.
b. White, R.E. and Coon, M.J.; (1980), Annu. Rev. Biochem., **49**, 315.
3. The Porphyrins, Vol. VII part B, ed. David Dolphin, Academic Press Inc., N.Y. (1979), pp. 325-345
4. a. Ibers, J.A.; Holm, R.H.; (1980), Science, **209**, 223-35.
b. Phillips, S.E.V.; Schoenborn, B.P.; (1981), Nature, **292**, 81-82.
c. Phillips, S.E.V.; (1980), J. Mol. Biol., **142**, 531-554.
d. Shaanan, B. (1982), Nature, **296**, 683.
e. Chang, C.K.; Traylor, T.G.; (1975), Proc. Natl. Acad. Sci., USA, **72**(3), 1166.
5. a. Drago, R.S.; Cannady, J.P.; Leslie, K.A.; (1980), J. Am. Chem. Soc., **102**, 6014.
b. Lavalette, D.; Tetreau, C.; Mispelter, J.; Momentau, M.; and LHoste, J-C., (1984), Eur. J. Biochem., **145**, 555-565.
c. Chang, C.K.; Ward, B.; Young, R.; Kondylis, M.P.; (1988), J. Macromol. Sci. Chem., 1307-1326.
d. Chang, C.K.; Kondylis, M.P.; (1986), J. Chem. Soc. Chem. Commun. 316.



6. a. Tsao, M.S.; Wilmarth, W.K.; (1962) Avan. Chem. Ser, **37**, 113.
b. Sehested, K.; Rasmussen, O.L.; Fricke, H.; (1968), **72**, 626.
c. Wood, P.M.; (1974), FEBS Letters, **44**, 22.
7. Poulos, T.L.; et. al., (1980), J. Biol. Chem., **255**, 575-580.
8. Poulos, T.L.; Kraut, J.; (1980), J. Biol. Chem., **255**, 8199-8205.
9. Poulos, T.L.; (1987), Adv. Inorg. Biochem., **7**, 1.
10. Ereinska, M.; Wilson, D.F.; (1978), Arch. Biochem. Biophys. Acta, **188**, 1.
11. Keilen, D.; Hartree, E.F.; (1939), Proc. Roy. Soc. London, **167**, B127.
12. a. Chance, B.; Power, L.; (1981), Biophys. J., **33**, 959.
b. Powers, L.; Chance, B.; Ching, Y.; (1981), Biophys J., **34**, 465.
13. Kean, R.T., "The Application of Optical Absorption and Resonance Raman Spectroscopy to the Study of Heme Proteins and Model Compounds," 1987, Dissertation.
14. Sehested, K.; Rasmussen, O.L.; Fricke, H.; (19668), J. Phys. Chem., **72**, 626.
15. a. Collman, J.P., et. al.; (1980), J. Am. Chem. Soc., **102**, 6027.
b. Durand, R.R. (1983), J. Am. Chem. Soc., 2710.
c. Collman, J.P.; (1979) J. Electroanal. Chem., **101**, 117.
16. a. Abdalmuhdi, I., "Pillared Cofacial Porphyrins: Synthesis, Structure and Application", 1985, Dissertation.
b. Liu, H.Y.; Weaver, G.B.; Chang, C.K. (1983), J. Electroanal. Chem., **145**, 439.
c. Chang, C.K.; Liu, H.Y.; Abdalmuhdi, I.; (1984), J. Am. Chem. Soc., **105**, 2725.
d. Liu, H.Y.; Abdalmuhdi, I.; Chang, C.K.; Anson, F.; (1985), J. Phys. Chem., **89**, 665.



Chapter 2

Decomposition of Co(II) Naphthoic Acid Porphyrin

Introduction

Kondylis¹ in his study of O₂ binding to Co(II) naphthalene model compounds (Figure 1-3) observed that Co(II) naphthoic acid porphyrin not only oxidizes in CH₂Cl₂ at room temperature, but decomposes as well (solution turns green). This behavior is very unusual, since, from numerous studies of O₂ binding to Co(II) porphyrin to bind oxygen it must be 5-coordinated and even then low temperatures are needed to achieve appreciable binding. Also, tetracoordinated Co(II) porphyrins are very stable when dissolved in noncoordinating solvents such as methylene chloride.^{2,3} He studied this decomposition in more detail and found that:

1. O₂ is needed for decomposition to occur. When the porphyrin was kept dissolved in CH₂Cl₂ under argon no decomposition took place (even after long periods of time). As soon as this solution was exposed to air, decomposition (evident color change) would start immediately.
2. Proton on carboxylic group is essential. The naphthoic ester and alcohol porphyrins did not show this decomposition. When a trace amount of ammonia was added to the CH₂Cl₂ solution before exposed to air, no decomposition was observed.

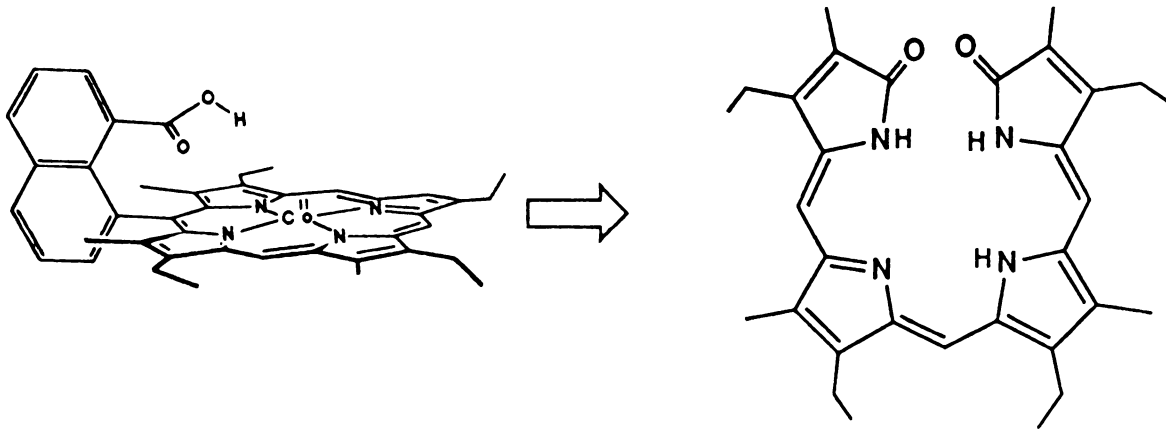


3. The reaction is catalyzed by external acid. Addition of HCl to the CH_2Cl_2 solution, decomposition takes place much faster.
4. Radical chain mechanism can be ruled out. Radical traps, such as duroquinone and galvinoxyl, do not inhibit the reaction.

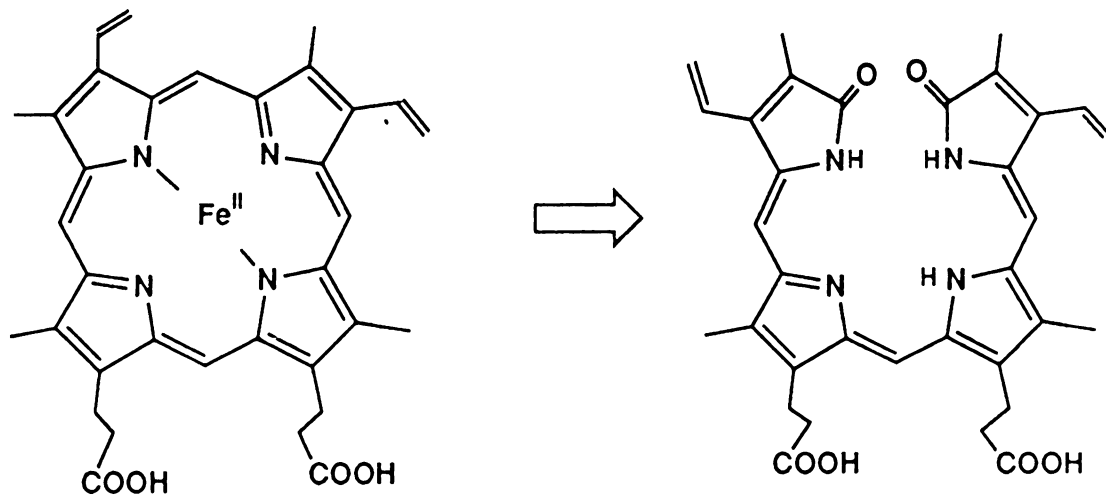
The most important result of the previous study is the isolation and characterization of the major product of this decomposition, namely the etiobiliverdin IV which suggests that the reaction involves oxygen attack of the meso position of the porphyrin ring where the naphthyl group is attached. This is contrary to the known examples of metallo-porphyrins decomposition by H_2O_2 where the phenyl-substituted meso positions are the most stable towards oxygen attack (because of steric reasons).⁴ Finally, he observed that Co(II) anthroic acid porphyrin (although binds O_2 with the same affinity as Co(II) naphthoic acid porphyrin) does not decompose when dissolved in CH_2Cl_2 . These two last results demonstrate the importance of the position of the carboxyl group.

It is interesting that one of the major products of this decomposition (etiobiliverdin IV) is of the same kind as the one observed in heme catabolism (biliverdin IX α) (Figure 2-1). Heme catabolism is an important biological process in which the heme is converted to bile pigments. This process has been the subject of intense study for more than 50 years⁵⁻⁷ and the main biocatabolic pathway has been



Co^{II} naphthoic acid porph.

Etiobiliverdin IV



HEME IX

biliverdin IX α

Figure 2-1. Final decomposition products of Co(II) naphthoic acid porphyrin and heme IX.



elucidated.^{6,7} The first step is assumed to be hydroxylation at the meso position to form an α -oxy derivative (catalyzed by heme oxygenase with the newly incorporated oxygen being supplied by molecular oxygen) (Figure 2-2). This α -oxyheme (b) is then converted to biliverdin by the addition of two molecules of oxygen and the loss of a molecule of CO. The reaction from oxyheme to biliverdin must necessarily involve

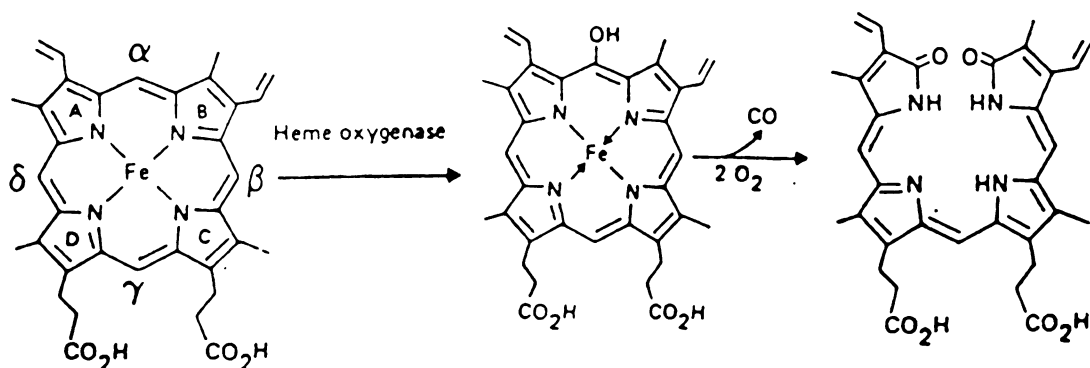


Figure 2-2. Heme catabolism main biocatabolic pathway.

additional intermediates, since the process involves loss of the iron atom and the α -methene carbon as CO, and incorporation of two oxygen atoms into the bile pigment, which were not present in the original haem compounds. Although the initiation of haem oxidation can be accounted for in terms of hydroxylation of a methene bridge, the



nature of the porphyrin-cleavage step itself remains uncertain, as well as the role of the possible intermediates between oxyhaem and biliverdin.

In an effort to understand what are the intermediates involved between the α -oxyhemin and biliverdin, model compounds (meso-hydroxyporphyrins and oxophlorins) were prepared⁸ and the steps followed in their degradation studied.⁹ In the in vitro system, the first step is also the hydroxylation at the meso position of the protohemin IX (Figure 2-3). Deprotonation and intramolecular electron transfer to reduce the Fe(III) to Fe(II) forms the α -oxyprotoheme IX.bis(py) π -neutral radical (2-3a). This activated intermediate then reacts with 1 equimolar amount of dioxygen to form intermediate 3b ($\lambda_{\max} = 893nm$) within 3 min., and this rapidly gives verdohemochrome IX (an oxaporphyrin, Figure 2-3c). Hydrolysis of the verdohemochrome IX gives then the biliverdin.

In our recent study of the decomposition of Co(II) naphthoic acid porphyrin, similar to the heme degradation, an oxaporphyrin species was identified as the major decomposition product. This led us to believe that the decomposition of Co(II) naphthoic acid porphyrin should follow a similar pathway. In this chapter we present the results obtained in our attempt to understand the decomposition of this porphyrin. A mechanism is proposed based on these results.



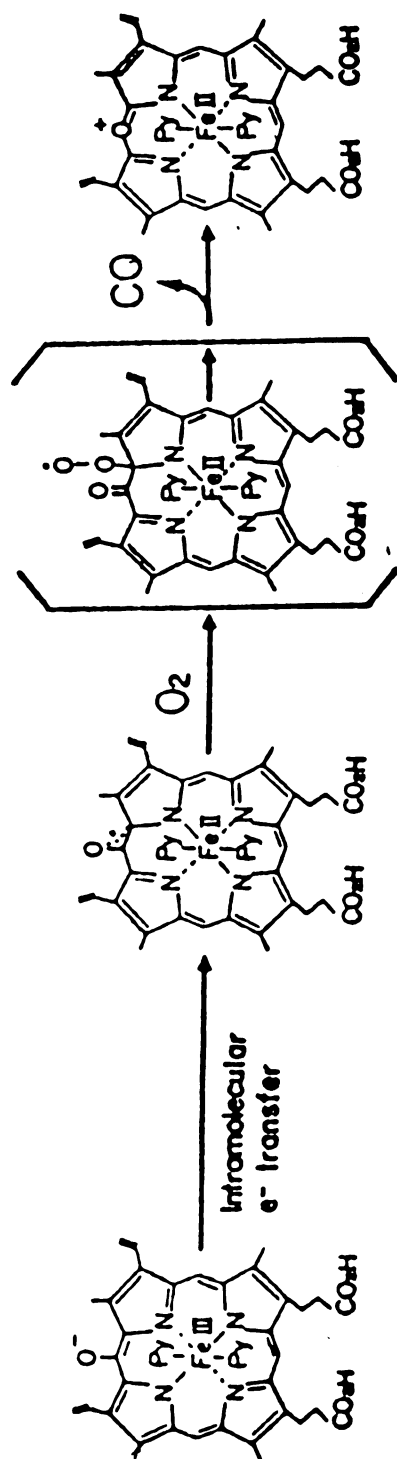


Figure 2-3. Mechanism followed in in vitro heme degradation.



Results

A. Final Decomposition Products

When a methylene chloride solution of Co^{II} naphthoic acid porphyrin was exposed to air it turns into green color in about 15 minutes. This was not observed when the solution was left under Argon. In addition to the color change, changes in the visible spectra were also observed. The Co^{II} naphthoic acid bands (399.5 (Soret), 526.0 and 559.0 nm) decreased and new bands at 423.0 and 651.0 nm appeared. After two hours visible absorption bands at 395.5 and 672.5 nm were observed. No additional changes in the visible spectra were observed. These results indicate that Co^{II} naphthoic acid porphyrin decomposes when exposed to oxygen.

Since the difference between this porphyrin and other cobalt porphyrins is the presence of a carboxylic acid near the Co-O_2 center we decided to see if the proton of the carboxylic acid is necessary for the decomposition to occur. In the presence of p-toluenesulfonic acid or HCl solution turned green immediately, giving a very complex visible spectrum. In the presence of 2,4,6-trimethylpyridine, NH_3 or when the porphyrin is dissolved in DMF no decomposition was observed. These results suggest that presence of a proton near the Co-O_2 center is necessary for the decomposition to occur.



Thin layer chromatography (silica-gel, 5% MeOH/CH₂Cl₂) showed that the porphyrin decomposes to two major compounds (a yellow and a blue-green compound). The visible spectra of the blue-green compound showed bands at 398, 511, 536 and 673 nm. This visible spectra was similar to the visible spectra of verdohemochrome (Figure 2-4), suggesting that this green compound was a cobalt oxaporphyrin. FAB mass spectra showed a peak at 538.05 (100.0) corresponding to the molecular ion of the cobalt oxaporphyrin cation (Figure 2-5). Infrared showed a strong absorption at 1261 cm⁻¹ corresponding to the asymmetric stretch of the C-O-C group. This peak was not observed in the IR of the Cu naphthoic acid porphyrin. The ESR of this compound is characteristic of a Co(II). From these results we can conclude that the blue-green decomposition product of Co^{II} naphthoic acid porphyrin is Co^{II} oxaporphyrin.

NMR and MS spectra of the purified yellow compound is identical to the commercial 1,8-naphthalic anhydride (Figure 2-6). Gas chromatography analysis of non purified decomposition product shows three major peaks with retention times of 9.51, 32.50 and 36.92 minutes. GC analysis of 1,8-naphthalic anhydride shows only one major peak at 37.57 minutes. The GC chromatogram of freshly prepared²³ 1,8-naphthaldehydic acid shows two major peaks with retention times of 33.67 and 38.54 minutes (Figure 2-7) corresponding to the 1,8-naphthaldehydic acid (33.67 min) and the 1,8-naphthalic anhydride (38.54 min). The 1,8-naphthaldehydic



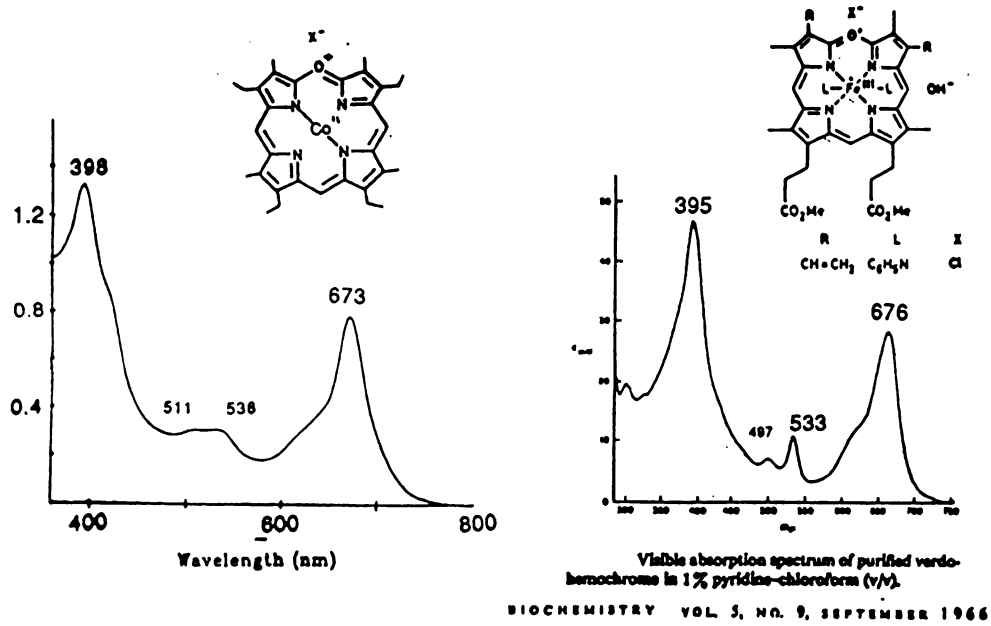


Figure 2-4. Visible absorption spectrum for Co^{II} oxaporphyrin and verdohemochrome.

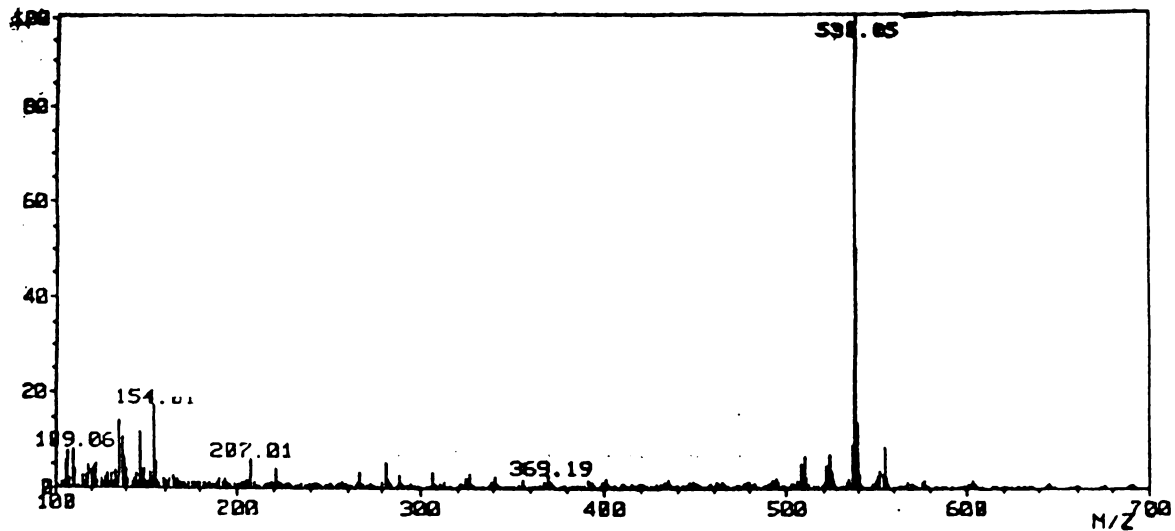


Figure 2-5. Mass spectrum for Co^{II} oxaporphyrin.



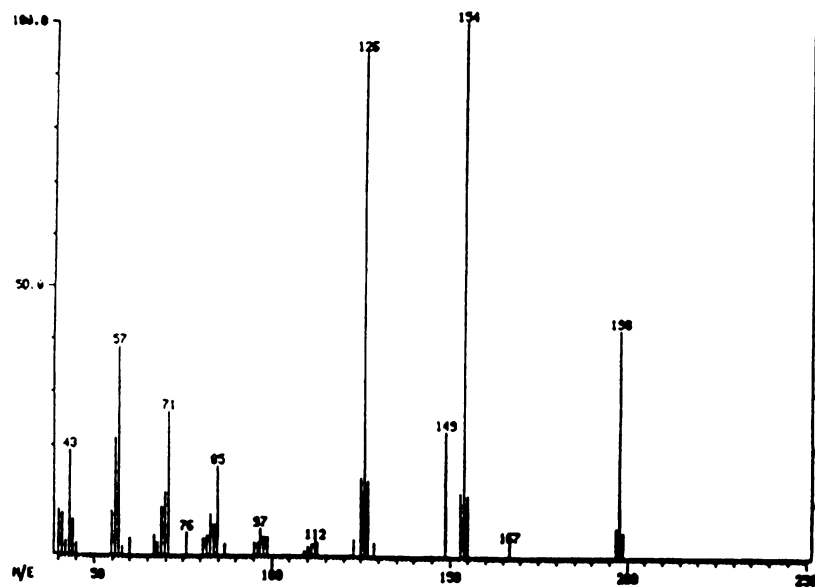
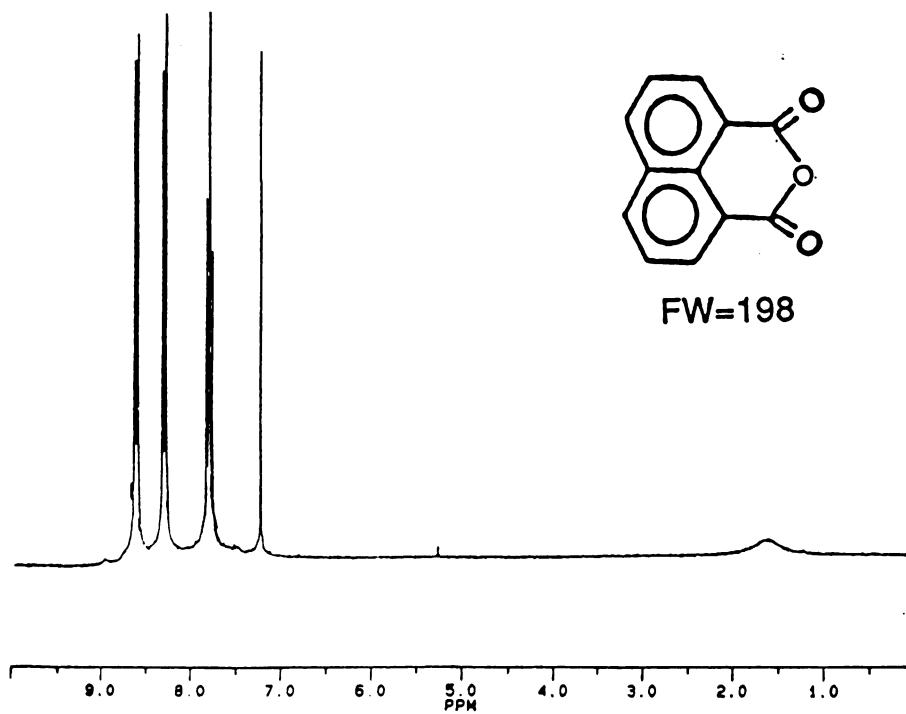


Figure 2-6. Proton NMR and e/I mass spectra of the yellow decomposition product.



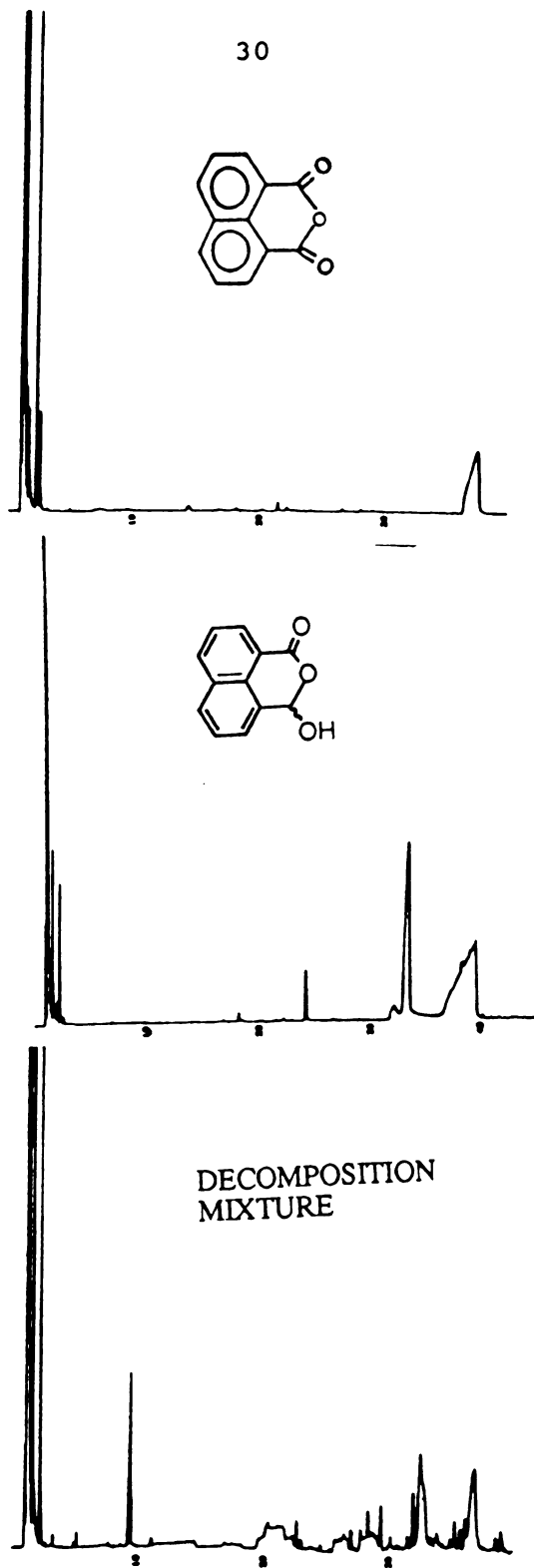


Figure 2-7. Gas chromatogram of: (a) 1,8-naphthalic anhydride; (b) 1,8-naphthaldehydic acid; (c) decomposition product.



acid oxidizes easily to the 1,8 naphthalic anhydride, therefore it is not surprising to see two peaks on its chromatogram. These results support the formation of 1,8-naphthaldehydic acid as the other major decomposition product which, upon purification oxidizes to the 1,8-naphthalic anhydride. In summary, the Co^{II} naphthoic acid porphyrin decomposes mainly to Co^{II} oxaporphyrin and 1,8-naphthaldehydic acid (Figure 2-8).

In order to quantify the decomposition reaction, the Co^{II} oxaporphyrin was converted to its biliverdin by treatment of base in the presence of air. Etio biliverdin was obtained in 91% yield indicating that the decomposition is almost quantitative. The etio biliverdin was identified by proton NMR, UV-vis and e/I mass spectra (Figure 2-9). In addition to the high yield of etio biliverdin obtained, it was also observed, that radical traps such as duroquinone and galvinoxyl did not prevent the decomposition. These results strongly suggest that the decomposition does not occur by radical chain mechanism.

B. Formation of Intermediate

When the Co^{II} naphthoic acid porphyrin was dissolved in dry CH_2Cl_2 (freshly distilled from CaH_2) and O_2 passed through, it was observed that changes in the visible spectrum of this green species showed absorption bands at 435, 569 and 673 nm (Figure 2-10). The visible spectra of this species has characteristics of N-alkyl Co^{II} TPP^{24a}



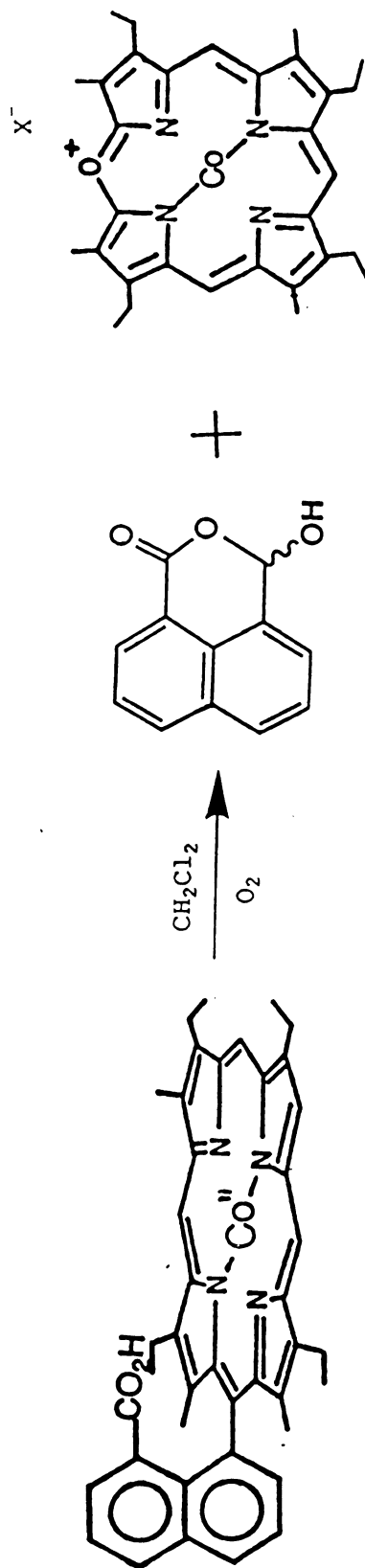


Figure 2-8. Co^{II} Naphthoic acid porphyrin final decomposition products.



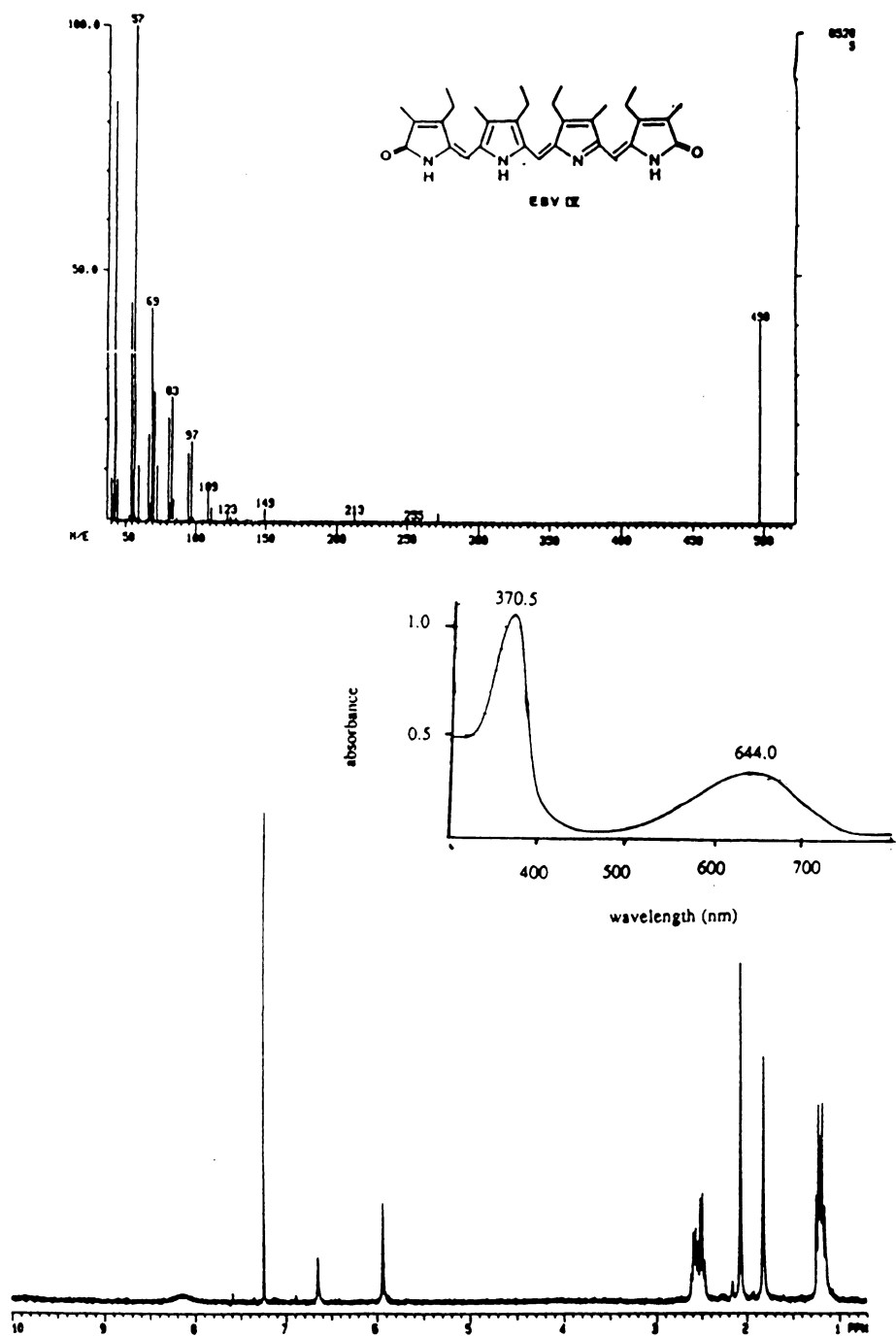


Figure 2-9. Physical data of Etio biliverdin obtained from decomposition: (a) e/I MS; (b) ¹H NMR; (c) UV-Vis.



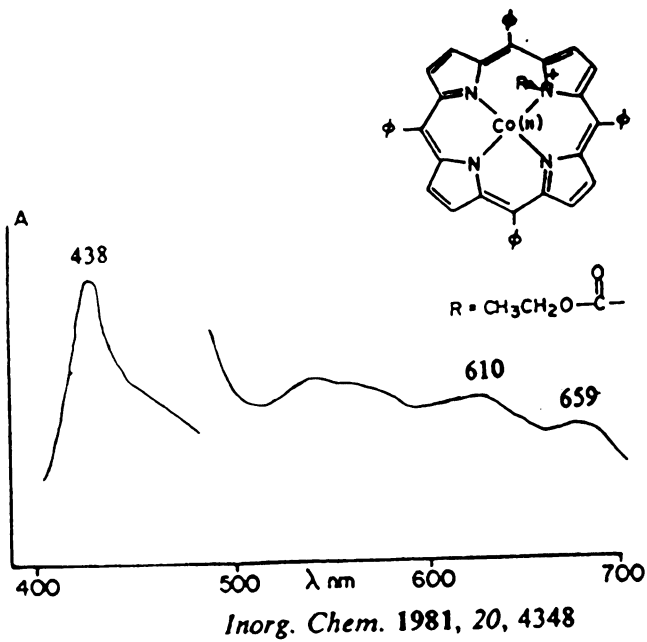
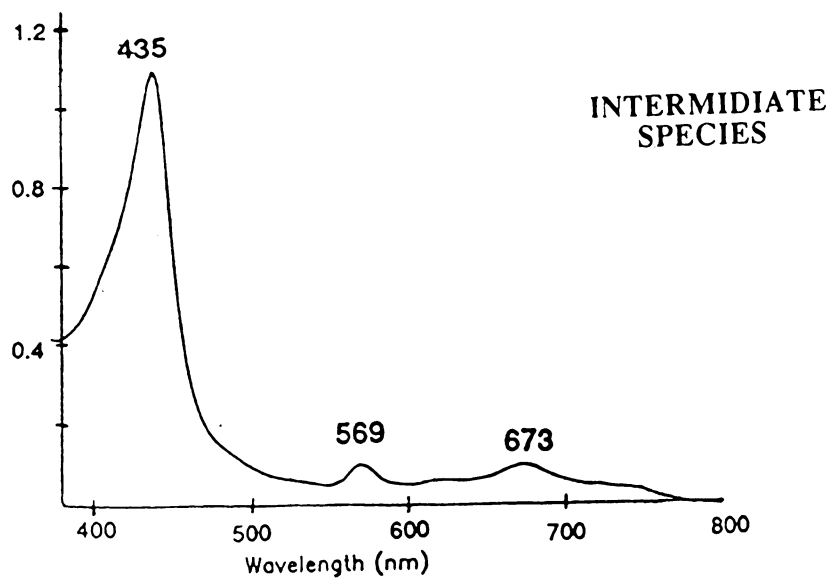


Figure 2-10. UV-Vis spectra of intermediate species and N-alkyl Co^{II} TPP.



(Figure 2-10), free base oxophlorin π -radical^{13b} (broad band at ~ 650 nm) and α -carbon substituted oxaporphyrins^{24b} (Soret at 430 nm). Field desorption mass spectra of this species shows in addition to the Co^{II} naphthoic acid ($M^+ = 705$) and Co^{II} oxaporphyrin ($M^+ = 538$) peaks at 737, 736 and 735 indicating addition of a molecule of oxygen to the Co^{II} naphthoic acid porphyrin with the consecutive loss of two hydrogen atoms (Figure 2-11). This species shows a very small ESR signal suggesting that in this species the Co is in the (+3) state, possibly a π -radical dimer or a Porph Co^{III}-O₂-Co^{III} Porph dimer. This species had a sharp proton NMR spectra that looked very similar to the NMR spectra of the naphthoic acid porphyrin. No major change in the meso positions were observed indicating that no major change in the ring aromaticity had occurred. The major difference with respect to the naphthoic acid porphyrin was the position of the methyl groups in the porphyrin ring. The methyls at positions 3 and 7 are shifted upfield by 0.2 ppm; and the methyls at positions 12 and 18 are shifted downfield by 1.1 ppm (from 2.1 to 3.2 ppm). When a drop of water or methanol was added to this species, further changes occurred, eventually yielding the oxaporphyrin. This is observed in the presence of oxygen or when the intermediate is left under Argon (Figure 2-12), suggesting that this stage of the reaction is probably independent of oxygen.



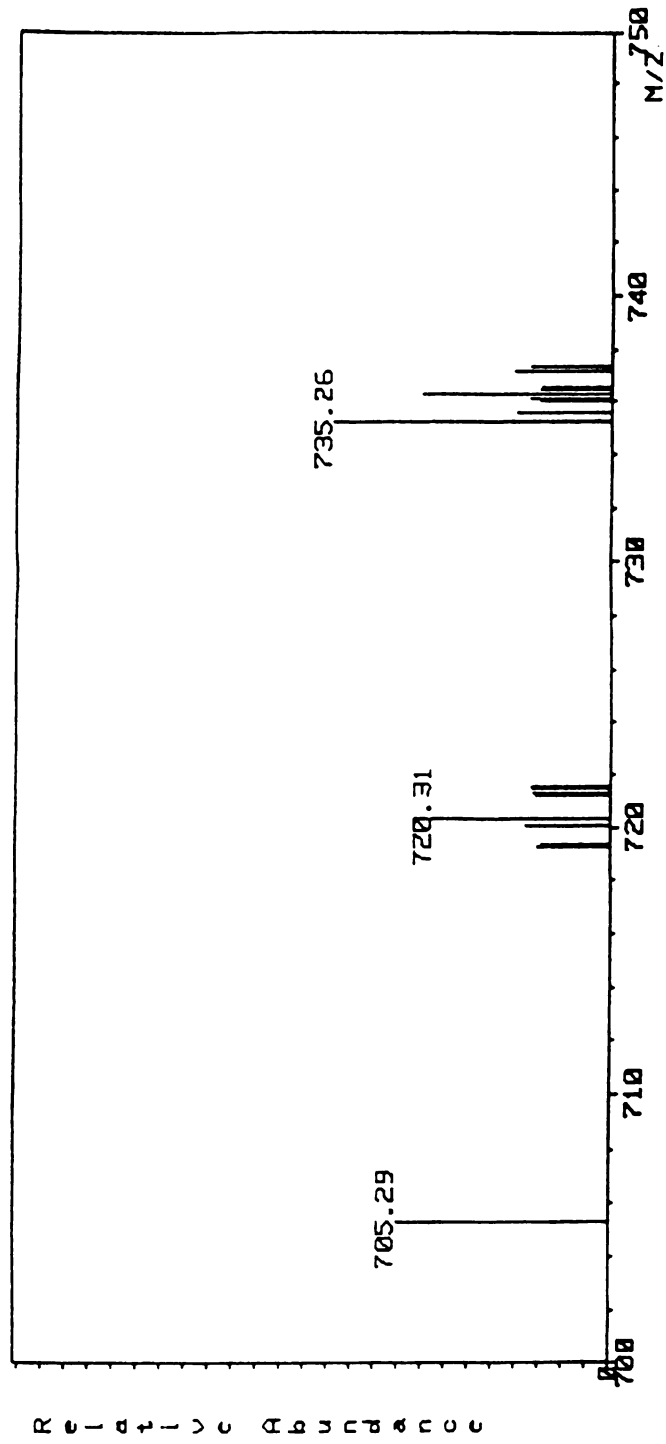


Figure 2-11. FD mass spectra of decomposition intermediate species.



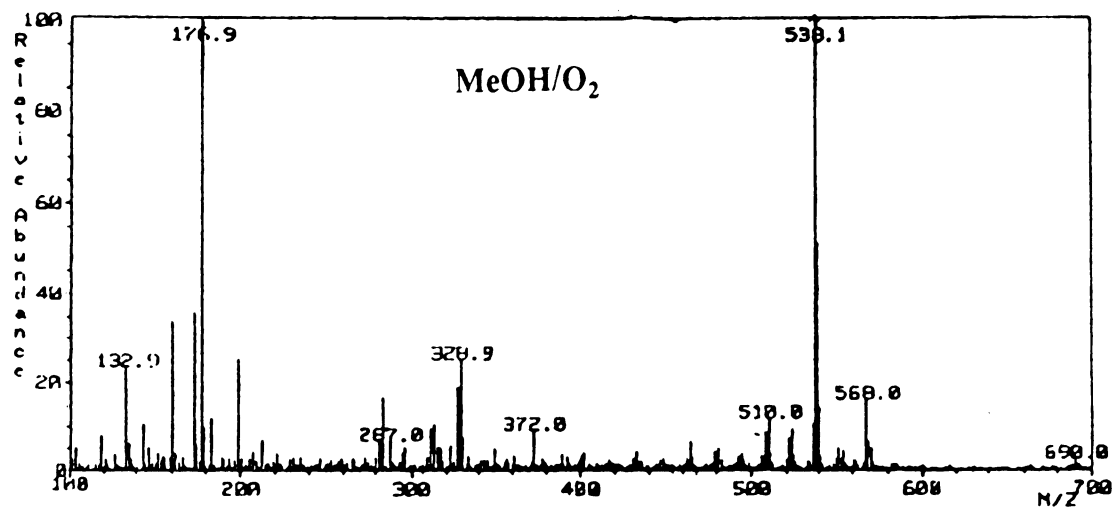
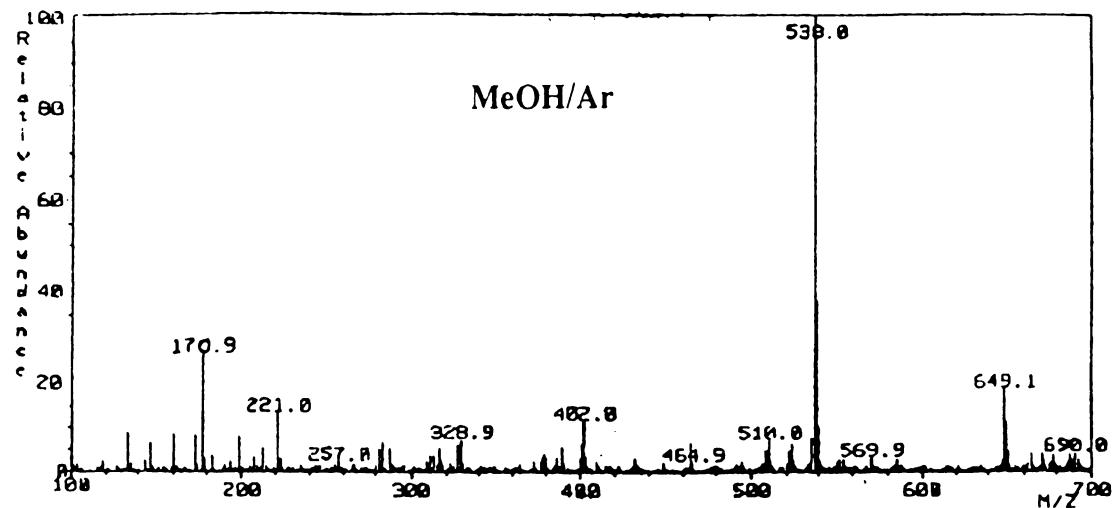


Figure 2-12. Mass spectra of decomposition products obtained when: (a) Methanol added under Argon; (b) Methanol added and O₂ bubbled through.



Discussion

Our results demonstrated that the Co(II) naphthoic acid porphyrin decomposes into Co(II) oxaporphyrin and 1,8-naphthaldehydic acid. After hydrolysis, the oxaporphyrin further changes into etio biliverdin. This final product in the decomposition of Co(II) naphthoic acid porphyrin is of the same kind as that derived from heme degradation (biliverdin IX α). Therefore, we assume that there are similarities in their formation mechanisms. The study of heme degradation has been most often carried out by couple oxidation in which pyridine hemochromes or hemoproteins are reacted with O₂ in the presence of hydrazine or ascorbate. In the following discussion we first present the literature results of the degradation of hemes. This is important in order to understand the mechanism we are proposing for the Co(II) naphthoic acid porphyrin.

A. Oxidation of Heme

Formation of verdohemochrome is a two-stage process. First, the heme ring is hydroxylated at the meso bridge to give meso-hydroxyheme. The hydroxylating species is most likely the electrophilic hydroxyl radical, $\bullet\text{OH}$, produced by action of ferric iron, ascorbate and oxygen; or by treatment of the ferrous porphyrin with hydrogen peroxide. Porphyrins and metalloporphyrins are susceptible to attack of electrophiles and radical at their meso positions.





treating the solution, still under nitrogen, with benzoyl chloride. Of the two tautomers (meso-hydroxy porphyrin and oxophlorin) the oxophlorin (oxyporphyrin) is the most stable.¹² The iron (III) octaethyl oxoporphyrin readily undergoes autoxidation in pyridine to give, after hydrolysis, octaethylbilatriene-abc. This is the first example of biliverdin (after hydrolysis of verdohemochrome) formed from an oxophlorin ring.

Besecke and Fuhrhop¹⁵ found that irradiating octaethyl- α -hydroxy-porphyrinatozinc(II) in benzene/methylene chloride in the presence of air with visible light leads to the formation of a neutral π -radical^{13,14} (Figure 2-14) which converts into a species whose visible spectrum is similar to the verdohemochrome. Treatment of this species with methanolic potassium hydroxide yielded the zinc complex of octaethylbiliverdin (Figure 2-14).

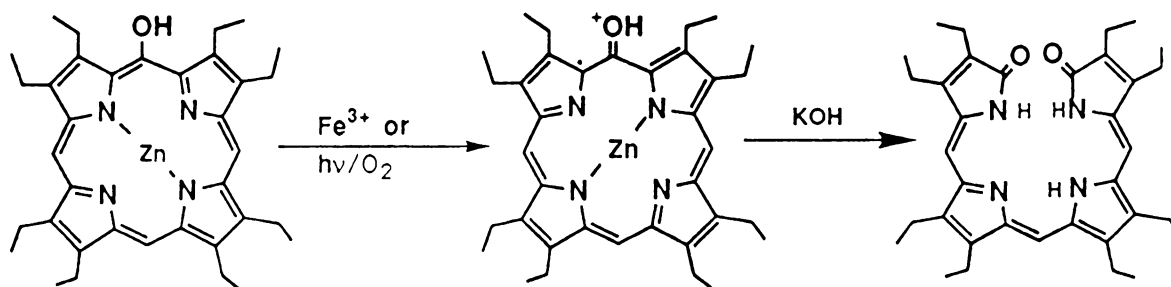


Figure 2-14. Formation of biliverdin from meso hydroxy porphyrin.



Sano and Morishima¹⁷ studied the autoxidation of α -oxyprotohemin IX to biliverdin IX α (Figure 2-15). They found that in anaerobic aqueous pyridine, α -oxyprotohemin (hexacoordinate) underwent autoreduction (intramolecular electron transfer) to yield an Fe(II) α -oxyprotoporphyrin π -neutral radical bis (pyridine) complex, which reacted with an equimolar amount of dioxygen to give pyridine verdohemochrome IX α and CO in 75-80% yield via an intermediate with an absorption maximum at 893 nm. Verdohemochrome IX α did not react with further dioxygen.

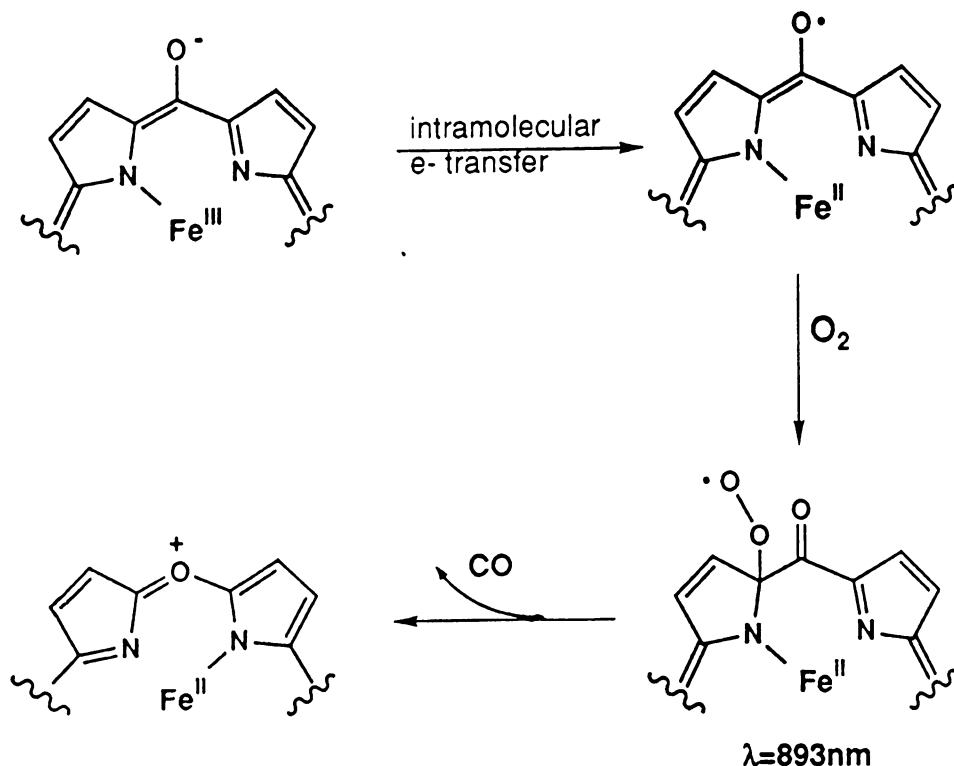


Figure 2-15. Intramolecular electron transfer of meso hydroxylate porphyrin and formation of oxaporphyrin.



From the results obtained by the different groups¹¹⁻¹⁷ that have studied the in vitro heme degradation a general mechanism can be proposed. The first step involves either one electron oxidation of the oxoporphlorin or autoreduction of the α -oxyprotohemin (Fe(III) \rightarrow Fe(II)) to form the oxyporphyrin π -neutral radical. This radical adds a molecule of O_2 to form an intermediate with an absorption band at 893 nm. Rapid decarbonilation of this intermediate will form the oxaporphyrin (Figure 2-16).

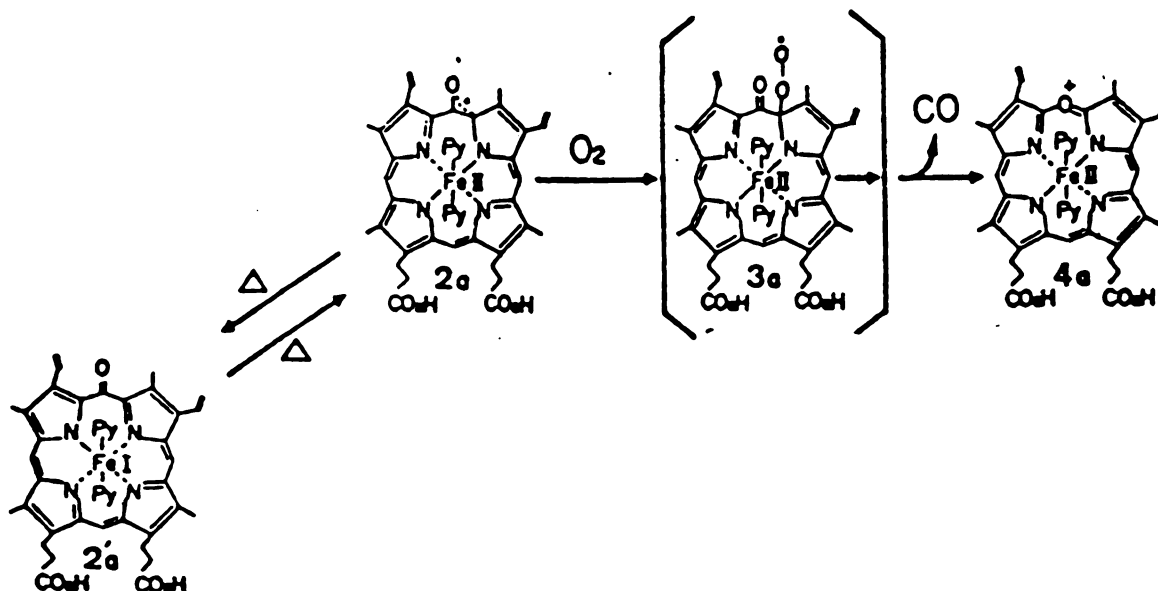


Figure 2-16. Suggested mechanism in the formation of Fe^{II} oxaporphyrin from Fe^{III} oxophlorin.



The reaction mechanism involved in the O₂ addition as well as the expulsion of CO, however, has not been determined.

B. Oxidation of Hemoproteins

The mechanism for the oxidation that is catalyzed by haem oxygenase, which uses oxygen and electrons (supplied by NADPH via reductase), is probably very similar to the analogous reaction in vitro, using oxygen and a reducing agent such as ascorbate. Formation of the biliverdin can be considered a two stage process: (1) oxygenation of heme and (2) decarbonylation and ring cleavage.

Experiments carried out using the microsomal heme oxygenase system and ¹⁸O₂ indicated that the oxygen liberated as CO as well as the oxygen found in each of the lactam carbonyls of biliverdin IX α was derived from O₂ and not from water.¹⁸ Moreover, when the enzymatic oxidation was carried out using ¹⁶O₂/¹⁸O₂ mixtures, it was found that the terminal oxygens of biliverdin are derived from separate O₂ molecules.¹⁹

By analogy to the in vitro process the first step would be formation of α -oxy-haemin. This step involves a molecule of O₂ and two NADPH. The mechanism of the oxygenation step is not known, but it is evident that a fundamental requirement must be fulfilled: generation of some reactive oxygen species, possibly \cdot OH.



The second step in the catabolism of heme in vivo involves elimination of CO from hydroxyporphyrin or oxyphlorin intermediate. In view of the ready autoxidation of oxophlorin-iron complexes^{11,21} this step probably occurs nonenzymatically by spontaneous addition of oxygen.

Sano and Morishima^{17b} reconstituted apomyoglobin α -oxyprotohemin IX complex (pentacoordinated), which reacted with an equimolar amount of dioxygen to form an Fe(II)oxy-porphyrin π -neutral radical intermediate, which rearranged to a green compound (λ_{\max} 660 and 704 nm) with elision of CO. The green product, which is probably an apomyoglobin-verdoheme π -radical complex, reacted with another equimolar amount of dioxygen to give Fe(III) • biliverdin IX α . Demetallation of this gave biliverdin IX α in overall yield of 70-75%. Their results indicate that the sequence of oxyheme autoxidation in the presence of apomyoglobin is:



A schematic representation of this mechanism is shown on Figure 2-17. Although this mechanism is speculative, it is consistent with most of the available experimental evidence.



Co^{II} Naphthoic Acid Porphyrin

The decomposition of Co^{II} naphthoic acid porphyrin and the in vitro heme degradation have two main characteristic features in common. First, for both systems one of the final products is an oxaporphyrin (Figure 2-18). Second, in order to get to this final product they both lose a meso carbon. In the in vitro heme degradation this carbon is lost as carbon monoxide and in the Co^{II} naphthoic acid porphyrin it is lost as a hydroxymethyl functional group.

Both of these reactions, opening of the ring and the elision of the meso carbon are highly unusual. The porphyrin macrocycle is particularly stable; coupled oxidation (in vitro) and decomposition of the Co^{II} naphthoic acid porphyrin are unique reactions in porphyrin chemistry in that permits this stable ring to be easily opened under extremely mild conditions. Therefore, the combined occurrence of both of these esoteric reactions suggests that analogous tetrapyrrole intermediate are involved in both systems (Figure 2-19).

The first step in the in vitro heme catabolism is hydroxylation¹¹ of the meso carbon (Figure 2-19). This process activates this position. Deprotonation of the hydroxyl group and intramolecular electron transfer gives the oxophlorin π -radical¹⁷ (19d). This radical reacts then with an equimolar amount of dioxygen to give the oxaporphyrin (19f).¹⁷ Our studies show that the presence of the carboxylic group near this position is essential for



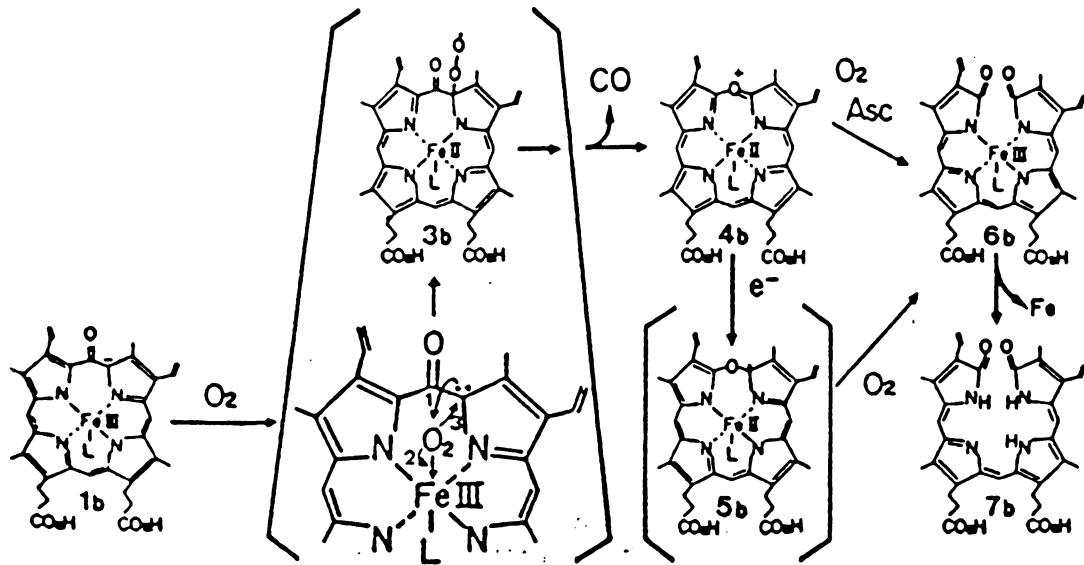


Figure 2-17. Possible mechanism involved in the oxidation of hemoproteins to biliverdin.

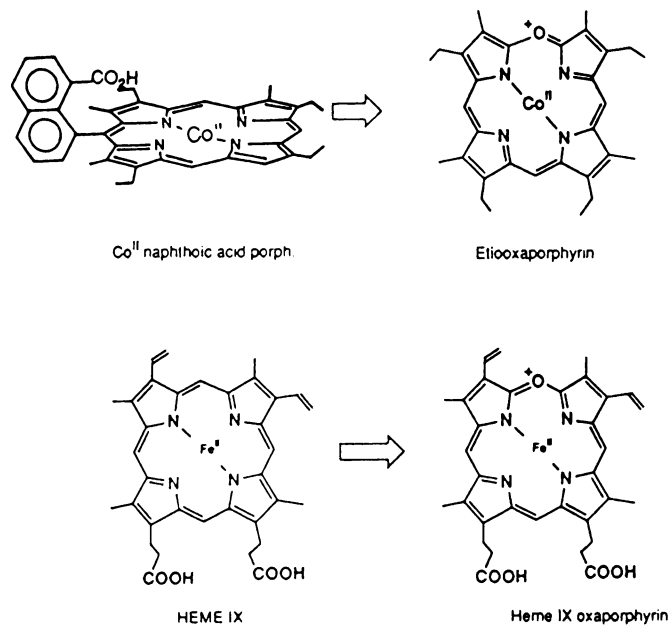


Figure 2-18. Oxaporphyrin formation from Co^{II} naphthoic acid porphyrin and protoheme IX.



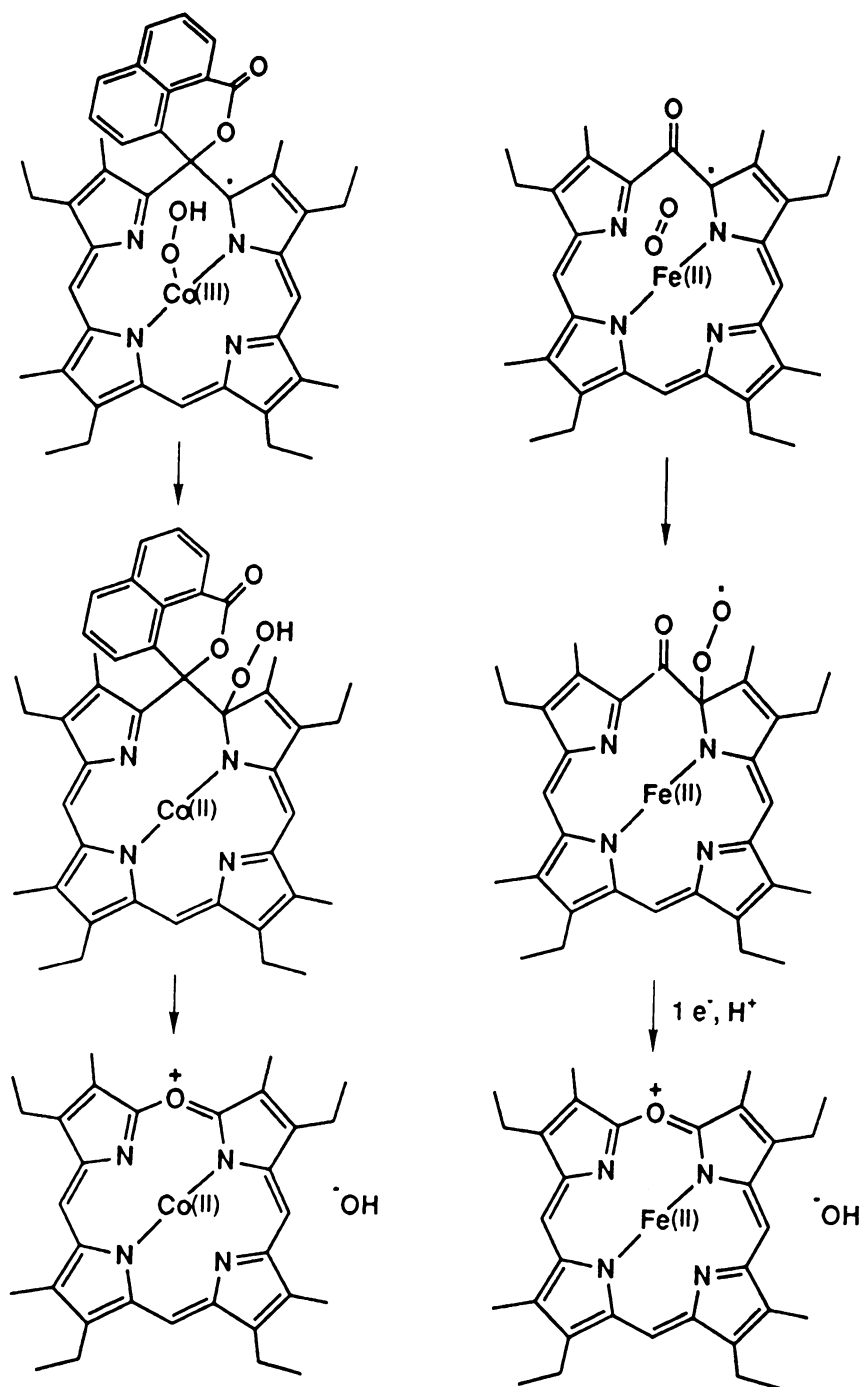
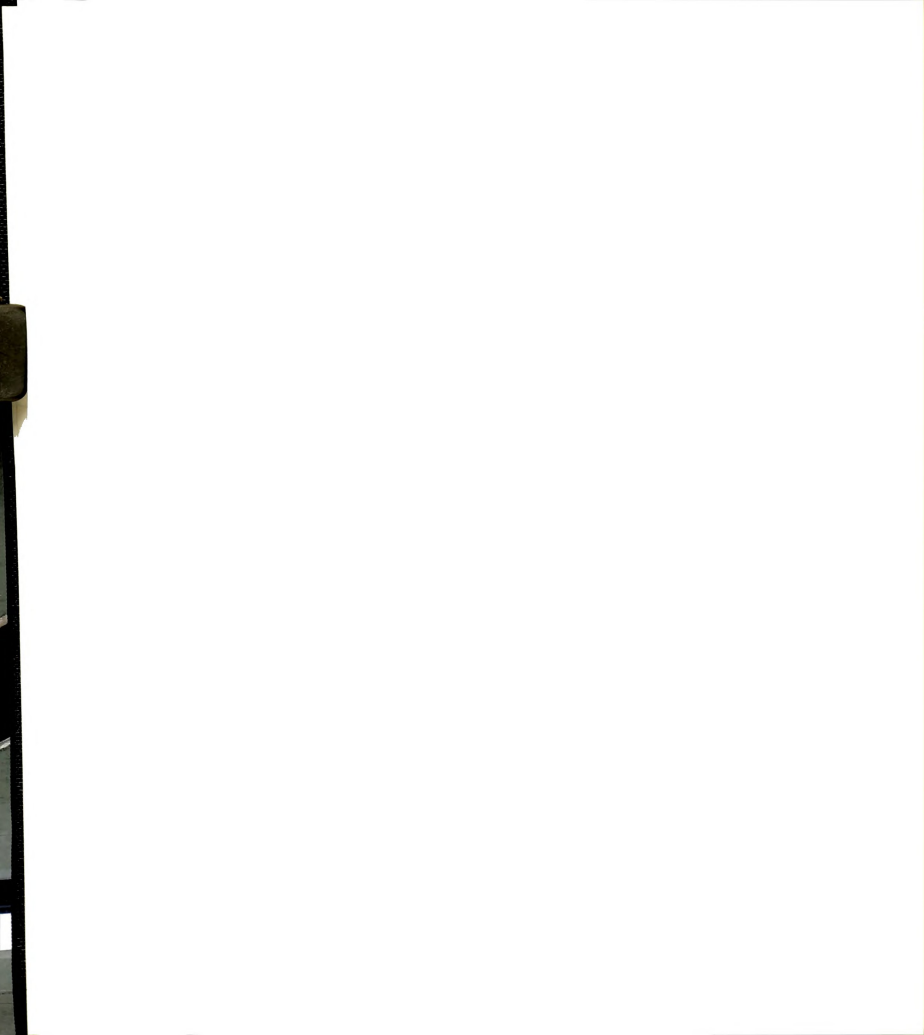


Figure 2-19. Suggested analogous pathway to heme degradation followed by the Co^{II} naphthoic acid porphyrin decomposition.



decomposition to occur (only Co^{II} naphthoic acid porphyrin is known to decompose under such mild conditions), therefore, we suggest that the carboxylate oxygen activates the porphyrin ring in analogy to the meso hydroxylation of the in vitro heme catabolism. To balance the chemical equation (reactants \rightarrow final products) only one molecule of dioxygen is needed. Therefore (in analogy to heme degradation), we suggest that the first step is the activation of the porphyrin ring by the carboxylate oxygen atom, followed by some activated dioxygen metal complex ($\text{Co}^{\text{III}} \cdot \text{O}_2^{-2}$ or $\text{Co}^{\text{III}} \cdot \text{O}_2^{-2} \cdot \text{Co}^{\text{III}}$) attack at the α -pyrrole carbon 19b. Rearrangement of this ring will then give the oxaporphyrin 19c.

To account for the Co^{II} naphthoic acid porphyrin decomposition we propose here a more detailed description (Figure 2-20). This mechanism is speculative, since we have not identified any of the intermediate species. Our mechanism is based on the final decomposition products (which are analogous to the products of heme catabolism) and the need of water or methanol to form the final decomposition products.

As mentioned earlier the first step in the decomposition of Co^{II} naphthoic acid porphyrin is the attack of the carboxylate oxygen to the meso carbon forming some π -radical species. Simultaneous intramolecular electron transfer of this electron to reduce the cobalt dioxygen complex (probably a cobalt-superoxide complex, $\text{Co}^{\text{III}} \cdot \text{O}_2\text{H}^{\cdot}$) and



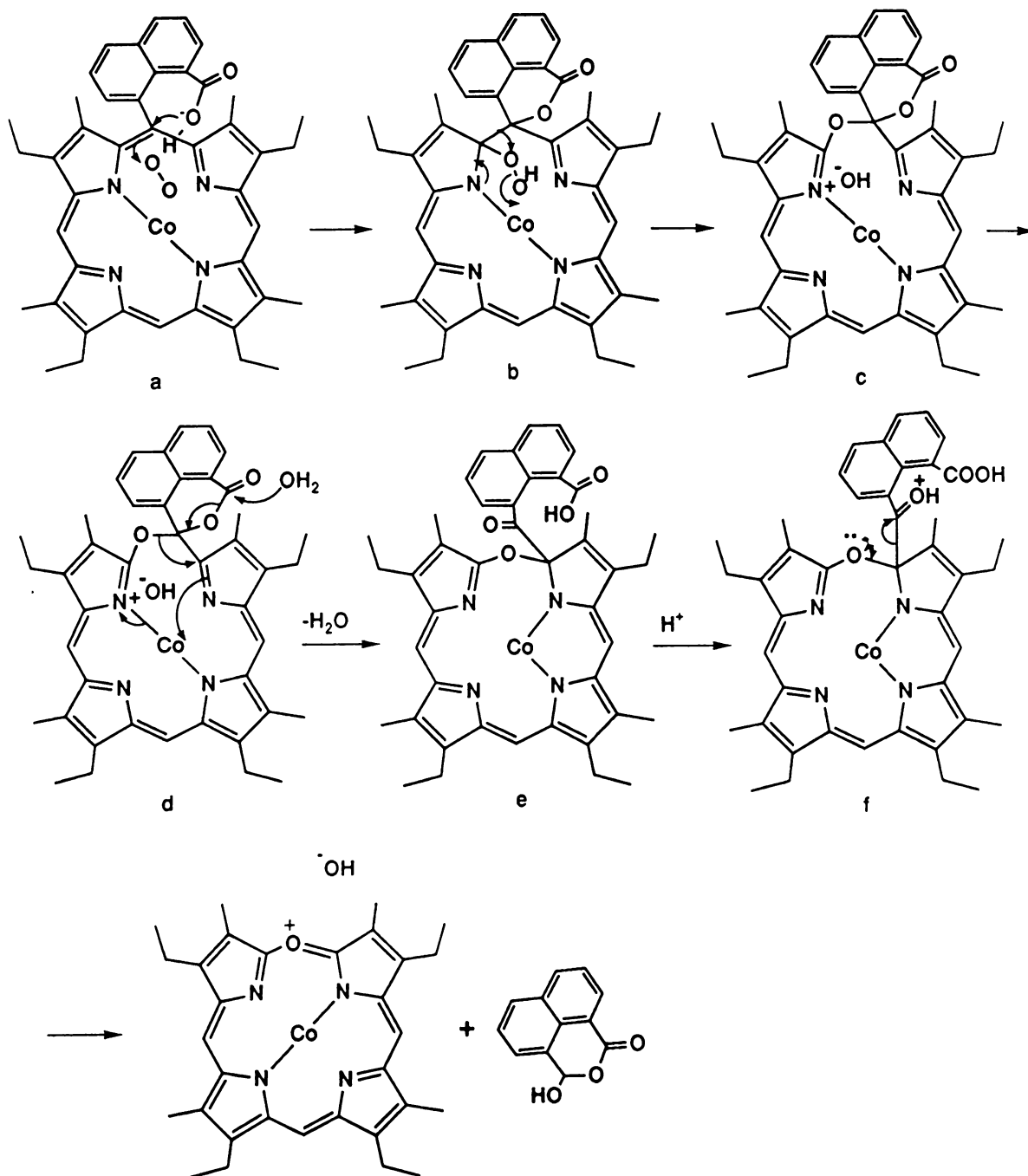


Figure 2-20. Proposed mechanism followed in the decomposition of Co^{II} naphthoic acid porphyrin.



attack of the dioxygen (probably a peroxide) to the α -pyrrole carbon near where the naphthalene is attached will form the species 20b. Intramolecular rearrangement of 20b will form 20c and hydrolysis of the ester bond will then give 20e. Protonation of the carbonyl group gives species 20f and final rearrangement of this species will form the final products.

During the decomposition of the Co^{II} naphthoic acid porphyrin we observe a green species with a visible spectrum showing absorption bands at 435, 569 and 673 nm. Because of the instability of this species, its structure has not been characterized. However, mass spectra of this species indicates that it has a molecule of dioxygen attached to the $\text{Co}(\text{II})$ naphthoic acid porphyrin. Also, in the presence of water or methanol, this species readily undergo further changes to form the $\text{Co}(\text{II})$ oxaporphyrin. We tentatively suggest structure 20b as the intermediate species but vigorous proof must await further studies.

Experimental

5-(8-Carboxyl-1-naphthyl)-2,8,13,17-tetraethyl-3,7,12,18-tetramethylporphyrin cobalt(II) (1)

The synthesis of the naphthoic acid porphyrin is described elsewhere.²⁷ Cobalt ion was incorporated into the porphyrin as follows: 5 mg of the naphthoic acid porphyrin was dissolved in 10 mL of dry (freshly distilled from CaH_2) methylene chloride. Then a solution of excess CoCl_2 (6 mg,



3x) and anhydrous sodium acetate (a pinch) in 5 mL of anhydrous methanol was added. The solution was then heated over a steam bath while Argon was continuously bubbled until all the solvent was evaporated. UV-Vis, λ_{\max} (rel. rat.), 559.0(0.770), 526.0(0.090), 399.5(1.000). MS (FAB) 705(70, M^+).

2,8,13,17-Tetraethyl-3,7,12,18-tetramethyl-5-oxaporphyrin cobalt(II) (2)

To the cobalt (II) naphthoic acid porphyrin 15 mL of methylene chloride was added. Air was bubbled into the solution. Solution turns brownish green immediately. Air was bubbled until no major changes in the visible spectra were observed. The oxaporphyrin was purified from silica gel column chromatography (started with pure CH_2Cl_2 and slowly increased the percentage of methanol up to 10%). Two major fractions were obtained: yellow fraction (corresponding to the naphthalic anhydride) and blue-green fraction (corresponding to the oxaporphyrin). The blue-green fraction was dissolved in CH_2Cl_2 and washed with saturated aqueous NaBF_4 and water, dried, and evaporated under reduced pressure. MS FAB 538.05 (100, M^+); UV-Vis, λ_{\max} (rel. rat.), 672.5(0.633), 536(0.300), 511.0(0.303), 398.0(1.000). The oxaporphyrin was ESR active (7 lines) indicating that the cobalt atom was in its (+2) state. IR showed band at 1261 cm^{-1} characteristic of C-O-C stretch.



1,8-Naphthalic anhydride from decomposition (3)

This compound was purified from preparative plates (Silica-gel, 5% MeOH/CH₂Cl₂). The resulting yellow fraction was then recrystallized from hexane. UV-Vis, λ_{\max} (rel. rat.), 329.4(1.000), 339.8(0.952); MS m/e (% RA), 198(42.05, M⁺), 154(100.00, -CO₂), 126(94.22, -CO); NMR δ , 7.81(2H, t), 8.31(2H, d), 8.62(2H, d).

Commercial 1,8-Naphthalic anhydride

Obtained from Aldrich Chemical Company, Inc. UV-Vis λ_{\max} (rel. rat.), 329.5(1.000), 339.5(0.942); MS m/e (% RA), 198(37.04, M⁺), 154(94.71, -CO₂), 126(100.00); NMR δ , 7.81(2H, t), 8.31(2H, d), 8.62(2H, d).

3,8,12,17-Tetraethyl-2,7,13,18-tetramethyl-1,19(21H,24H)-dione (Etio biliverdin) (4)

The naphthoic acid porphyrin (5.6 mg, 8.6 μ mole) was dissolved in 10 mL of CH₂Cl₂. The solution was deaerated for 5 min. To this solution, a solution of CoCl₂ (3x excess), anhydrous sodium acetate in methanol was added. The final mixture was then heated under argon until all solvent had evaporated. 25 mL of methylene chloride was added and oxygen bubbled through. The oxaporphyrin formed was extracted with 25% NaOH (3x), 75% HCl, saturated NaHCO₃, water and dried over sodium sulfate. The blue compound was purified by preparative tlc (silica gel/CH₂Cl₂) to give 3.9 mg (91%) of the etio biliverdin. UV-Vis, λ_{\max} (rel. rat.),



644(0.31), 370.5(1.00). MS m/e (% RA), 498(40.20, M⁺), 69(42.50), 57(100.00). NMR δ , 8.25 (1H, broad), 6.64(1H,s), 5.93(1H, S), 2.58(4H, q), 2.48(4H, q), 2.04(6H, s), 1.81(6H, s), 1.12-1.22(12H, m).

Decomposition Intermediate

To a flame dried round bottom flask, the naphthoic acid porphyrin (5 mg) was added followed by 10 mL of dried CH₂Cl₂ (freshly distilled from CaH₂). This solution was then deaerated for 15 min. Then 6 mg of CoCl₂ (3x excess) in 5 mL of dry methanol (freshly distilled from CaH₂) was added. The solution heated on oil bath (90°C) until completely dry. To the Co^{II} naphthoic acid porphyrin formed 50 mL of dry CH₂Cl₂ (freshly distilled from CaH₂) was added and oxygen bubbled through until no more changes in the visible spectra were observed. UV-Vis, λ_{\max} (rel. rat.), 673.0(0.22, 569.0(0.23), 435.0(1.00). MS Field Desorption, 737.47(M), 736.27(M-H), 735.26(M-2H), 720.3(M-OH), 705.29. NMR δ , 9.70(2H, s), 9.66(1H, s), 8.62(2H, d), 8.29(2H, d), 7.80(2H, t), 3.70-3.63(8H, 2q); 3.23(6H, s), 3.18(6H, s), 1.76-1.66(6H, 2t). Compound showed very small ESR signal.

Method used in the G.C. Study

All samples were dissolved in THF (dist. from CaH₂) and ran for 60 min. G.C. were done on a Perkin Elmer instrument using a 25M 0.25UM Ethyl Silicone capillary column.



	1(initial)	2(final)
Oven Temp. (°C)	70	250
Iso time (min)	0	0
Ramp Rate (°C/min)	3.0	-
Inj. Temp (°C) 300	Flow 10 mL/min	
Carrier gas: He	Pressure: 10.0 psig	

1,8-Naphthaldehydic Acid

To a suspension of acenaphthenequinone (5 g, 28 mmole) in DMSO (64g), 45% aqueous KOH (104g) was added all at once under vigorous stirring. After stirring at room temperature (external 34°C), under argon for 7 hours, the reaction mixture was poured into an erlenmeyer and diluted with 110 mL of water and neutralized with concentrated HCl.. The yellow solid formed was filtered and washed 3 times with water. The solid was dried at 70° in a vacuum oven. NMR δ 6.86(1H, s), 7.70-8.36(6H_{arom}, 1H_{OH}).



LIST OF REFERENCES

1. Kondylis, Michail "Distal Steric and Hydrogen Bonding Effects in Heme-Dioxygen Interactions," 1985, 127 pages, Dissertation.
2. a. Ibers, J.A.; Stynes, D.V.; Stynes, H.C.; James, B.R. J. Am. Chem. Soc. (1974), **96**, 1358.
b. Drago, R.S.; Beugelsdijk, T.; Breese, J.A.; Cannady, J.P. J. Am. Chem. Soc. (1978), **100**, 5374.
c. Drago, R.S.; Stahlbush, J.R.; Kitko, D.J.; Breese, J. J. Am. Chem. Soc. (1980), **102**, 1884.
d. Drago, R.S.; Corden, B.B. Acc. Chem. Res. (1980), **13**, 353-360.
e. Collman, J.P.; Browman, J.I.; Boxsee, K. M.; Halbert, T.R.; Hayes, S.E.; Suslick, K.S. J. Am. Chem. Soc. (1978), **100**, 2761.
3. Jameson, G.B.; Drago, R.S. J. Am. Chem. Soc. (1985), **107**, 3017-3020.
4. a. Dolphin, D.; Felton, R.H.; Borg, D.C.; Fajer, J. J. Am. Chem. Soc. (1970), **92**, 743.
b. Bonnett, R.; Dimsdale, M.J. J. Chem. Soc. Perkin I (1972), 2540.
5. a. Lemberg, R.; Cortis-Jones, B.; Norrie, M.; Biochem. J. (1938), **32**, 171.
b. Levin, E.Y. Biochemistry (1966), **5**, 2845.
6. Schmid, R. and McDonagh, A. in "The Porphyrins" (David Dolphin, ed.), Vol. VI, pp. 257-291, Academic Press, New York, 1979.
7. a. Lightner, D.A.; McDonagh, A.F. Acc. Chem. Res. (1984), **17**, 417.
b. Frydman, R.B.; Frydman, B. Acc. Chem. Res. (1987), **20**, 250-256.
8. a. Jackson, A.H.; Rao, K.R.N.; Wikins, M.; J. Chem. Soc. Perkin Trans I (1987), 307.
b. Bonett, R.; Dimsdale, M.J. Tetrahedron Letters (1968), 731-733.



9. Norman, R.O.C. and Lindsay Smith, J.R. Oxidases Relat. Redox Syst., Proc. Symp. 1964, Vol. 1, p. 131 (1965).
10. a. Libowitsky, H. and Fischer, H. Hoppe-Leyler's Z. Physiol. Chem. (1938) **255**, 209.
b. Libowitsky, H. Hoppe-Leyler's Z. Physiol. Chem. (1941) **265**, 191.
c. Stier, E. Hoppe-Leyler's Z. Physiol. Chem. (1942) **272**, 239.
11. Bonett, R.; Dimsdale, J.J. J. Chem. Soc. Perkin Trans I (1972), 2540.
12. a. Clezy, P.S.; Lim, C.L.; Shannon, J.S. Aust. J. Chem. (1974), **27**, 1103-20.
b. Jackson, A.H.; Kenner, G.W.; Smith, K. M. J. Chem. Soc. (c) (1968), 302.
13. a. Bonett, R.; Dimsdale, M.J.; Sales, K.D. J. Chem. Soc. Chem. Commun. (1970), 962.
b. Fuhrhop, J-H.; Besecke, S.; Subramanian, J. J. Chem. Soc. Chem. Commun. (1973), 1.
14. Clezy, P.S.; Liepa, A.J.; Smythe, G.A. Austral. J. Chem. (1970), **23**, 603.
15. Besecke, S.; Fuhrhop, J-H. Angew. Chem. Internat. Ed. (1974), **13**, 150.
16. Fuhrhop, J-H.; Besecke, S.; Subramanian, J.; Mengersen, Chr.; Riesner, O. J. Am. Chem. Soc. (1975), **97**, 7141.
17. a. Sano, S.; Sugira, Y.; Maeda, Y.; Ogawa, S.; Morishima, I. J. Am. Chem. Soc. (1981), **103**, 2888.
b. Sano, S.; Sano, T.; Morishima, I.; Shiro, Y.; Maeda, Y. Proc. Natl. Acad. Sci. (1986), **83**, 531.
c. Morishima, I.; Fujii, H.; Shiro, Y.; Sano, S. J. Am. Chem. Soc. (1986), **108**, 3858.
18. Tenhunen, R.; Marver, H.S.; Pimstone, N.R.; Trager, W.F.; Cooper, D.Y.; Schmid, R. Biochemistry (1972), **11**, 1716.
19. a. King, R.F.G.J.; Brown, S.B. Biochem. J. (1978), **174**, 103.
b. Troxler, R.F.; Brown, A.S.; Brown, S.B. J. Biol. Chem. (1979), **254**, 3411.
c. Rajananda, V.; Brown, S.B. Tetrahedron (1983), **39**, 1927.
20. Woodward, R.B. Ind. Chim. Belge (1962), **2**, 1293.



21. Jackson, A.H.; Kenner, G.W.; Smith, K.M. J. Chem. Soc. C (1968), 302.
22. Foote, C.S.; Wexler, S; Ando, W.; Higgins, R. J. Am. Chem. Soc. (1968), **90**, 975.
23. Bader, H.; Chiang, Y.H. Synthesis (1976), 249.
24. Hempenius, M.A.; Koek, J.H.; Lugtenburg, J.; Fokkens, R. Recl. Trav. Chim. Pays - Bas. (1987), **106**, 105-112.
25. Newton, J.; Hall, M.B. Inorg. Chem. (1984), **23**, 4627-4632.
26. a. Nishinaga, A.; Tomita, H. J. Mol. Catalysts (1980), **7**, 179-199.
b. Schaefer, W.P.; Marsh, R.E. J. Am. Chem. Soc. (1966), **88**, 178.
27. Buchler, J.W. In Porphyrins and Metalloporphyrins (Kevin Smith, Ed.), Elsevier Scientific Publishing Co., (1975), p. 179.



Chapter 3

Synthesis of Novel Porphyrins and their Study of O₂ Binding to Co(II) and ¹⁵N-NMR of Iron-bound C¹⁵N

Introduction

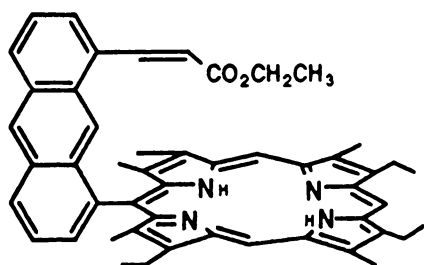
As already mentioned in Chapter 1, Chang and Kondylis through the use of the Co(II) naphthoic acid model, clearly demonstrated that the presence of H-bonding increases the Co-O₂ formation constant. Although hydrogen bonding is thought to (see Chapters 1 and 2 for more details):

- promote heterolysis of peroxides in cytochrome c peroxidase.
- assist in the reduction of O₂ to water in the monometallated pac-man porphyrin.
- promote the decomposition of the Co(II) naphthoic acid porphyrin when dissolved in methylene chloride.

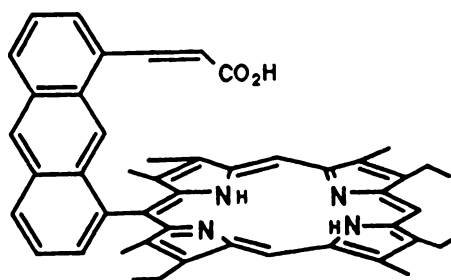
the influence of H-bonding in the O₂ activation and reduction is not yet clear.

In an effort to provide a better understanding on the influence of H-bonding in O₂ activation and reduction we prepared a new series of model compounds: anthracene acrylic acid and anthracene Kemp acid porphyrins (Figure 3-1). The anthracene Kemp acid porphyrin offers several advantages. First, an intramolecular proton is coming from the heme normal (axial direction) to interact with the terminal oxygen atom of the coordinated dioxygen, and there is a very restricted freedom of motion between the proton source and

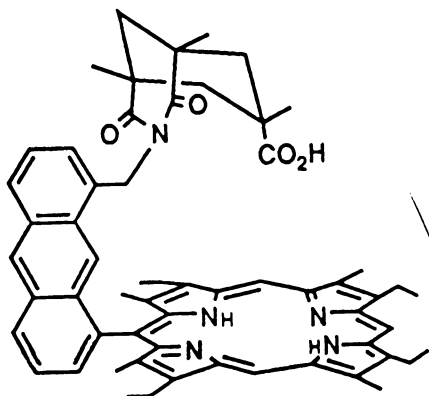




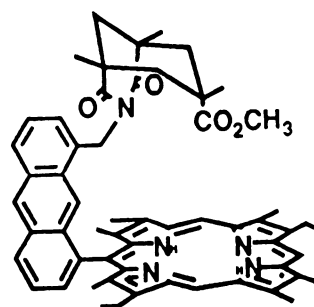
Anthracene Acrylic Ester Porphyrin



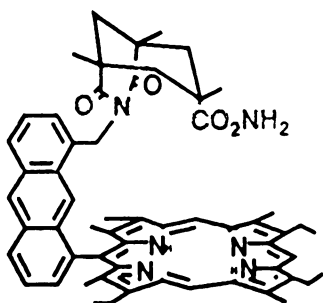
Anthracene Acrylic Acid Porphyrin



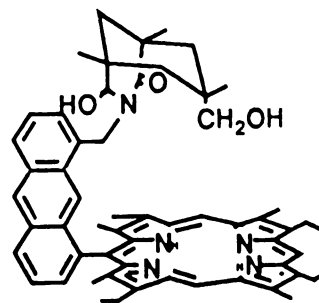
Anthracene Kemp Acid Porphyrin



Anthracene Kemp Ester Porphyrin



Anthracene Kemp Amide Porphyrin



Anthracene Kemp Alcohol Porphyrin

Figure 3-1. Structures of the series of anthracene acrylic and anthracene Kemp porphyrins.



O₂. Secondly, the conformation of the H-bonding should minimize the intramolecular attack on the porphyrin ring to avoid self decomposition, thus allowing further studies on the reaction of H-bonded heme-O₂ species. The study of O₂ binding to the series of the Co(II) Kemp acid porphyrins was examined and the results are presented here.

In addition of the O₂ binding studies, we also studied the H-bonding effects on heme coordinated cyanide and CO. ¹⁵N has an unusually large response in its NMR chemical shift due to changes in its environment. Changes in protonation state, hydrogen bonding and metal ligation produce large shifts. In the ¹⁵N NMR study of the dicyano Fe(III) protoporphyrin Goff demonstrated that hydrogen bonding can cause an 82 ppm upfield shift of the signal.¹ For the cyano and carbon monoxide iron porphyrin complexes the N≡C-Fe^{III} and O≡C-Fe^{II} angles are of ~180°. Therefore, ¹⁵N NMR of the dicyano Fe(III) naphthoic acid, acrylic acid and Kemp acid porphyrins is a good indication of the proximity and conformation of the proton to the nitrogen of the Fe-CN center. The results of the ¹⁵N NMR study of the dicyano Fe(III) complexes of these porphyrins (naphthoic acid, acrylic acid and Kemp acid) are presented here. These results indicate that the proton on the Kemp acid porphyrin interacts more efficiently with the nitrogen of the Porph Fe^{III}(NC)₂⁻ complex than the proton on the naphthoic or acrylic acid porphyrins.



Results and Discussion

A. Synthesis of the Anthracene Acrylic Acid Porphyrins

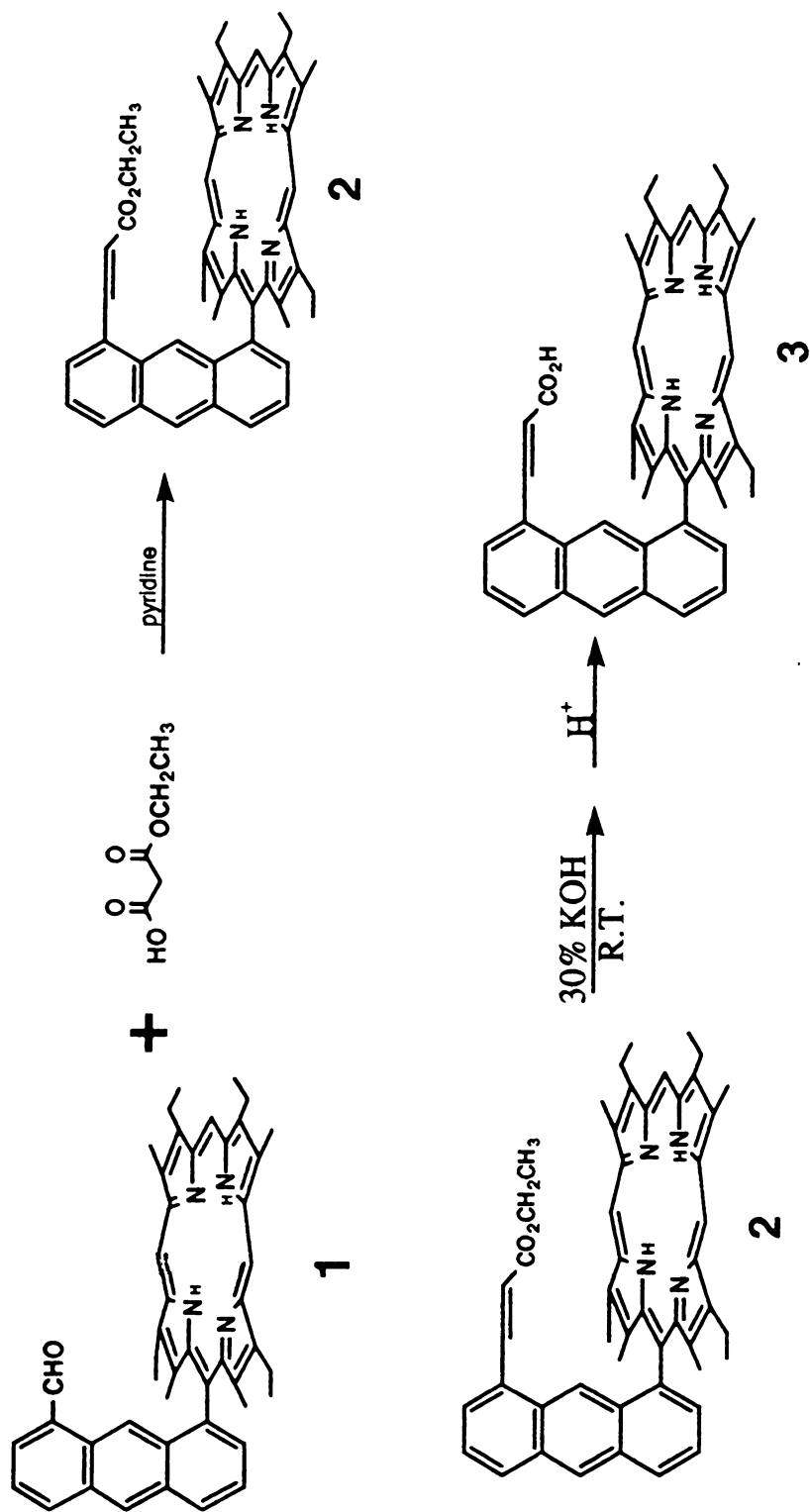
The anthracene formyl porphyrin (1) was prepared as reported previously.² The anthracene acrylic ester porphyrin (2) was prepared in 98% yield by the condensation of the anthracene formyl porphyrin with monoethyl ester malonic acid (Scheme 1). The proton coupling constant (J) of the protons attached to the double bond is 16Hz which is characteristic of trans protons on a double bond. Therefore, we assign the trans structure to the anthracene acrylic ester porphyrin. The ethyl ester protons are moved upfield by ~2.0 ppm (-CH₂ at 2.38 ppm and -CH₃ at -1.21 ppm) when compared to the ethyl acrylate protons (-CH₂ at 4.2 ppm and -CH₃ at 1.3 ppm), indicating that the ethyl group is close to the porphyrin center.

Hydrolysis of the anthracene acrylic ester porphyrin (2) (30% KOH) gave the anthracene acrylic acid porphyrin (3) (Scheme 1).

B. Synthesis of Kemp Isomer Porphyrins

The naphthalene alcohol (4) was prepared according to previous procedure.³ The naphthalene mesylate porphyrin was prepared by dissolving the porphyrin in sufficient amount of methanesulfonyl chloride. The reaction was conducted at room temperature since heating the porphyrin in mesyl chloride would decompose it. Reaction of this mesylate with the potassium Kemp imide carboxylate salt (5) was expected





Scheme 1

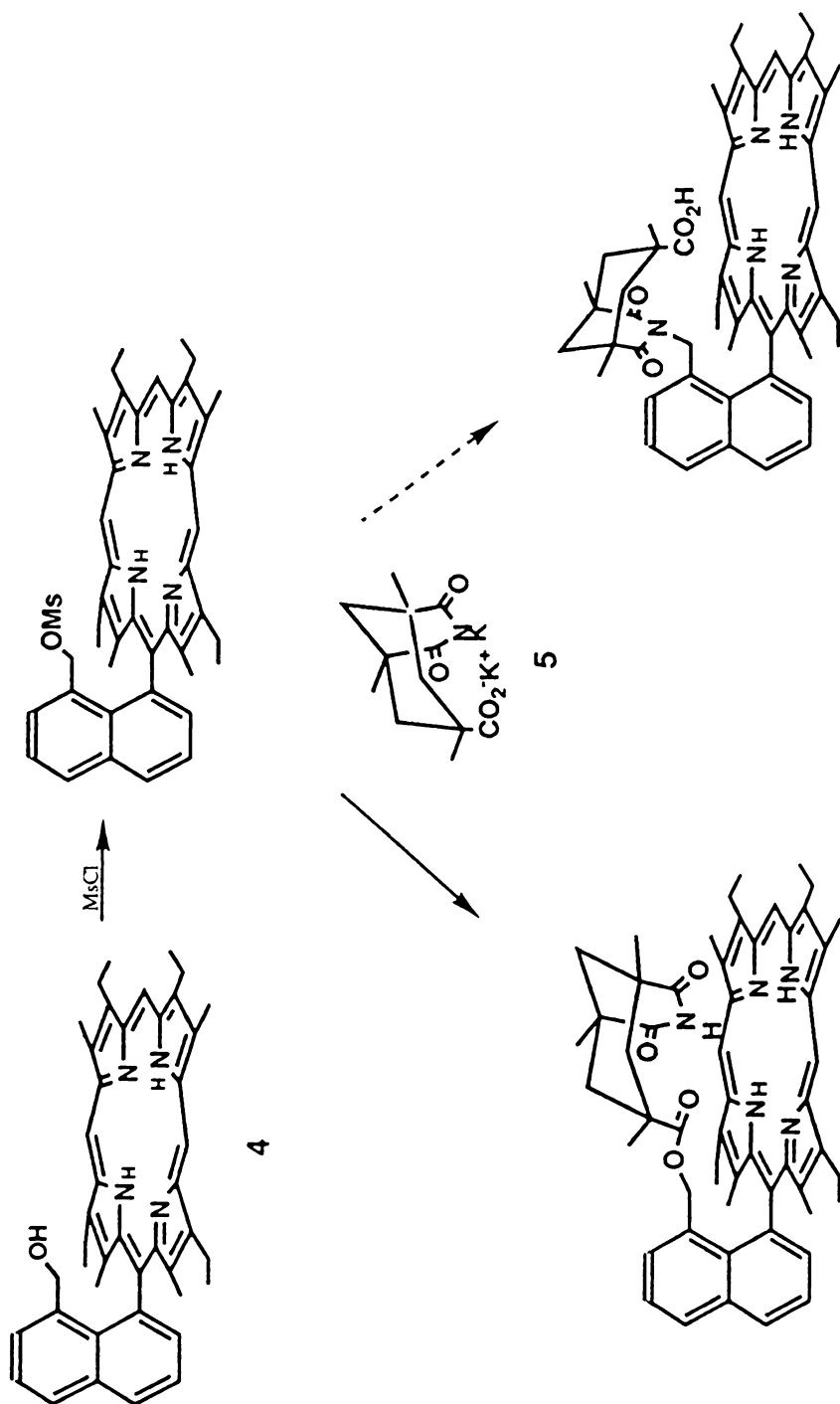


to give the naphthalene Kemp acid porphyrin (Scheme 2) but instead we obtained the naphthalene Kemp isomer porphyrin (6). The anthracene Kemp isomer porphyrin was prepared by the same procedure (Scheme 3). The first evidence that these compounds (6 and 8) were not the desired Kemp acid porphyrins came when the proton we thought belonged to the carboxylate (δ around 6 ppm for both compounds) did not exchange in the presence of deuterated water nor would it react with diazomethane. We decided then to prepare the anthracene Kemp acid porphyrin by a different route (Scheme 4).

The NMR and MS of the anthracene Kemp isomer (8) and anthracene Kemp acid (12) porphyrins were very different. MS of the anthracene Kemp acid (12) shows the loss of CO_2 which is typical of carboxylic acid compounds, this is not observed for the anthracene Kemp isomer. Proton NMR of the anthracene Kemp acid, anthracene acrylic acid and naphthoic acid porphyrins do not show the carboxylate proton or the porphyrin N-H protons indicating that there is exchange between them, the anthracene and naphthalene Kemp isomer porphyrins show these protons.

In conclusion, the reaction of the mesylate porphyrins (4a and 7a) with the potassium Kemp imide carboxylate (5) is not a good route for the synthesis of the Kemp acid porphyrins. The carboxylate side of the molecule (5) reacts easier (less sterically hindered) than the imide side of the



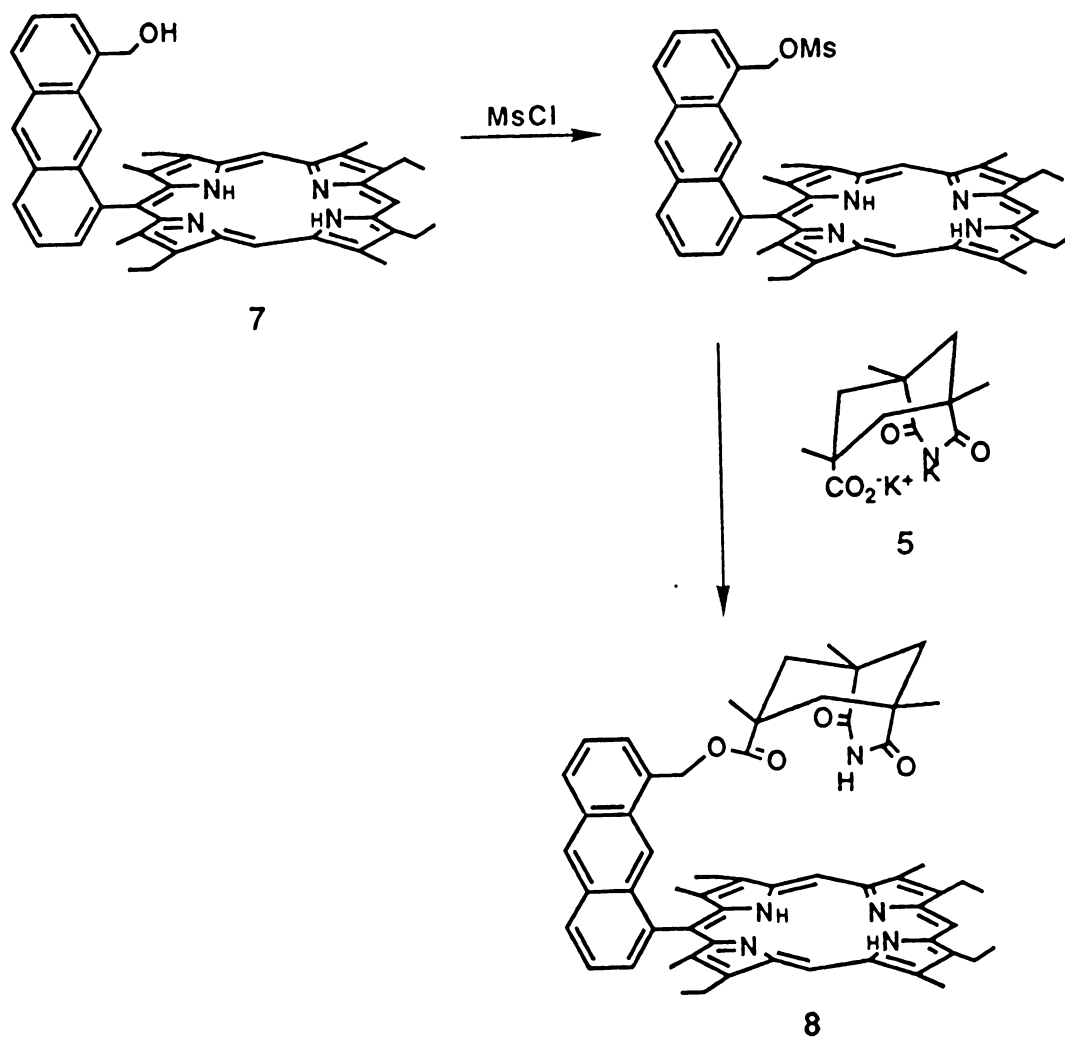


Naph Kemp acid porph

6

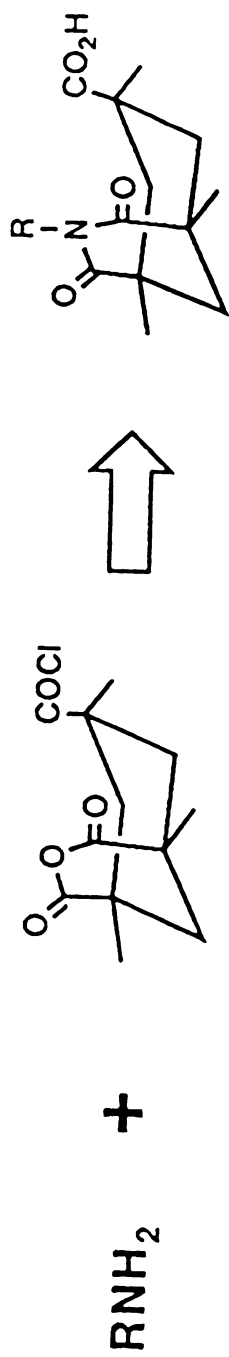
Scheme 2





Scheme 3





Scheme 4



molecule (5) and therefore attacks the mesylate carbon much faster than the imide.

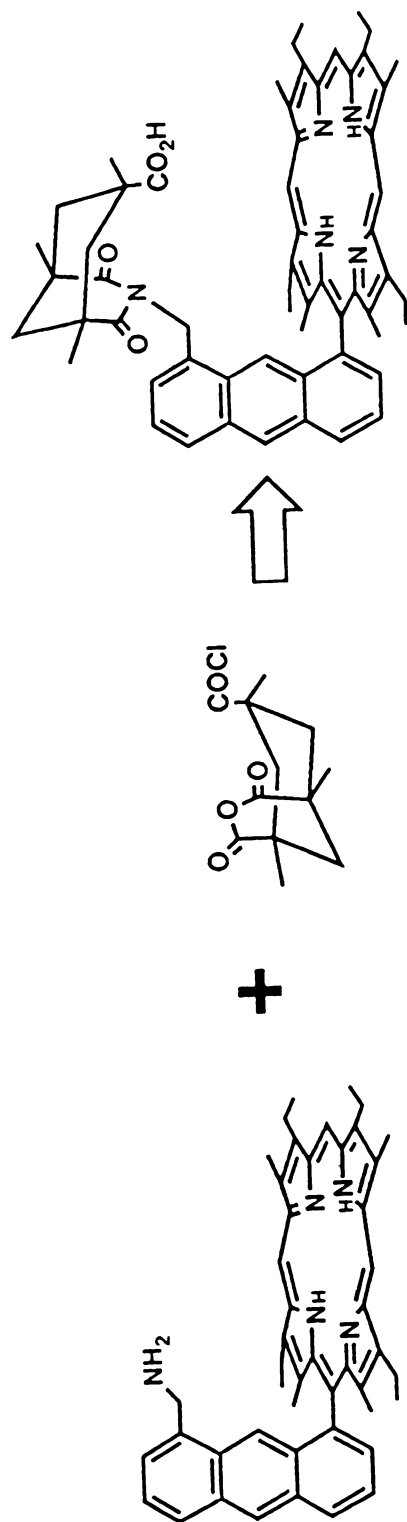
C. Synthesis of the Anthracene Kemp Acid Porphyrins Series

Since the reaction of the mesylate porphyrin with the potassium Kemp imide carboxylate salt (5) prove to be unsuccessful, an alternative route for the synthesis of the anthracene Kemp acid porphyrin was followed. Rebeck has reported the successful condensation of different amines with the Kemp anhydride acid chloride to form the alkylated Kemp imide acid⁸ (Scheme 4). Therefore, the route we followed involved the condensation of the anthracene amine porphyrin with the Kemp anhydride acid chloride (Scheme 5).

Our first major concern was the preparation of the anthracene amino porphyrin. This was accomplished in three steps. The anthracene mesylate was prepared from the anthracene alcohol porphyrin (7) as mentioned earlier, and was then reacted with sodium azide to form the azido porphyrin 9. IR spectrum of this porphyrin showed strong absorption band at 2096 cm^{-1} characteristic of azido stretch. The azide porphyrin 9 was reduced to the amino porphyrin 10 by treatment with LiAlH_4 . Reaction of the amine porphyrin 10 with the Kemp anhydride acid chloride 11 (prepared as reported previously⁵) gave the anthracene Kemp acid porphyrin 12 in 75% yield.

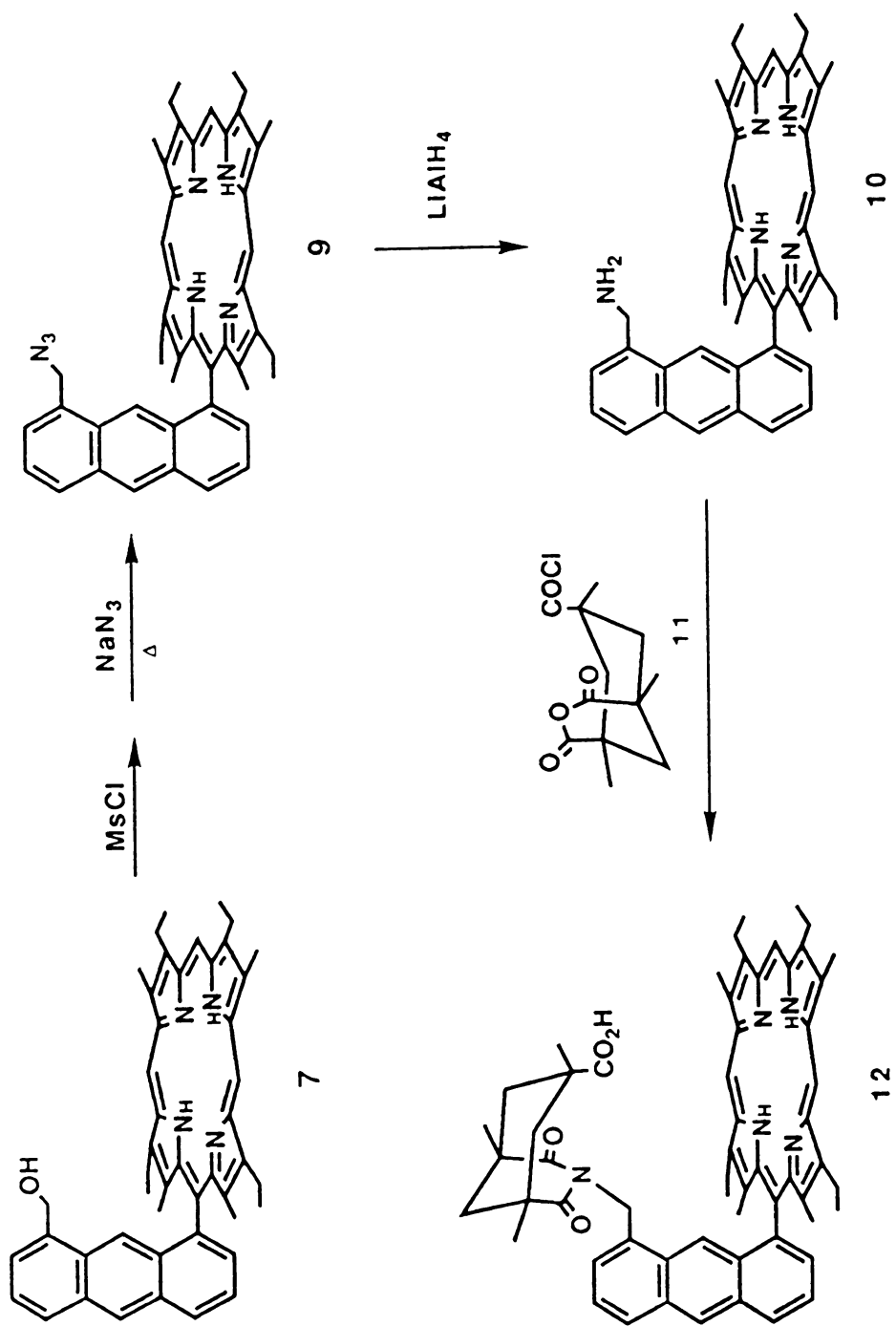
The anthracene Kemp ester 13 was obtained in quantitative yield from the reaction of the anthracene Kemp





Scheme 5





Scheme 6



acid with diazomethane. The Kemp amide **14** was obtained from the reaction of the Kemp acid **12** first with thionyl chloride followed by ammonia. The reduction of the Kemp ester **13** with LiAlH_4 was expected to give the Kemp alcohol porphyrin but instead it gave a mixture of the reduction on the imide carbonyl **15** and what we called the Kemp diol **16**. Recently, Rebeck reported the facile reduction of the imide carbonyls in the presence of LiAlH_4 ⁹ corroborating what we observed when we treated the Kemp ester porphyrin **13** with LiAlH_4 (Scheme 7).

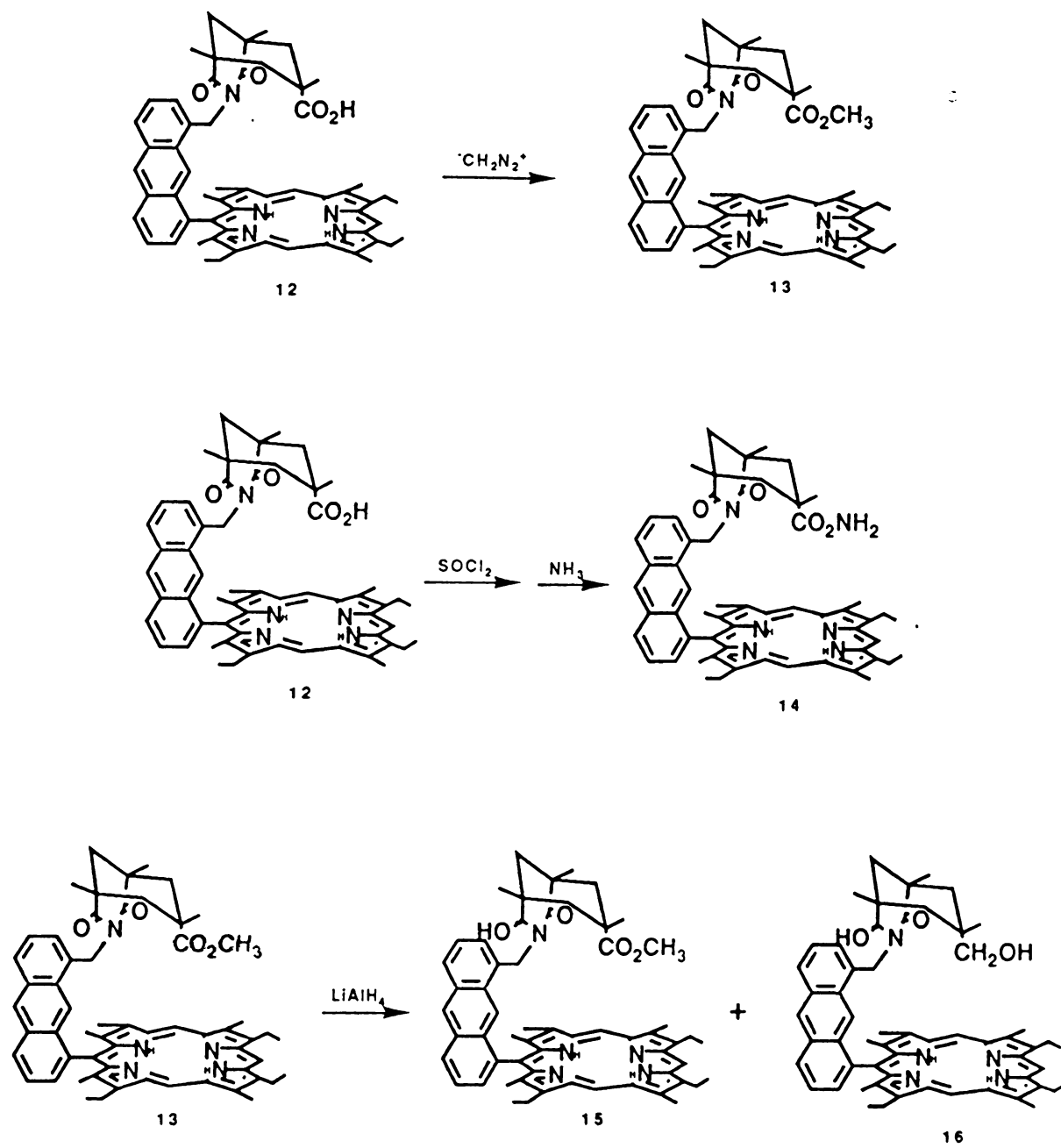
D. O_2 Binding to Co^{II} Kemp Isomer and Kemp Porphyrins

From the results obtained from O_2 binding to the Co^{II} Kemp porphyrin series (Table 3-1) we observed an O_2 affinity increase of 90 fold on going from the Co^{II} Kemp ester porphyrin (**13**) to the Kemp acid porphyrin (**12**). We also

Table 3-1. Results of O_2 Binding to Cobalt Porphyrins
(Solvent: DMF; Temp; (-42°C))

Porphyrin	$P_{1/2}$ (Torr)
Naphthalene Kemp isomer (6)	0.9 ± 0.09
Anthracene Kemp isomer (8)	8.0 ± 0.8
Anthracene Kemp acid (12)	2.4 ± 0.3
Anthracene Kemp alcohol (16)	34 ± 5
Anthracene Kemp ester (13)	214 ± 7
Naphthoic acid ³	0.028 ± 0.005





Scheme 7

observed that the O₂ affinity increased as the hydrogen-bonding ability of the model compound increased. O₂ affinity for the Co^{II} Kemp acid model (12) is 14 times better than the O₂ affinity for the Co^{II} Kemp alcohol (16). This is in agreement with the results obtained by Kondylis.² The naphthoic acid porphyrin still has a much larger O₂ affinity ($P_{1/2}=0.028$) than the anthracene Kemp acid porphyrin ($P_{1/2}=2.4$) at -42°C. This could be due to the >4Å distance between the Kemp acid and porphyrin ring so that the carboxylic proton may not achieve an optimal interaction with the terminal oxygen of the Co-O₂ complex in order to stabilize it.

In our O₂ binding to Co^{II} study we also found that the O₂ affinity for the Naphthalene Kemp isomer (6) is ~2.5 times better than O₂ affinity for the anthracene Kemp acid (12). This is very interesting since the carboxylic group of the anthracene Kemp acid is expected to be a better proton donor ($pK_a \sim 4.6$) than the imide of the naphthalene Kemp isomer ($pK_a \sim 9.6$). We suspect that the better O₂ binding ability observed for the naphthalene Kemp isomer (6) is because the imide proton in this model is positioned closer to the Co-O₂ center, thereby stabilizing it more than the anthracene Kemp acid porphyrin (Figure 3-2). If this is true, the O₂ affinity to Co^{II} naphthalene Kemp acid porphyrin (Scheme 2) should be even better. The preparation of the naphthalene Kemp acid porphyrin is being attempted by another member of our group. Once the O₂ binding of this model is done we will have a definite answer.

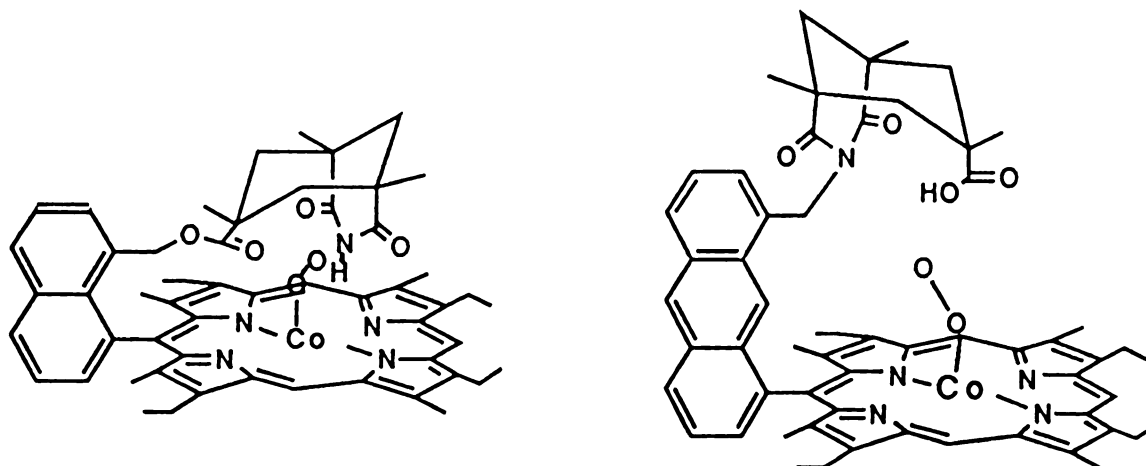


Figure 3-2. Co-O₂ complex of naphthalene Kemp isomer and anthracene Kemp acid porphyrins.

E. H-Bonding Effects on Heme Coordinated Cyanide

¹⁵N has an unusually large response in its NMR chemical shift due to its environment. Changes in protonation state, hydrogen bonding and metal ligation all produce large shifts. In the ¹⁵N NMR study of the dicyano Fe(III) protoporphyrin Goff¹ demonstrated that hydrogen bonding can cause an 82ppm upfield shift of the signal. Furthermore, as we have found (see Chapter 4), geometric distortions in the coordinated NC-Fe^{III} complex can also be monitored by the NMR shift. Therefore, ¹⁵N NMR of the dicyano Fe(III) anthroic acid, acrylic acid, naphthoic acid anthracene Kemp acid porphyrins should provide some indication of the proximity



and conformation of the proton to the nitrogen of the Fe-CN center.

The NMR of the models studied showed three peaks (except Fe^{III}OEP which has only two). All of them had a peak at -100 ppm which corresponded to the free cyanide, and the other two peaks arising from the two bound cyanide ligands (see Table 3-2). For the anthracene Kemp acid porphyrin the peaks appeared at 621.7 and 490.3 ppm. The peak at 490.3 ppm was assigned to the CN on the side where the Kemp acid substituent is (Top), and the peak at 621.7 ppm was assigned to the side where there was no substituent (bottom). In a similar way, for the ¹⁵N-NMR of the other models studied the peak that was most upfield was assigned to be near the polar substituents (Table 3-2). As can be seen in Table 3-2 these were the peaks that shifted the most when the substituents vary (in comparison with Fe^{III}OEP).

The results obtained showed that within the same series of models (anthracene Kemp acid and its ester; acrylic acid and its ester; naphthoic acid and its ester) the presence of a proton donor caused an upfield shift of the signal. This is in agreement with the results obtained by Goff¹ in which hydrogen bonding caused an 82 ppm upfield shift of the signal. This upfield shift of the signal is caused by the presence of hydrogen bonding which weakens the axial ligand field, reduces the magnetic anisotropy and σ -basicity towards the metal ion, decreasing the spin transfer from

Table 3-2. ^{15}N Chemical Shift for Fe^{III} Porphyrin Models

Porphyrin Complex*	^{15}N Chemical Shift (ppm)
OEP	720
Anthracene Kemp isomer (8)	641; 618.9
Naphthalene Kemp isomer (6)	669.2; 667.6
Anthracene Kemp acid (12)	621.7; 490.3
Anthracene Kemp ester (13)	630; 628.7
Anthracene acrylic acid (3)	708.5; 653
Anthracene acrylic ester (2)	685.1; 657.5
Naphthoic Acid	627.3; 551.8
Naphthalene methyl ester	644.8; 642.1
Anthroic acid	698.3; 669.6

* All of the Fe^{III} porphyrin models also show a peak at -100 ppm due to free C^{15}N^-

iron to cyanide¹² (in the next chapter the theory involved will be explained in more detail).

Table 3-2 and Figure 3-3 showed the largest upfield shift for the anthracene Kemp acid porphyrin (upfield shift of 230 ppm in comparison to Fe^{III}OEP). These results indicate that the proton on the anthracene Kemp acid porphyrin interacts more efficiently with the nitrogen of the Porph Fe^{III}(CN)₂⁻ complex than the protons of the other acid porphyrin models. Even though the distance between the Kemp acid and the porphyrin ring may not be ideal for the best O₂ ligand, the linear CN ligand apparently has a better appreciation of the over-hanging proton. From these results we expect that the proton of the anthracene Kemp acid porphyrin will also interact more efficiently with CO in carbonylhemes and, therefore, may show some influence on the Fe-CO formation constant.

Experimental

5-(8-(trans-2-Ethoxycarbonylethenyl)-1-anthryl)-2,8,13,17-tetraethyl-3,7,12,18-tetramethylporphine (2)

50 mg (0.07 mmol) of the anthracene formyl porphyrin² 1 were added to a solution consisting of 2.2 mL of pyridine and 2.2 mL of toluene. The solution was then heated to reflux (under argon). A mixture of 40 mg (0.30 mmol) of monoethyl ester malonic acid, 0.5 mL toluene, 2 drops of glacial acetic acid and 2 drops of piperidine were added. Solution was refluxed for 4 more hours (under argon). The

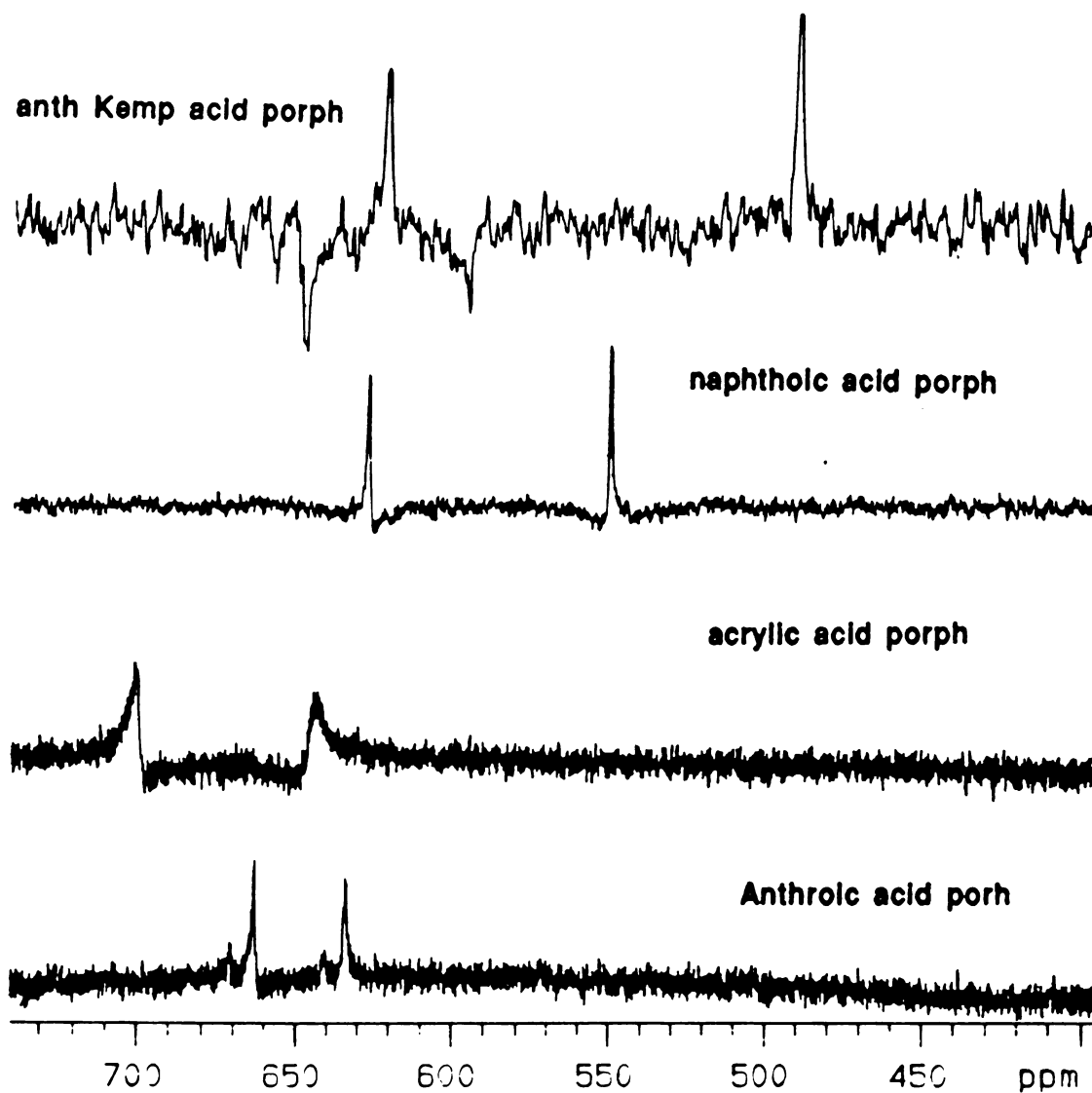


Figure 3-3. ^{15}N -NMR spectra of the dicyano Fe^{III} complex of anthroic acid, acrylic acid, naphthoic acid and anthracene Kemp acid porphyrins.



mixture was then rotoevaporated to dryness. Purification (silica-gel/ CH_2Cl_2) and recrystallization (CH_2Cl_2 / CH_3OH) gave 98% of the anthracene acrylic ester porphyrin (2). NMR, δ -3.09(2H, d, NH), - 1.21(3H, t, Et), 1.70(6H, t, Et), 1.88(6H, t, Et), 2.08(6H, s, Me), 2.38(2H, q, Et), 3.64(6H, s, Me), 3.92(4H, q, Et), 4.09(4H, q, Et), 5.58(1H, d, Acr., J=16 Hz), 6.94(1H, d, Acr., J=16 Hz), 9.97(1H, s, meso), 10.17(1H, s, meso), anthryl: 7.35(1H, s), 7.37(1H, d), 7.92(1H, dd), 8.08-8.16(3H, m), 8.48(1H, d), 8.75(1H, s). MS (FAB): 753(M+1, 40). UV-Vis, λ_{max} nm (rel. rat.): 625.0(1.0), 570.5(10.3), 536.5(10.8), 501.0(15.2), 406.0(95).

5-(8(trans-2-Hydroxycarbonylethenyl)-1-anthryl)-2,8,13,17-tetraethyl-3,7,12,18-tetramethylporphine (3)

10 mg (0.01 mmol) of the anthracene acrylic ester porphyrin (2) was added to 10 mL of a 30% KOH/Ethanol solution and stirred overnight under argon. After this period of time 10 mL of water was added, the solution was cooled using ice-bath and neutralized by adding (dropwise) conc. HCl. The ethanol was evaporated and the purple solid filtered and washed with plenty of water. Recrystallization from CH_2Cl_2 /Hexane gave 99% of the anthracene acrylic acid porphyrin (3). NMR δ 1.54(6H, t, Et), 1.79(6H, t, Et), 2.05(6H, s, Me), 3.44(6H, s, Me), 3.79(4H, q, Et), 3.97(4H, q, Et), 5.42(1H, d, Acrylic, J=16 Hz), 7.02(1H, d, Acrylic, J=16 Hz), 9.88(1H, s, meso), 10.01(1H, s, meso), anthryl:



7.28(1H, d), 7.37(1H, t), 7.88(1H, dd), 8.05(1H, d),
8.12(1H, d), 8.27(1H, s), 8.47(1H, d), 8.77(1H, s). MS
(FAB): 725 (M+1, 70). UV-Vis, λ_{\max} nm (rel. rat.): 624.0(1),
570.5(1.7), 537.0(1.7), 504.0(3.0), 412.5(10.8).

Naphthalene Kemp acid isomer porphyrin (6)

The naphthalene alcohol porphyrin (4) was prepared according to previous procedure.³ The cis, cis-Kemp imide acid was prepared according to previous procedure.⁵ The potassium Kemp imide carboxylate salt was prepared by adding 1.4 g of the Kemp imide acid (5.8 mmole) to 130 mL of absolute ethanol. The solution was brought to boil. When almost all of the Kemp imide had dissolved a solution of 0.82 g (14 mmol) KOH in 20 mL of absolute ethanol was added and refluxed continuously for 15 minutes. The solution was cooled and the salt (white solid) filtered, washed with 3mL absolute ethanol and dried under vacuum (60°C) for 3 hours.

15 mg (0.024 mmol) of the naphthalene alcohol porphyrin was placed in a 50 mL round bottom flask (flame dried) under argon. A sufficient amount of mesityl chloride to dissolve all of the alcohol porphyrin (~ 3mL) was added. The solution was stirred under argon for 14 hours. After this period of time the excess mesityl chloride was evaporated (without heating) to almost dryness using a vacuum pump. The temperature was then brought to 60°C under vacuum until the residue was completely dry (5 hours). 30 mg (0.091 mmol) of the Kemp imide potassium salt and 20 mL of dry

toluene (distilled from LiAlH_4) was added. The solution was refluxed (125-130°C) while stirring under argon for 12 hours. The excess potassium salt was removed by filtration. The toluene was removed by rotoevaporation, the porphyrin dissolved in fresh CH_2Cl_2 and purified by tlc plates (silica-gel, 1% $\text{CH}_3\text{OH}/\text{CH}_2\text{Cl}_2$). Recrystallization from $\text{CH}_2\text{Cl}_2/\text{CH}_3\text{OH}$ gave 14% of the naphthalene Kemp isomer porphyrin (6). NMR, δ porphyrin: -3.06(2H, d, NH), 1.71(6H, t, Et), 1.86(6H, t, Et), 2.12(6H, s, Me), 3.61(6H, s, Me), 3.86(2H, q, Et), 4.04(6H, m, Et), 9.91(1H, s, meso), 10.11(2H, s meso); naphthyl: 3.96(2H, s, CH_2), 7.42(1H, d), 7.64(1H, t), 7.71(1H, t), 7.83(1H, d), 8.21(1H, d), 8.31(1H, d); chair: -0.60(3H, s Me), 0.31(1H, d), 0.64(6H, s, Me), 0.78(1H, d), 1.40(1H, d), 1.63(2H, d), 6.36(1H, NH). MS (FAB): 856(M+1, 100). UV-Vis λ_{max} nm (rel. rat.): 626.5(1.0), 573.5(8.3), 539.0(10.2), 504.0(15.5), 408.5(219.7).

Anthracene Kemp acid isomer porphyrin (8)

The anthracene alcohol porphyrin (7) was prepared as described.² The anthracene Kemp isomer porphyrin (8) was prepared following the same procedures as for the naphthalene Kemp isomer (6). Purification by tlc plate (silica-gel, 1% $\text{CH}_3\text{OH}/\text{CH}_2\text{Cl}_2$) and recrystallization from $\text{CH}_2\text{Cl}_2/\text{CH}_3\text{OH}$ gave 56% yield of the anthracene Kemp isomer. NMR δ porphyrin ring: -3.12(2H, d, NH), 1.68(6H, t, Et), 1.87(6H, t, Et), 2.08(6H, s, Me), 3.64(6H, s, Me), 3.82(2H,

m, Et), 3.99(2H, m, Et), 4.08(4H, q, Et), 9.96(1H, s, meso), 10.15(2H, s, meso); anthryl: 4.38(2H, s, CH₂), 7.17(1H, d), 7.34(1H, dd), 7.86(1H, dd), 8.03-8.10(3H, m), 8.48(1H, d), 8.77(1H, s); chair: -1.28(3H, s, Me), -0.34(2H, d), 0.19(6H, s, Me), 0.50(1H, d), 0.97(2H, d), 1.22(1H, d), 6.55(1H, s, NH). MS(FAB): 906(M+1, 100), UV-Vis $\lambda_{\text{max}}^{\text{nm}}$ (rel. rat.): 624.0(1.0), 569.5(1.5), 534.5(1.6), 502.0(2.4), 406.5(19.6).

5-(8-(Azidomethyl)-1-anthryl)-2,8,13,17-tetraethyl-3,7,12,18-tetramethylporphine (9)

The anthracene alcohol porphyrin was prepared following Abdalmuhdi's procedure.² To 95 mg (0.14 mmol) of the anthracene alcohol porphyrin (7) under argon was added enough mesityl chloride to dissolve the porphyrin (~10 mL). The solution was stirred under argon for 14 hours. The excess of mesityl chloride was evaporated using a vacuum pump (room temperature until almost dry, then 60°C for 5 hours). 35 mL of acetone (reagent grade) was added followed by 100 mg (1.5 mmol) NaN₃ in 5mL H₂O. The solution was refluxed for 5 hours under argon. After which, water, CH₂Cl₂ and a drop of HCl were added and the solution stirred for a few minutes. The solvent was evaporated, fresh CH₂Cl₂ added and extracted with sat. NaHCO₃, water and dried over sodium sulfate. Purification from short column chromatography (silica-gel, CH₂Cl₂) and recrystallization (CH₂Cl₂/CH₃OH) gave 77% of the anthracene azido porphyrin.



NMR δ porphyrin: -3.08(2H, d, NH), 1.65(6H, t, Et), 1.87(6H, t, Et), 2.06(6H, s, Me), 3.65(6H, s, Me), 3.91(4H, m, Et), 4.09(4H, q, Et), 10.00(1H, s, meso), 10.18(2H, s, meso); anthryl: 3.56(2H, s, CH₂), 7.15(1H, d), 7.35(1H, dd), 7.89(1H, dd), 7.94(1H, s), 8.09-8.11(2H, m), 8.49(1H, d), 8.78(1H, s). MS(FAB): 709(M, 65%). UV-Vis λ_{\max}^{nm} (rel. rat.): 622.0(1.0), 571.0(1.7), 535.5(1.8), 503.5(3.1), 409.5(16.8). IR shows strong absorption band at 2096 cm⁻¹ characteristic of azido group stretch.

5-(8-(Aminomethyl)-1-anthryl)-2,8,13,17-tetraethyl-3,7,12,18-tetramethylporphine (10)

50 mg (0.07 mmol) of the anthracene azide porphyrin (9) was dissolved in 20 mL of dry THF (freshly distilled from CaH₂) under argon. The solution was cooled (ice-bath) and 40 mg of LiAlH₄ was slowly added. The mixture was stirred at room temperature under argon for 3 hours. Afterwards 0.5 mL of 0.1N HCl was added dropwise to decompose the excess LiAlH₄. The THF was evaporated, CH₂Cl₂ was added (~20 mL) and the mixture was extracted with H₂O, sat. NaHCO₃, H₂O, and dried over sodium sulfate. The compound was purified from tlc plates (silica-gel, 5% CH₃OH/CH₂Cl₂) and recrystallized from CH₂Cl₂/Hexane to give 73% of the anthracene amino porphyrin. NMR δ porphyrin: -3.18(2H, d, NH), 1.68(6H, t, Et), 1.92(6H, t, Et), 2.11(6H, s, Me), 3.68(6H, s, Me), 3.93-3.97(4H, m, Et), 4.13(4H, q, Et), 10.07(1H, s, meso), 10.23(2H, s, meso); anthryl: 3.00(2H, s, CH₂), 7.14(1H, d),



7.34(1H, dd), 7.89-8.01(3H, m), 8.10(1H, dd), 8.52(1H, d), 8.79(1H, s). MS(FAB): 684(M+1), 668(-NH₂). UV-Vis $\lambda_{\max, nm}$ (rel. rat.): 622.0(1.0), 570.5(1.5), 535.5(1.6), 503.5(2.5), 407.5(19.5).

5-(8-Kemp acid-1-anthryl)-2,8,13,17-tetraethyl-3,7,12,18-tetramethylporphine (12)

The imide acid chloride (11) was prepared as reported previously.⁵ 62.8 mg (0.09 mmol) of the anthracene amine porphyrin was added to 5mL of dry toluene (freshly distilled from LiAlH₄) and stirred under argon. To this mixture a catalytic amount of DMAP, 46 mg of 2,6-di-*t*-butylpyridine and 28 mg (1.0 mmol) of the imide acid chloride was added. The mixture was refluxed under argon for 19 hours (at 125°C). The solvent was then evaporated and fresh CH₂Cl₂ added. Purification from tlc plates (silica-gel, 1% CH₃OH/CH₂Cl₂) and recrystallization from CH₂Cl₂/CH₃OH gave 75% of the anthracene Kemp acid porphyrin (12). NMR δ porphyrin: 1.72(6H, t, Et), 1.93(6H, t, Et), 2.17(6H, s, Me), 3.69(6H, t, Me), 3.88-3.92(2H, m, Et), 4.09-4.13(6H, m, Et), 10.11(1H, s, meso), 10.31(2H, s, meso); anthryl: 4.14(2H, s, CH₂), 6.37(1H, d), 7.26(1H, dd), 7.86(1H, s), 7.95-8.01(2H, m), 8.13(1H, d), 8.56(1H, d), 8.81(1H, s); chair: 0.37(3H, s), 0.62(2H, d), 0.89(6H, s), 1.08(1H, d), 1.71-1.74(1H, hidden by porphyrin triplet), 1.79(2H, d). MS(FAB) 906(M+1, 100%), 878(-H₂O), 862(-CO₂). UV-vis $\lambda_{\max, nm}$



(rel. rat.): 619.5(1.0), 567.5(1.8), 539.0(1.8),
505.0(2.9), 407.5(22.9).

5, (8-Kemp methylester-1-anthryl)-2,8,13,17-tetraethyl-
3,7,12,18-tetramethylporphine (13)

8 mg (0.0088 mmole) of the anthracene Kemp acid porphyrin was dissolved in 10 mL of dry THF. To this solution 20 mL of freshly prepared diazomethane in ether was added and solution stirred under argon at room temperature for 1/2 hour. After this period of time 1mL of 5% HCl was added. The solvent was then evaporated and the compound dissolved in CH_2Cl_2 , extracted with water, sat. solu. NaHCO_3 , water and dried over sodium sulfate. Recrystallization from $\text{CH}_2\text{Cl}_2/\text{CH}_3\text{OH}$ gave the anthracene Kemp ester porphyrin (13) in 99% yield. NMR δ porphyrin: -3.2(2H, d, NH), 1.73(6H, t, Et), 1.92(6H, t, Et), 2.14(6H, s, Me), 3.69(6H, s, Me), 3.90-4.15(8H, m, Et), 10.04(1H, s, meso), 10.24(2H, s, meso); anthryl: 3.58(2H, s, $-\text{CH}_2$) 6.34(1H, d), 7.24(1H, dd), 7.77(1H, s), 7.93-7.99(2H, m), 8.17(1H, d), 8.54(1H, d), 8.79(1H, s); chair: -1.04(3H, s, OCH_3), 0.32(3H, s, CH_3), 0.58(2H, d), 0.85(6H, s, Me), 1.01(1H, d), 1.65(1H, d), 1.90-1.94(2H, hidden by porphyrin triplet). MS(FAB): 920(M+1, 100%), 905($-\text{CH}_3$). UV-Vis $\lambda_{\text{max}} \text{nm}$ (rel. rat.): 623.5(1.0), 570.0(1.7), 535.5(1.9), 502.0(3.4), 405.5(30.3).

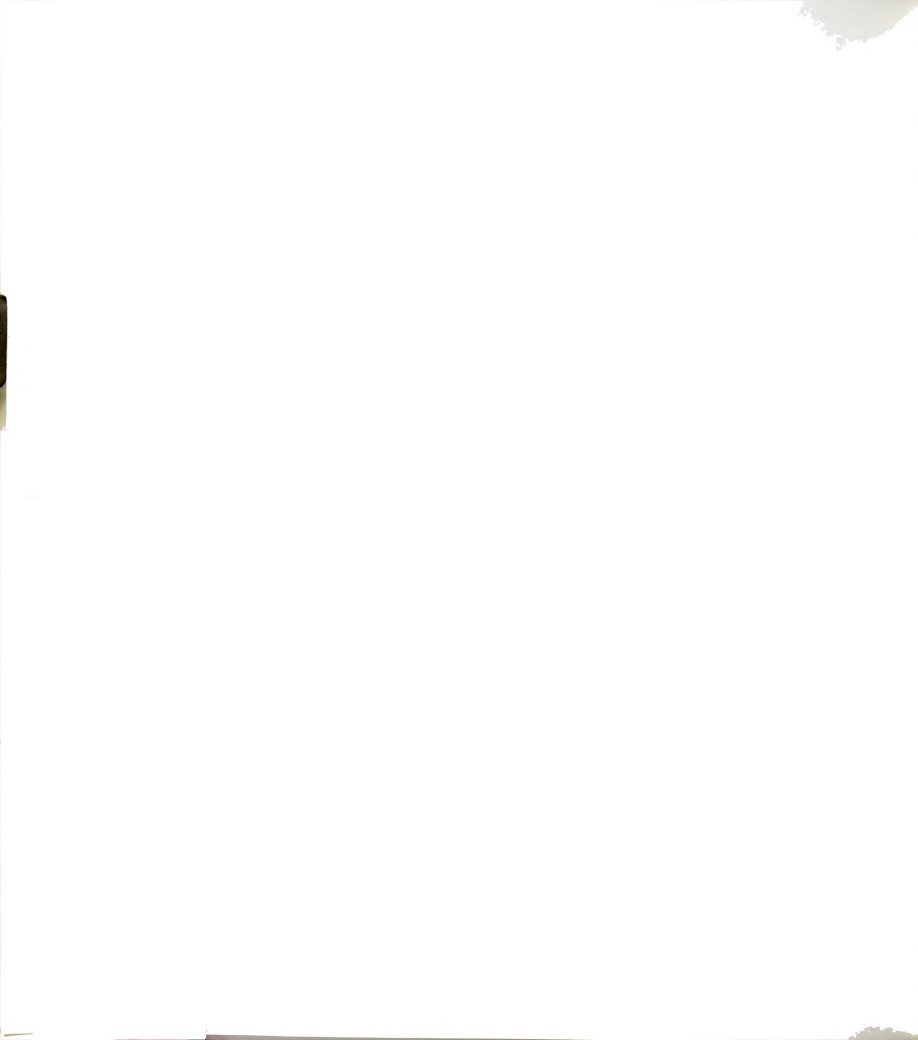


5-(8-Kemp amide-1-anthryl)-2,8,13,17-tetraethyl-3,7,12,18-tetramethylporphine (14)

All glassware was flame dried. To 10mg (0.01 mmol) of the anthracene Kemp acid porphyrin (12) 1.5 mL of freshly distilled thionyl chloride was added and the solution stirred under argon for 14 hours. The excess thionyl chloride was evaporated at room temperature using vacuum pump. The compound was left under argon for 8 more hours to ascertain that thionyl chloride was completely removed. Then 30mL of dry THF (freshly distilled from CaH₂) was added and NH₃ bubbled in for 15 min. The solution was stirred under argon overnight and purified from tlc plates (silica-gel, 1% CH₃OH/CH₃OH) to give 77% yield of the anthracene Kemp amide porphyrin (14). NMR δ porphyrin: -3.41(2H, d, NH), 1.74(6H, t, Et), 1.89(6H, t, Et), 2.21(6H, s, Me), 3.69(6H, s, Me), 3.81-3.92(2H, m, Et), 4.04-4.2(6H, m, Et), 10.08(1H, s, meso), 10.30(2H, s, meso); anthryl: 3.00(2H, s, CH₂), 6.91(1H, d), 7.31(1H, dd), 7.49(1H, s), 8.16(1H, dd), 8.39(1H, d), 8.64(1H, dd), 8.99(1H, d); chair: -1.41(2H, d, NH₂), -0.73 (3H, s, Me), 0.03(2H, d), 0.58(6H, s, Me), 0.61(1H, d), 1.13(1H, d), 1.25(2H, d). MS(FAB): 905(M+1, 100%). UV-Vis λ_{\max} nm (rel. rat.): 621.0(1.0), 568.5(1.8), 538.5(1.9), 505.0(3.0), 407.5(28.2).

5-(8-Kemp diol-1-anthryl)-2,8,13,17-tetraethyl-3,7,12,18-tetramethylporphine (15)

10 mg (0.01 mmol) of the anthracene Kemp ester porphyrin



(13) was added to a solution of 15 mg LiAlH_4 in 4 mL of dry THF (freshly distilled from CaH_2). The solution was stirred at room temperature under argon for 10 minutes. At this time tlc (silica-gel, 1% $\text{CH}_3\text{OH}/\text{CH}_2\text{Cl}_2$) showed that all the Kemp ester (13) had reacted. Then the solution was neutralized by adding 0.3mL (dropwise) of 0.1 N HCl. The solvent was then evaporated, CH_2Cl_2 was added and the solution extracted with water, sat soln. NaHCO_3 , water and dried over sodium sulfate. Purification from preparative plates gave the Kemp diol porphyrin (15) and Kemp hydroxylester (16). The Kemp hydroxylester (16) was only analyzed by mass spectra (MS(FAB)): 922(M+1, 100). The Kemp diol porphyrin (15) was analyzed by NMR and mass spectra. NMR δ porphyrin: -3.20(2H, broad, NH), 1.63(6H, t, Et), 1.86(6H, t, Et), 2.10(6H, s, Me), 3.61(3H, s, Me), 3.66(3H, s, Me), 9.98(1H, s, meso), 10.14(1H, s, meso), 10.18(1H, s, meso); anthryl: 3.42(2H, s, CH_2), 6.98(1H, d), 7.30(1H, d), 7.76(1H, s), 7.90-7.97(2H, m), 8.21(1H, d), 8.46(1H, d), 8.70(1H, s); chair: 0.45(2H, s CH_2OH), 0.12(3H, s, Me), 0.20(6H, s, Me), 0.37(2H, d), 0.91(1H, d), 1.50(1H, d), 1.93(2H, d), 4.23(1H, d). MS(FAB): 894(M+1, 55%).

Cobalt Insertion

Cobalt ion was incorporated into the porphyrin following the cobaltous chloride method.⁶ 5 mg of the porphyrin was dissolved in 10mL of CH_2Cl_2 and the solution deaerated by



bubbling argon for 15 min. Then a solution of excess $\text{CoCl}_2(\text{H}_2\text{O})_6$ (6mg, 3x) and anhydrous sodium acetate (a pinch) in 5 mL of anhydrous methanol was added. The solution was then heated over a steam bath while argon was continuously bubbled until all the solvent was evaporated. Fresh CH_2Cl_2 was added and the excess CoCl_2 removed by extraction with water.

Iron Insertion

Insertion of the iron was accomplished by using the ferrous sulfate method.⁷ 5 mg of the porphyrin was placed in a pear-shaped flash equipped with a gas inlet tube, dissolved in pyridine (1.5mL), and diluted with glacial acetic acid (30mL). A stream of argon was passed into the solution from the center tube while the mixture was placed in an oil bath preheated to 80°C. A saturated aqueous solution of iron(II) sulfate was syringed into the mixture, through the gas-outlet side arm. The temperature was raised to 90°C and the reaction kept at this temperature for 30 minutes. The flask was then removed from the heating bath, the argon bubbling stopped, and the mixture cooled to room temperature. A stream of air was passed through briefly to allow the autoxidation of the unstable iron(II) porphyrin. The solution was then diluted with water and extracted with CH_2Cl_2 . The organic phase was extracted once more with water. The iron(III) porphyrin was purified by a short



silica-gel column using 1-5% MeOH/CH₂Cl₂ as elutant (a pasteur pipet was used as the column) depending on the porphyrin. The iron(III) μ -oxo dimer porphyrin obtained from the column was washed with 0.1N HCl saturate NaCl solution to give the [Fe(III)Por]⁺Cl⁻.

Dioxygen binding to Co(II) porphyrins

The Co(III) porphyrins were dissolved in distilled DMF (approximately 4mL, 1×10^{-5} M). The solutions were degassed in a 60mL tonometer by freeze-pump-thaw cycles at 10^{-5} Torr. To this solution a drop of dilute sodium dithionite in H₂O (2mg/mL) was added to reduce the Co(III) to Co(II). Oxygenation was monitored spectrophotometrically at -42°C. The low temperature was achieved by immersing the tonometer in a dewar filled with liquid propane (b.p.: -42°C). The O₂ affinities were determined by direct titration of CoP with pure O₂, using a standard spectrophotometric procedure used by Halpern and coworkers¹³ (Figure 3-3). The solubility of O₂ in DMF at low temperatures is not known and all the equilibrium constants are calculated at the standard state of 1 Torr. The titration curves typically had correlation coefficients of 0.990 to 0.997 and varied between experiments by less than 15%. The equilibrium constants given in Table 3-1 are the average value of 2-3 runs (Table 3-1).



^{15}N NMR of Dicyano Iron (III) Porphyrin Models

Solutions for ^{15}N spectroscopy were accomplished by dissolving the desired high-spin ferric complexes in 0.60 mL of deuterated DMSO (3-5 mM porphyrin solutions). A 10 fold excess of KC^{15}N powder (98% N-15, Icon Inc.) was dissolved in the porphyrin/DMSO solution to produce a distinctive color change. Measurements were made on a Varian VXR 500 spectrometer. ^{15}N spectra were typically obtained in sweepwidths of 100 KHz at 50.6 MHz with pulse repetitions of 0.12s. A 200 μs delay prior to acquisition serve to diminish acoustic probe ringing. Spectra of heme contained in an 8-mm tube required 30,000 to 60,000 scans. Chemical shift values are referenced to external nitrate ion (aqueous ammonium nitrate) and downfield chemical shift were giving positive sign.



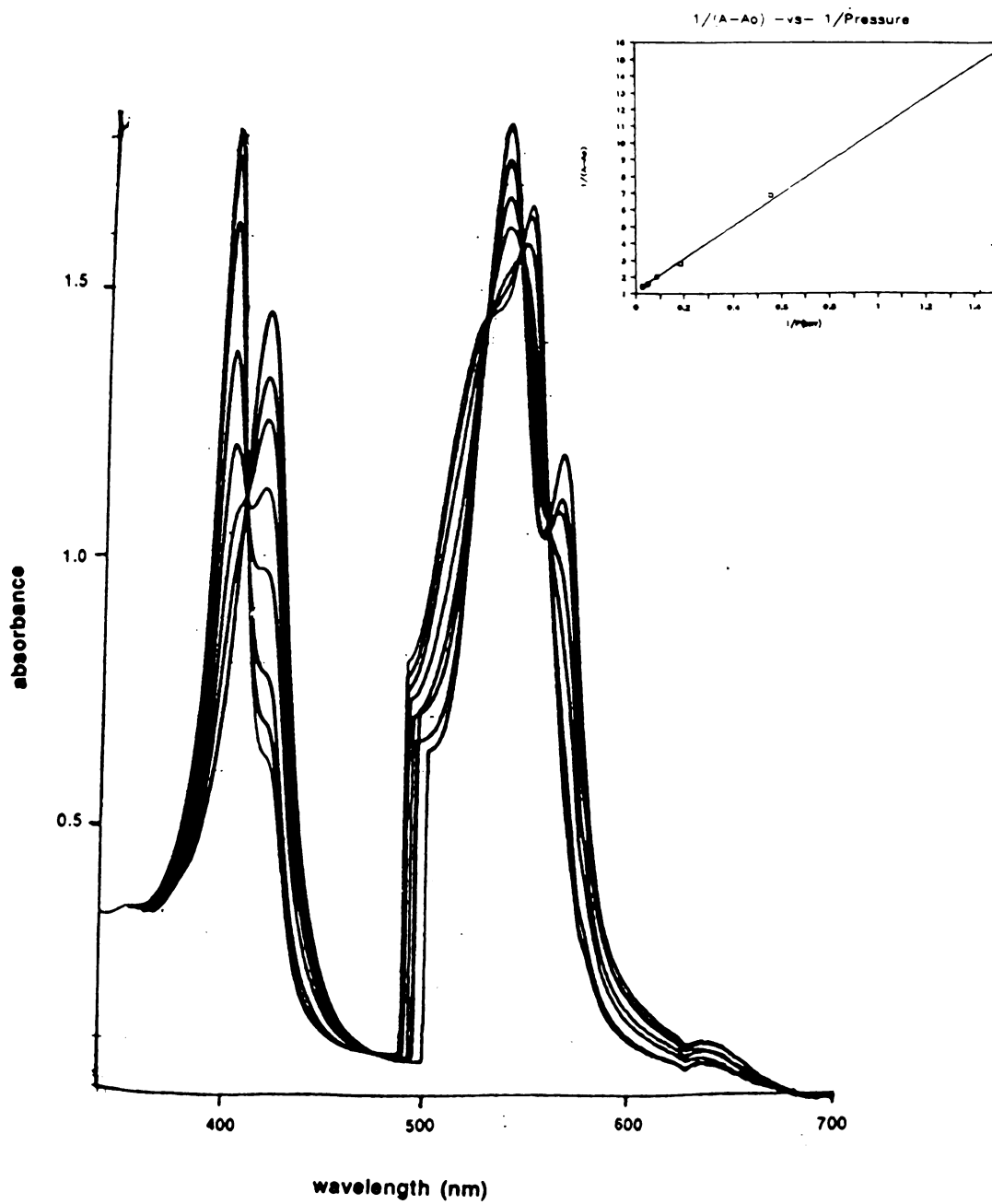
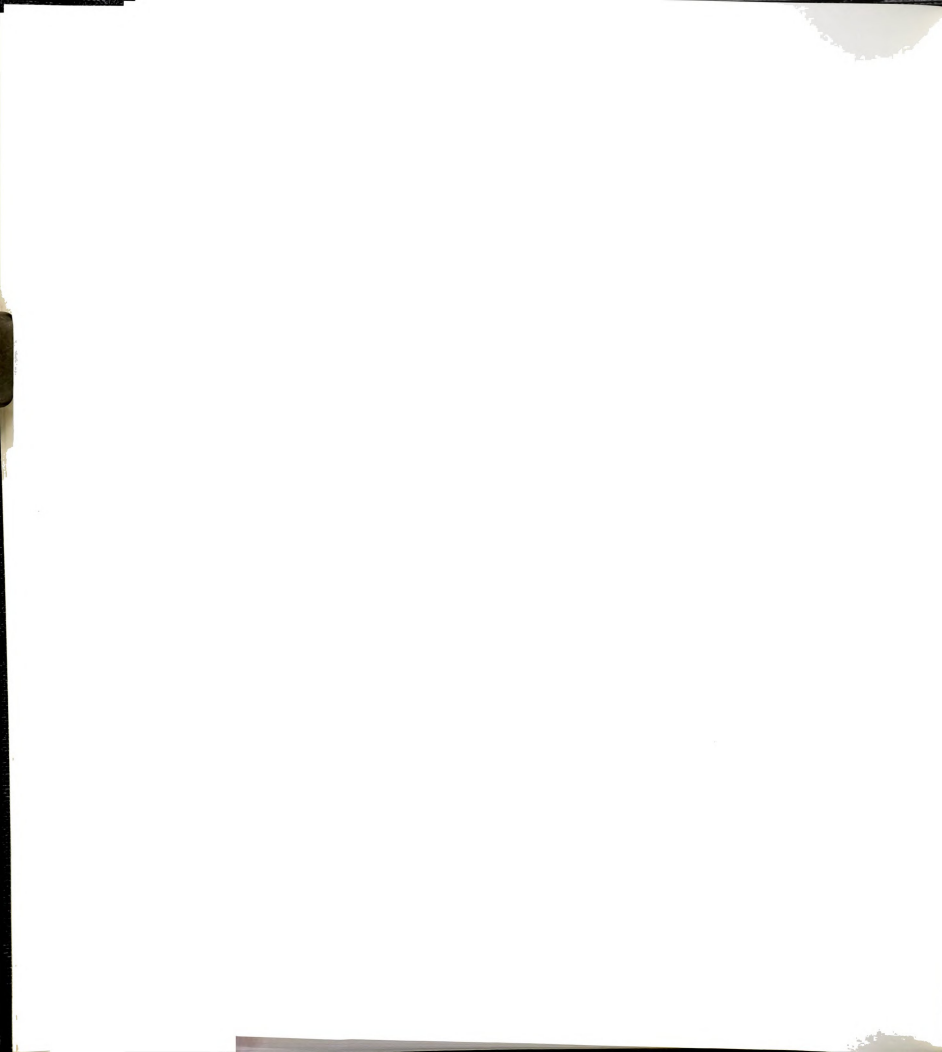


Figure 3-4. Spectrophotometric titration of Co anthracene Kemp isomer porphyrin.



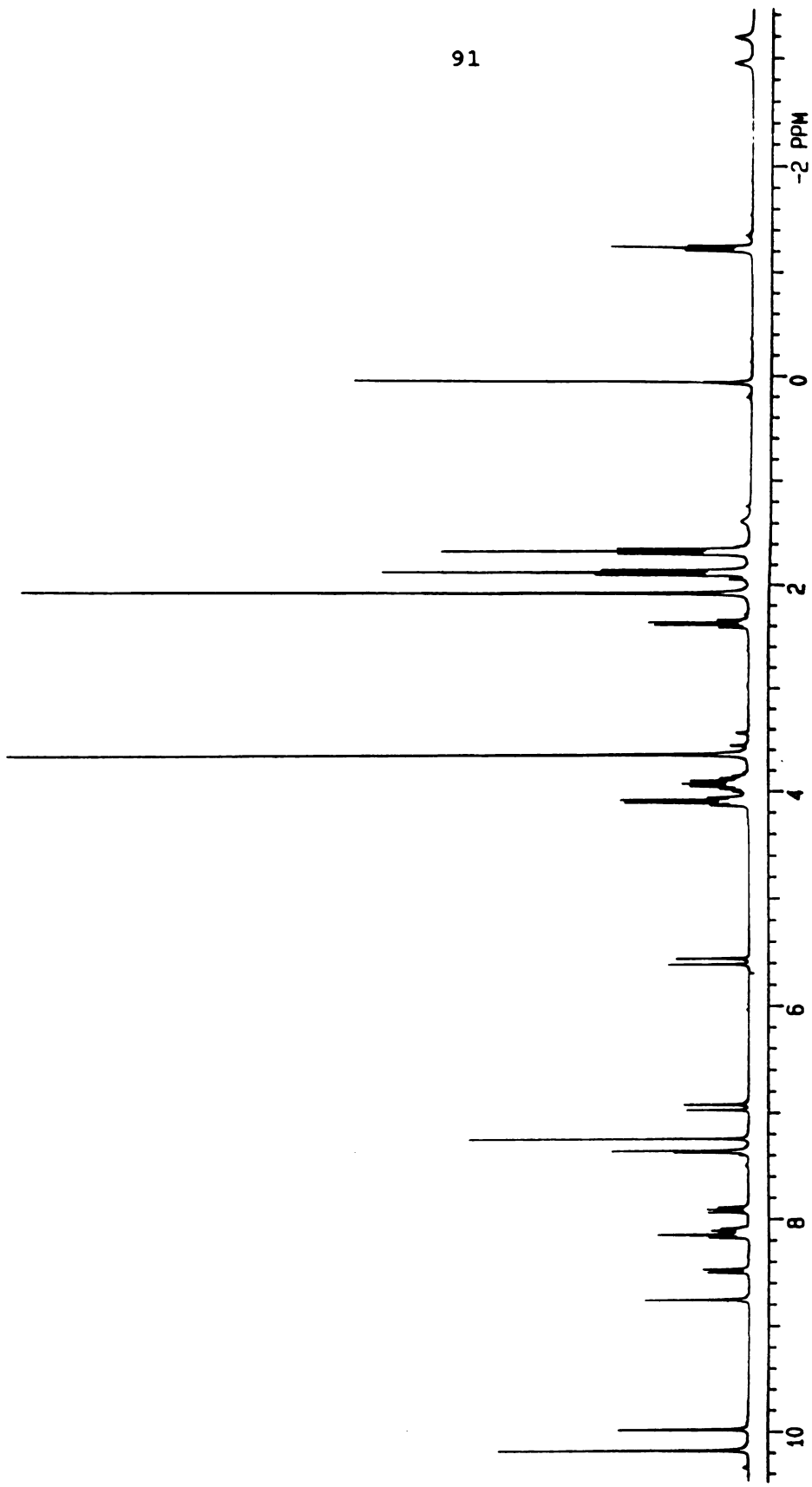
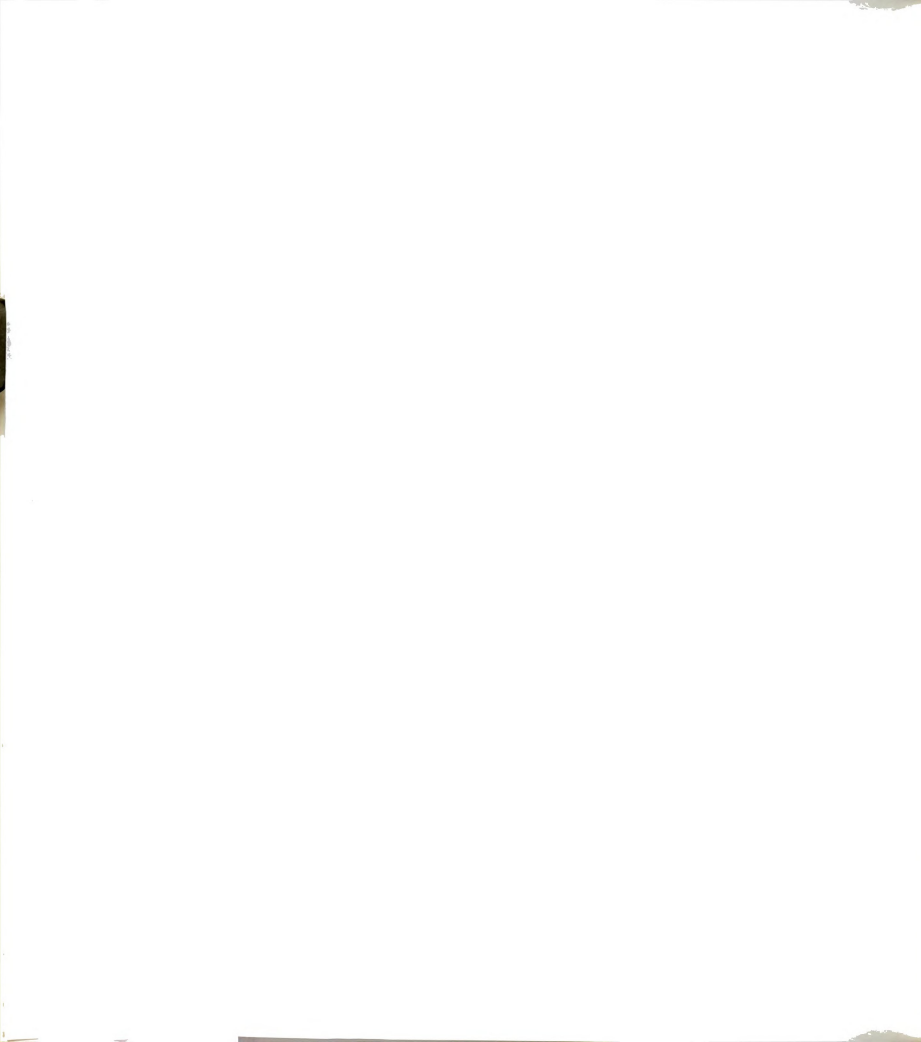


Figure 3-5. ¹H-NMR spectrum of anthracene acrylic ester porphyrin (2)



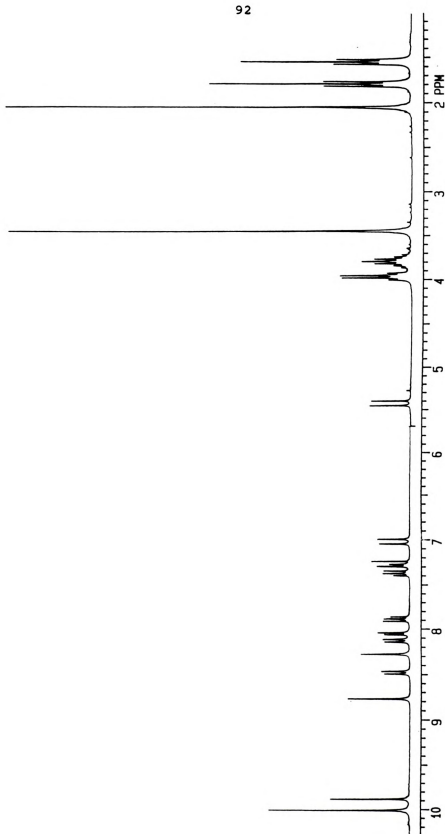


Figure 3-6. ¹H-NMR spectrum of anthracene acrylic acid porphyrin (3)

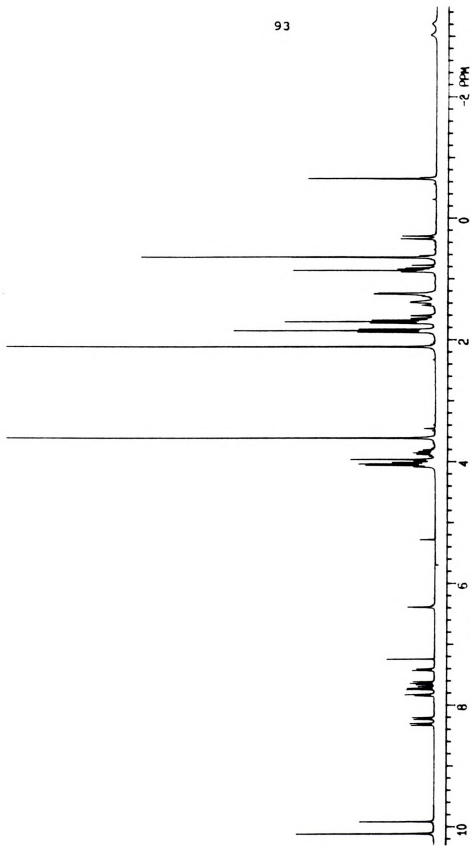


Figure 3-7. $^1\text{H-NMR}$ spectrum of naphthalene Kemp isomer porphyrin (6)



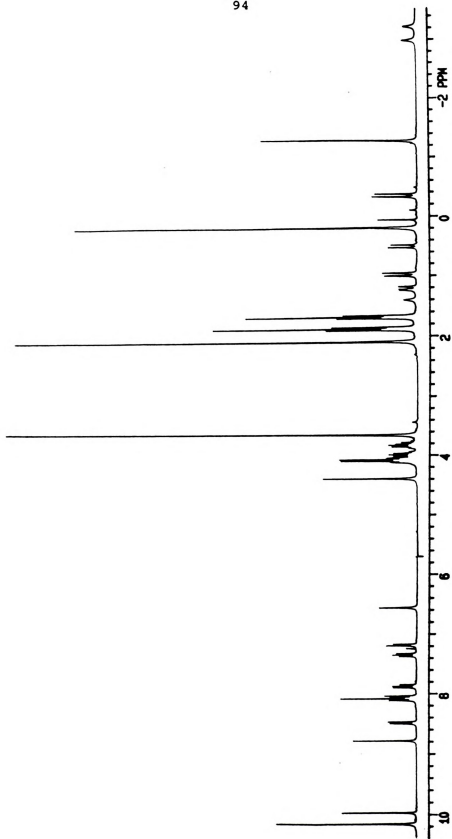


Figure 3-8. $^1\text{H-NMR}$ spectrum of anthracene Kemp isomer porphyrin (8)



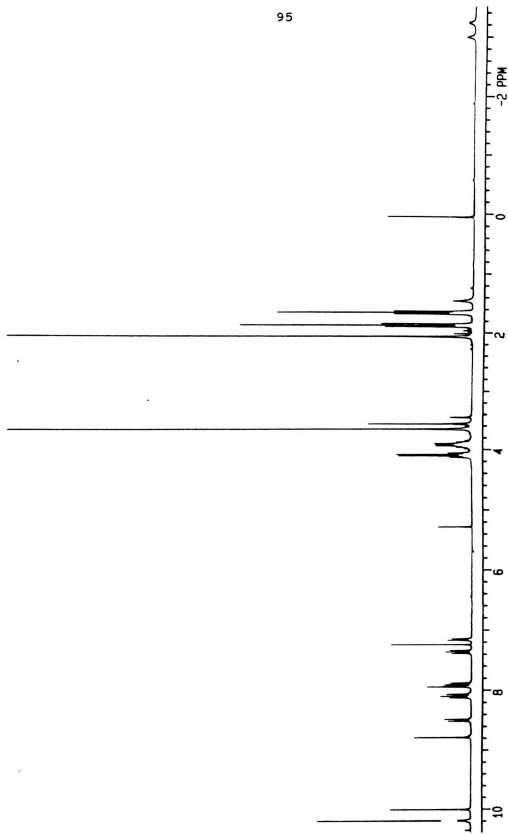
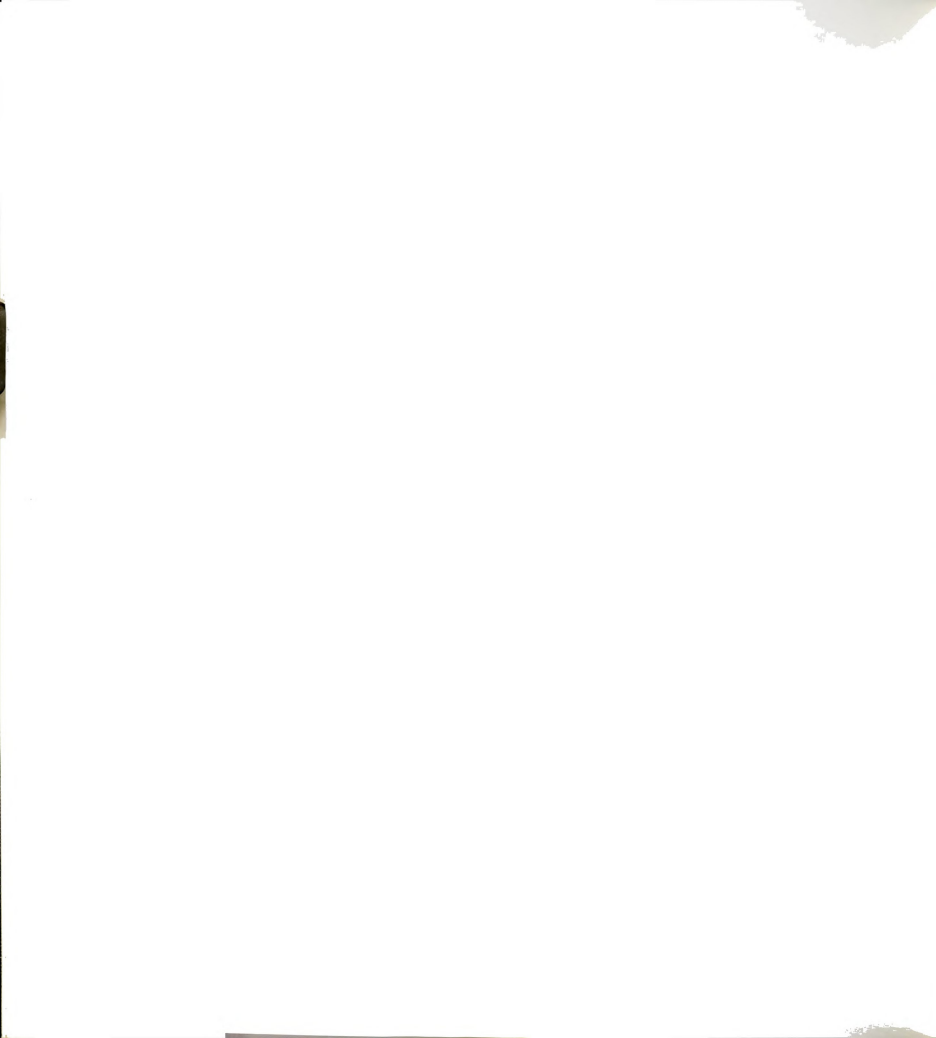


Figure 3-9. $^1\text{H-NMR}$ spectrum of anthracene azido porphyrin (9)



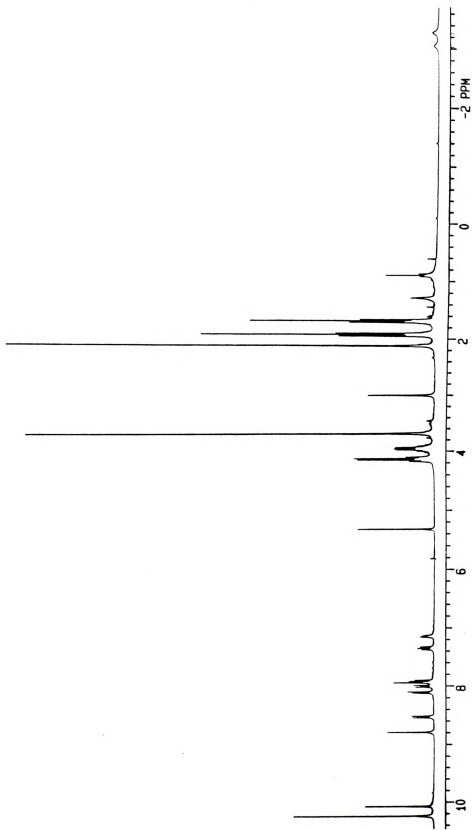


Figure 3-10. $^1\text{H-NMR}$ spectrum of anthracene amino porphyrin (10)



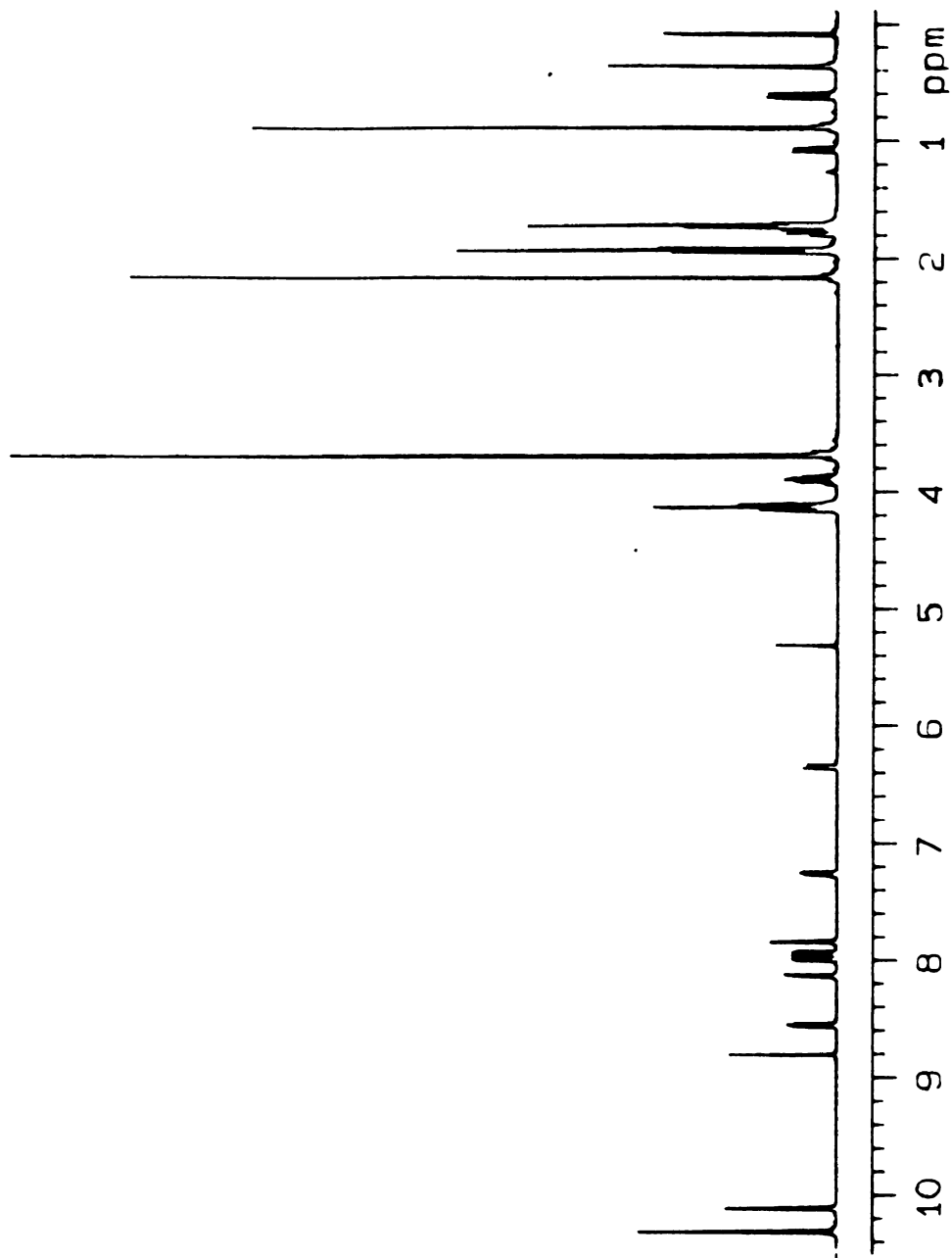


Figure 3-11. $^1\text{H-NMR}$ spectrum of anthracene Kemp acid porphyrin (12)



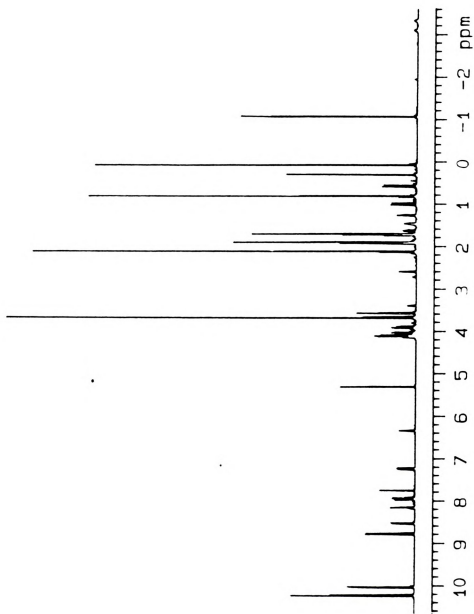
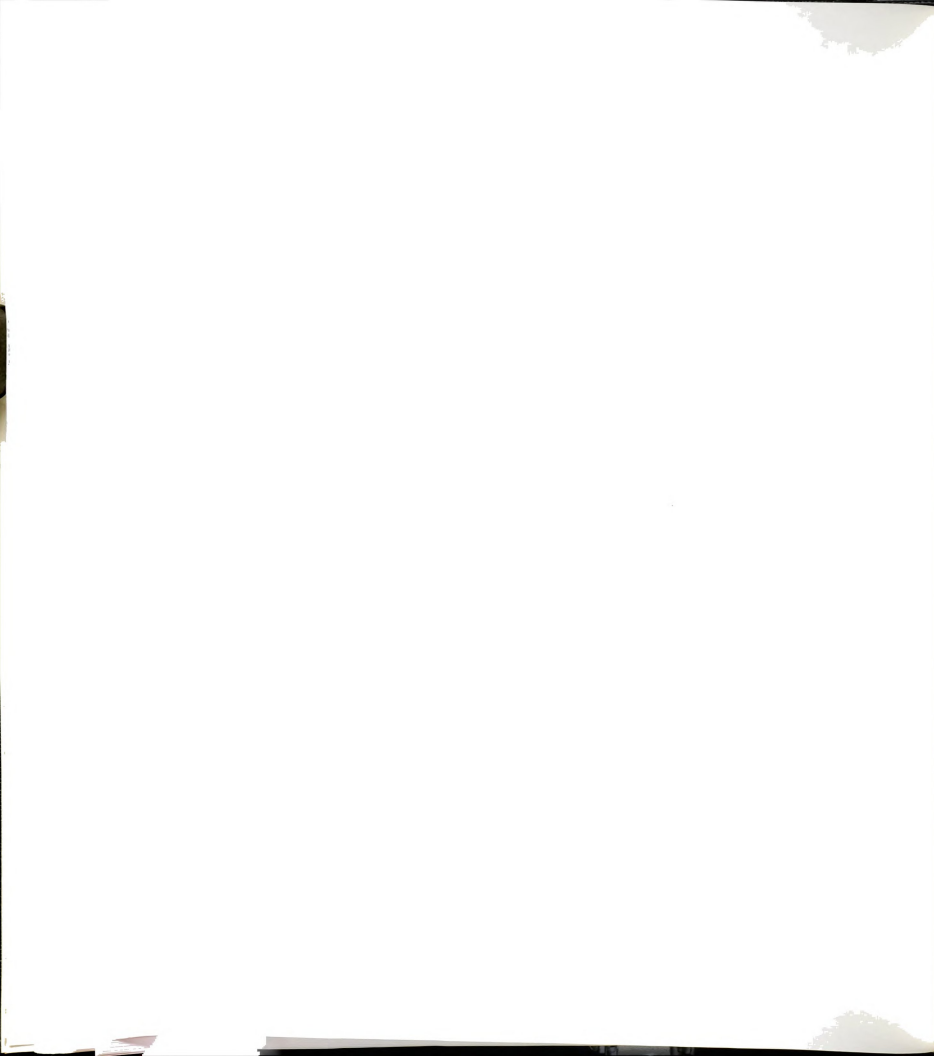


Figure 3-12. $^1\text{H-NMR}$ spectrum of anthracene Kemp ester porphyrin (13)



LIST OF REFERENCES

1. Behere, D.V.; Gonzalez-Vergara, E.; Goff, H.M. Biochim. Biophys. Acta (1985) **871**, 285-292.
2. Abdalmuhdi, I., "Pillard Cofacial Porphyrins: Synthesis, Structure and Application", 1985, Dissertation.
3. Kondylis, M., "Distal Steric and Hydrogen Bonding Effects in Heme-Dioxygen Interactions", 1985, 127 pages, Dissertation.
4. CO references
5. a. Askew, B; et. al. J. Am. Chem. Soc. (1989), **111**, 1082-1090.
b. Rebeck, J.; et. al. J. Am. Chem. Soc. (1985), **107**, 7476-7481.
6. Porphyrins and Metalloporphyrins, Ed. Kevin M. Smith, Elsevier Scientific Publishing Co., N.Y. (1975), p. 179-181.
7. Chang, C.K.; DiNello, R.K.; Dolphin, D. Inorg. Chem. (1980), **20**, 147.
8. a. Tadayoni, B.M.; Parris, R.J. J. Am. Chem. Soc. (1989), **111**, 4503-4505.
b. Rebeck, J.; et. al. J. Am. Chem. Soc. (1985), **107**, 7476-7481.
9. Ballester, P.; Tadayoni, B.M.; Branda, N.; Rebeck, J. J. Am. Chem. Soc. (1990), **112**, 3685-3686.
10. a. Drago, R.S.; Cannady, J.P.; Leslie, K.A. J. Am. Chem. Soc. (1980), **102**, 6014.
b. Lavalette, O; Tetreu, C.; Mispelter, J.; Momentou, M; LHoste, J-C. Eur. J. Biochem. (1980), **145**, 555-565.
c. Chang, C.K.; Kondylis, M.P. J. Chem. Soc. Chem. Commun. (1986), 316.



11. a. Ibers, J.A.; Holm, R.H. Science (1980), **209**, 223-35.
b. Phillips, S.E.V.; Schoenborn, B.P. Nature (1981), **292**, 81-82.
c. Phillips, S.E.V. J. Mol. Biol. (1980), **142**, 531-554.
d. Shaanan, B. Nature (1982), **296**, 683.
e. Chang, C.K.; Traylor, T.G. Proc. Natl. Acad. Sci., USA (1975), **72**(3), 1166.
12. a. Morishima, I.; Inubushi, T. J. Chem. Soc. Chem. Commun. (1977), 616.
b. Frye, J.S.; LaMar, G.N. J. Am. Chem. Soc. (1975), **97**, 3561.
13. Marzilli, G.L.; Marzilli, P.A.; Halpern, J. J. Am. Chem. Soc. (1971), **93**, 1374.



¹⁵N Nuclear Magnetic Resonance Studies of Iron-Bond C¹⁵N in Ferric Low-Spin Cyanide Complexes of Various Strapped Hemins. Importance of C¹⁵N as a Reporter Molecule.

Introduction

¹⁵N has an unusually large response in its NMR chemical shift due to changes in its chemical environment. Changes in protonation state, hydrogen bonding and metal ligation produce large shifts [1-3]. This makes the ¹⁵N nucleus a very useful "reporter group" for measuring these interactions in small molecules, proteins and nucleic acids. ¹⁵N has a low natural abundance (0.37%) and a small negative magnetogyric ratio (-0.1013 times that of the proton) which make this nucleus one of the more difficult common nuclei to study by NMR. Nevertheless, since 1970 ¹⁵N-NMR has become increasingly accessible with the advent of wide-bore high-field spectrometers and polarization transfer techniques for sensitivity enhancement, as well as by the wide availability of isotopically enriched compounds.

Ferric hemoproteins and Iron (III) porphyrin centers exhibit a high affinity for cyanide coordination. Cyanide ion binding may be monitored by either ¹³C or ¹⁵N-NMR spectroscopy of the respective isotope-enriched ion. ¹³C-NMR exhibits extreme line-broadening of the signal [4]. The cyano nitrogen atom is further removed from the iron (III) center and the NMR signals are sharper. The C¹⁵N NMR study of various hemoproteins and peroxidases has been reported



(Table 4-1) [5-12]. The hemoproteins and cytochrome c have signals between 1055 and 847 ppm with $^{15}\text{NO}_3^-$ as reference signal. The peroxidases and cytochrome P-450 have signals between 578 and 412 ppm.

In the ^{15}N NMR study of the dicyano iron (III) protoporphyrin Goff [10] demonstrated that hydrogen bonding can cause an 82 ppm upfield shift of the signal (Table 4-1). Goff also studied the ^{15}N NMR of mixed imidazole cyano-iron (III) protoporphyrin. Their study showed an upfield shift of 277 ppm associated with the deprotonation of the trans imidazole residue (Table 4-1). These results demonstrate that a trans ligand and hydrogen bonding can clearly play a major role in dictating the C^{15}N^- signal position. A third factor in cyanide binding that may be revealed by ^{15}N NMR is the geometric distortion of the cyanomet complex [13]. Up to now the steric constraints effect on the C^{15}N^- signal position was unknown. Geometric distortions may play a major effect in the ability of proteins to bind certain ligands.

The X-ray crystal structures of carbon monoxide liganded hemoglobins (Hb) and myoglobins (Mb) exhibit a bent or tilted FeCO linkage with respect to the porphyrin ring [14-18], whereas in heme model compounds the FeCO bond is linear or perpendicular to the heme plane [19-20]. The origin of the distorted configuration in the proteins is



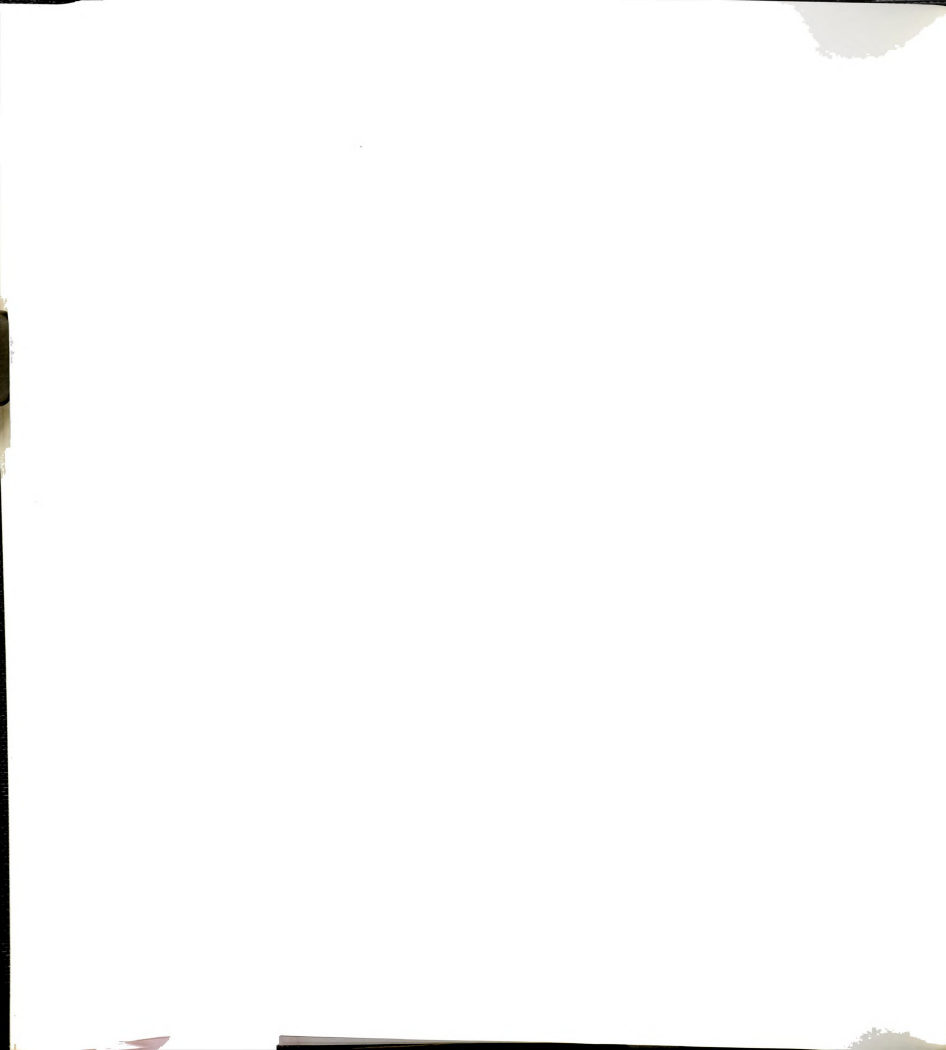
Table 4-1. ^{15}N Chemical Shifts For Proteins and Protoporphyrin

Complex	Solvent	^{15}N Chemical Shift (ppm)
<u>Cyano-hemoprotein</u>		
Horseradish peroxidase	H_2O , pH 7.0	576 ^a
Lactoperoxidase	H_2O , pH 7.2	423 ^a
Chloroperoxidase	H_2O , pH 6.1	412 ^a
Cytochrome P-450	H_2O , pH 7.2	433 ^b
Cytochrome C	$^2\text{H}_2\text{O}$, p ² H 7.8	847 ^c
Myoglobin	$^2\text{H}_2\text{O}$, p ² H 8.0	936 ^c
Hemoglobin	$^2\text{H}_2\text{O}$, p ² H 7.7	985(α) 1055(β) ^c
<u>Dicyano-iron (III) porphyrin</u>		
$(\text{CN})_2\text{FeProtDME}^-$	benzene	769 ^a
$(\text{CN})_2\text{FeProtDMF}^-$	benzene, 2- $\text{CH}_3\text{Imidazole}$	687 ^a
<u>Mixed cyano-iron (III) porphyrin</u>		
(Imid H)(CN)FeProtDME	DMSO	1015 ^a
(Imid ⁻)(CN)FeProtDME ⁻	DMSO	738 ^a

a. Data reference 10

b. Data reference 12

c. Data reference 9



attributed primarily to nonbonding steric interactions of the axial ligand with residues at the distal side. An assumption is made that ligands such as O_2 and NO, which preferentially form bent complexes, should encounter less steric interactions when bound in the heme pocket [21-22]. It has been proposed that in Hb and Mb, the distal steric effect would decrease the affinity ratio of CO vs. O_2 and is responsible for the detoxification of CO poisoning in respiratory systems [23-26]. It is therefore of importance to examine the steric effects on ligand affinity using synthetic models equipped with varying degrees of steric hindrance at the distal side.

Ward and Chang studied the equilibria and kinetic rates of CO and O_2 binding to two hindered heme systems [27]. One was mixed cofacial diporphyrins in which an inert copper porphyrin [28] is tightly linked to the heme, thereby providing a compression from above to the coordinating ligand (Figure 4-1). The second system was iron cyclophane porphyrins where a hydrocarbon chain is strapped across one face of the heme (Figure 4-1). Depending on the chain length, the strap would mostly exert a side-ways shearing strain to the gaseous ligand. In their study they demonstrated that, indeed, distal steric hindrance affects ligand binding, but this effect is manifested only in the ligand association rate constants and has almost no effect on the off rates. When they compared only the association rate data, they found, that relative to chelated mesoheme,



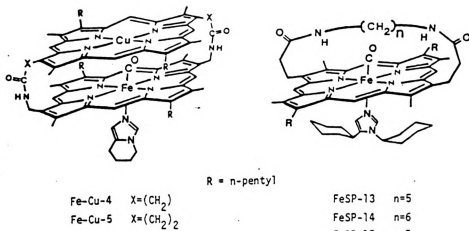


Figure 4-1. Chemical Structures of Cofacial Diporphyrins and Strapped Hemes.

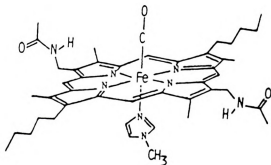
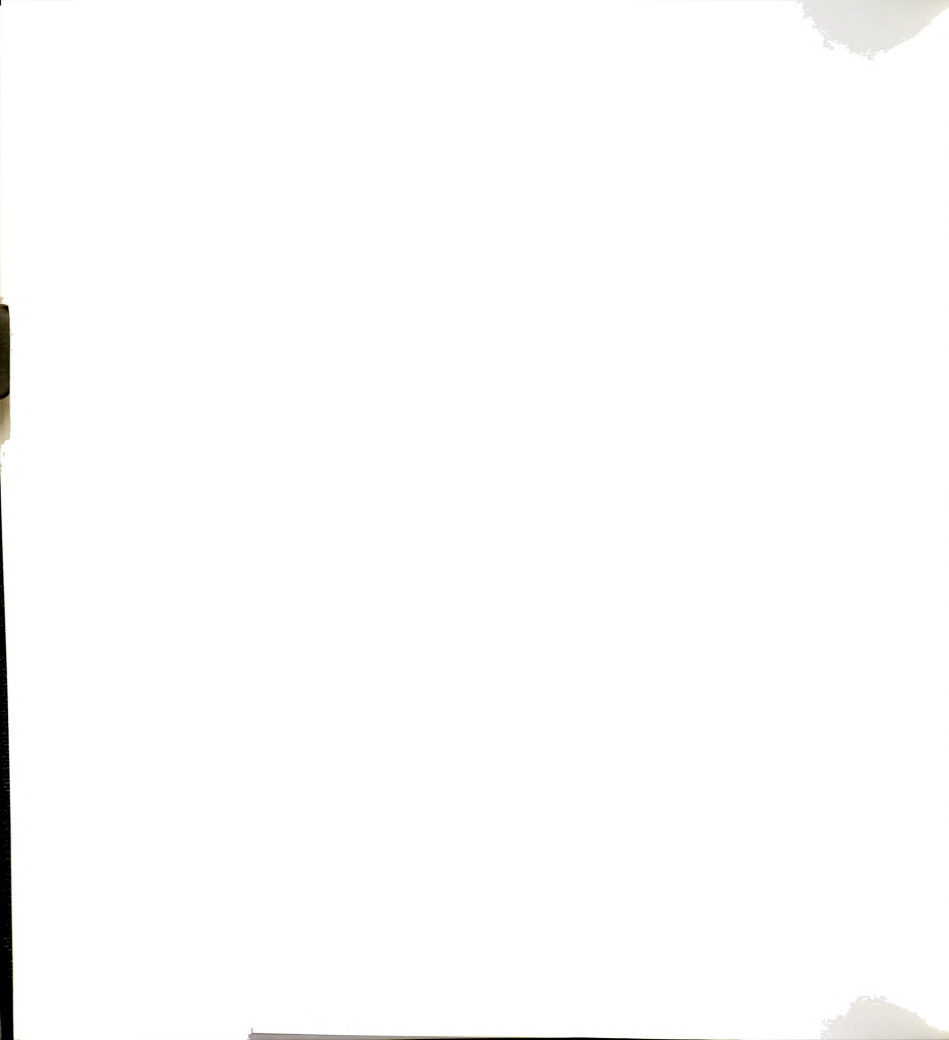


Figure 4-2. Chemical Structure of Heme 5.



for FeCu-5 a CO reduction of 90-fold while O₂ was reduced by 30 and for FeCu-4 a CO reduction of 400-fold with O₂ being reduced by 100. Although small, this unequal reduction of CO and O₂ association rates may be considered as evidence for the steric differentiation of O₂ and CO. A 240 fold reduction in the P_{1/2}(CO) of FeSP-13 is observed when compared to FeSP-15, demonstrating that steric constraints reduce the CO binding ability.

Resonance Raman studies of the Fe-CO distortion in sterically hindered strapped heme-CO complexes has been done (Figures 4-1 and 4-2) [29]. Increasing the steric hindrance (by decreasing the chain length), which reduces the CO binding affinity, is found to increase the Fe-CO stretching frequencies. In other words, the weaker the CO binding the stronger the iron-carbon (CO) bond. This has been interpreted in terms of a decrease in the CO effective mass and increased interactions between the C atom of CO and the N atom(s) of the pyrrole ring(s). The resonance Raman studies of sterically hindered cyanomet "strapped" hemes [13] indicated that the $\nu(\text{Fe-CN})$ frequency decreases as the chain length is decreased, in contrast with the CO complexes. In other words, the weaker the CN⁻ binding the weaker the iron-carbon (CN⁻) bond. Cyanomet heme-5 and strapped hemes exhibit predominantly σ -bonding interactions between iron (Fe^{III}) and cyanide (CN⁻), therefore, the weaker these σ interactions the lower the (Fe-CN) frequencies. These studies indicate that changes in the geometric



distortion of heme-ligand complex have an effect in the ligand binding ability of the porphyrin complex.

^{15}N has an unusual large response in its NMR chemical shift due to changes in its chemical environment. In this paper we clearly demonstrate that small changes in the geometric distortion of the cyanomet complex produces a large shift in the C^{15}N signal position making this nucleus a good "reporter group." Differences in the steric effects within the heme pocket may play a major role in dictating the functionality of hemoproteins.

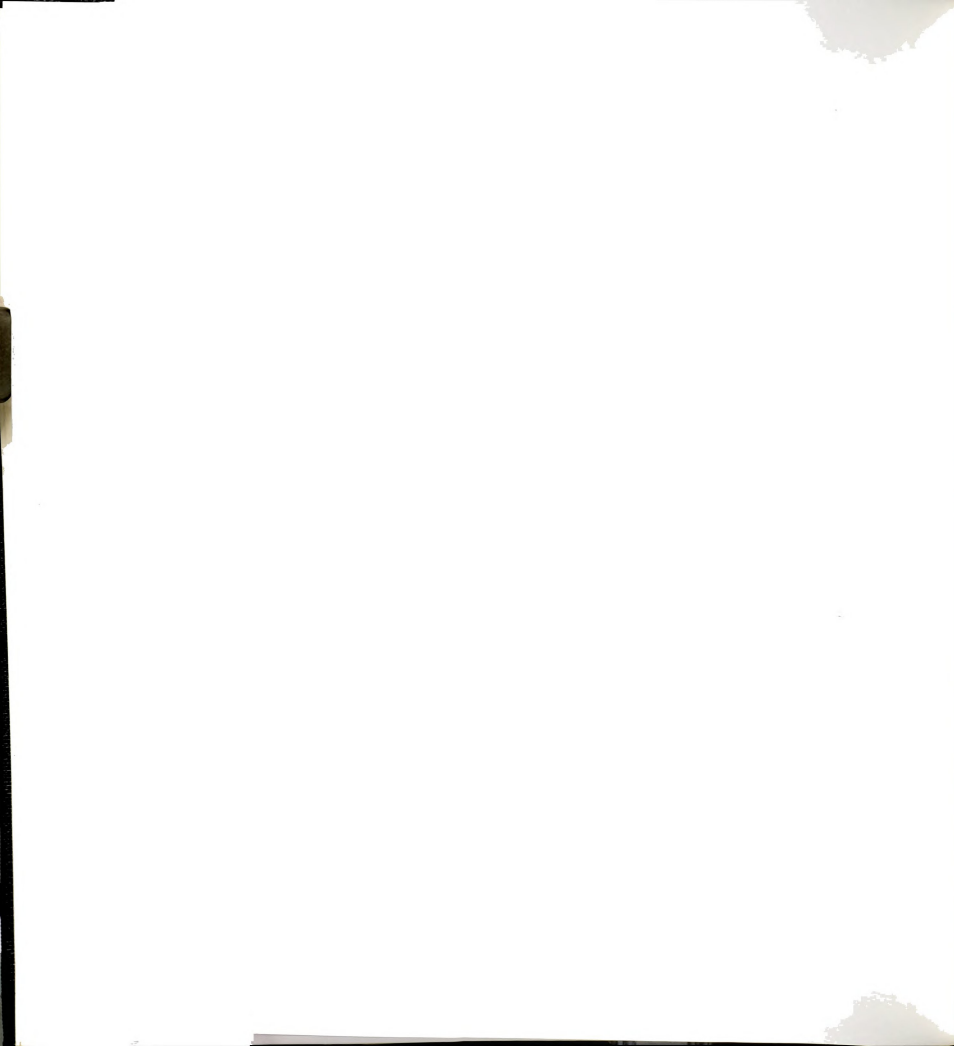
Experimental

Dicyano Iron (III) Porphyrin Models

The strapped porphyrins and octaethyl porphyrin were prepared and characterized as described [27, 30]. Insertion of iron was accomplished by using the ferrous sulfate method [31]. Solutions for ^{15}N spectroscopy were accomplished by dissolving the desired high-spin ferric complexes in 0.6 mL of deuterated DMSO (3-5 mM porphyrin solutions). A 10 fold excess of KC^{15}N powder (98% N-15, Icon Inc.) was dissolved in the porphyrin/DMSO solution to produce a distinctive color change.

Mixed Imidazole Cyano-Iron (III) Porphyrin Complexes

Solutions for ^{15}N spectroscopy were accomplished by dissolving the desired high-spin ferric complexes in 0.6 mL of deuterated DMSO (3-5 mM porphyrin solutions) 1.5 times of



1,3-dicyclohexyl-imidazole powder was dissolved in the porphyrin/DMSO solution. Finally, equal amount (with respect to the porphyrin) of the $KC^{15}N$ powder was added.

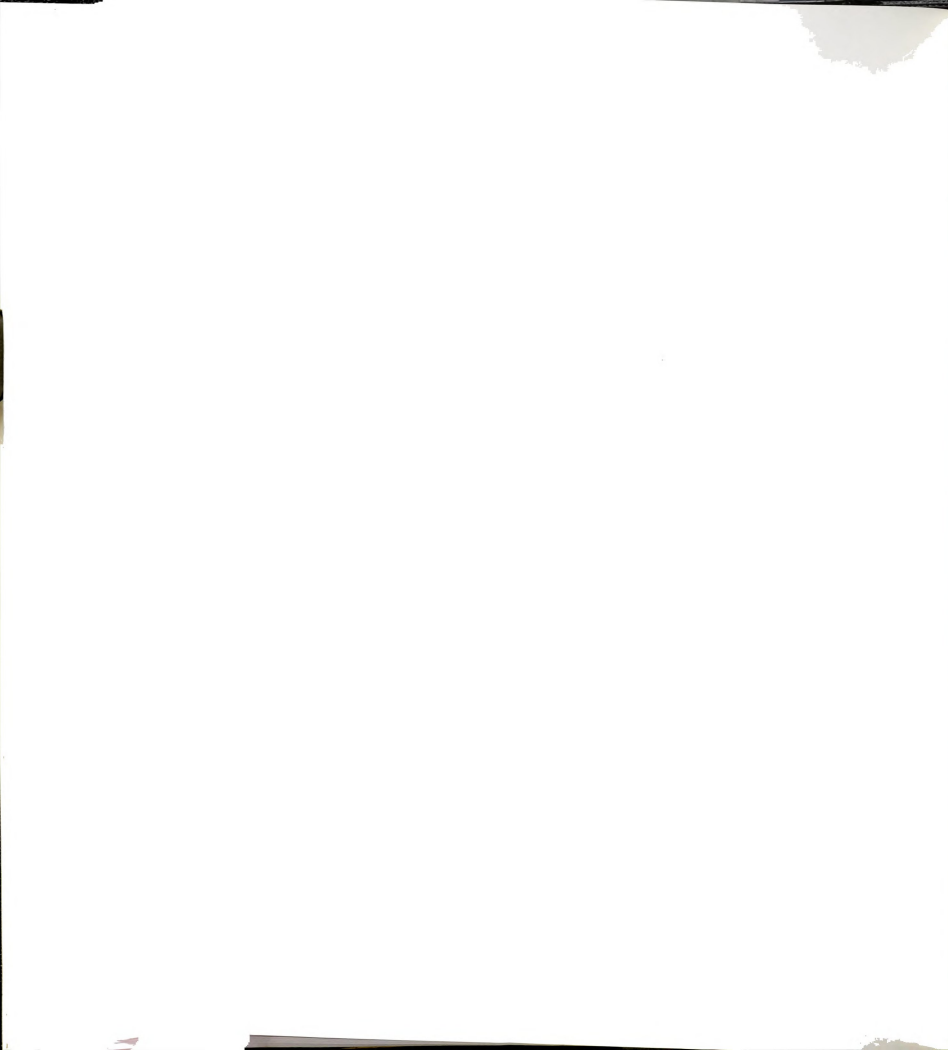
Measurements

Measurements were made on a Varian VXR-500 spectrometer. ^{15}N spectra were typically obtained in sweepwidths of 100 KHz at 50.6 MHz with pulse repetitions of 0.12s. A 200 μ s delay prior to acquisition serve to diminish acoustic probe ringing. Spectra of heme contained in an 8-mm tube required 30,000 to 60,000 scans. Chemical shift values are referenced to external nitrate ion (aqueous ammonium nitrate) and downfield chemical shift are giving positive sign.

Theory

The interaction between the unpaired electron spin of a metal center and an adjacent nuclei produce a magnetic field that can potentially be larger than the applied static field H_0 [32]. This interaction may take place through chemical bond (contact contribution) and/or through space (dipolar or pseudocontact contribution). Together the values constitute the measured isotropic (hyperfine) shift.

$$\left(\frac{\Delta H}{H}\right)_{ISO} = \left(\frac{\Delta H}{H}\right)_{dip} + \left(\frac{\Delta H}{H}\right)_{con} \quad (1)$$



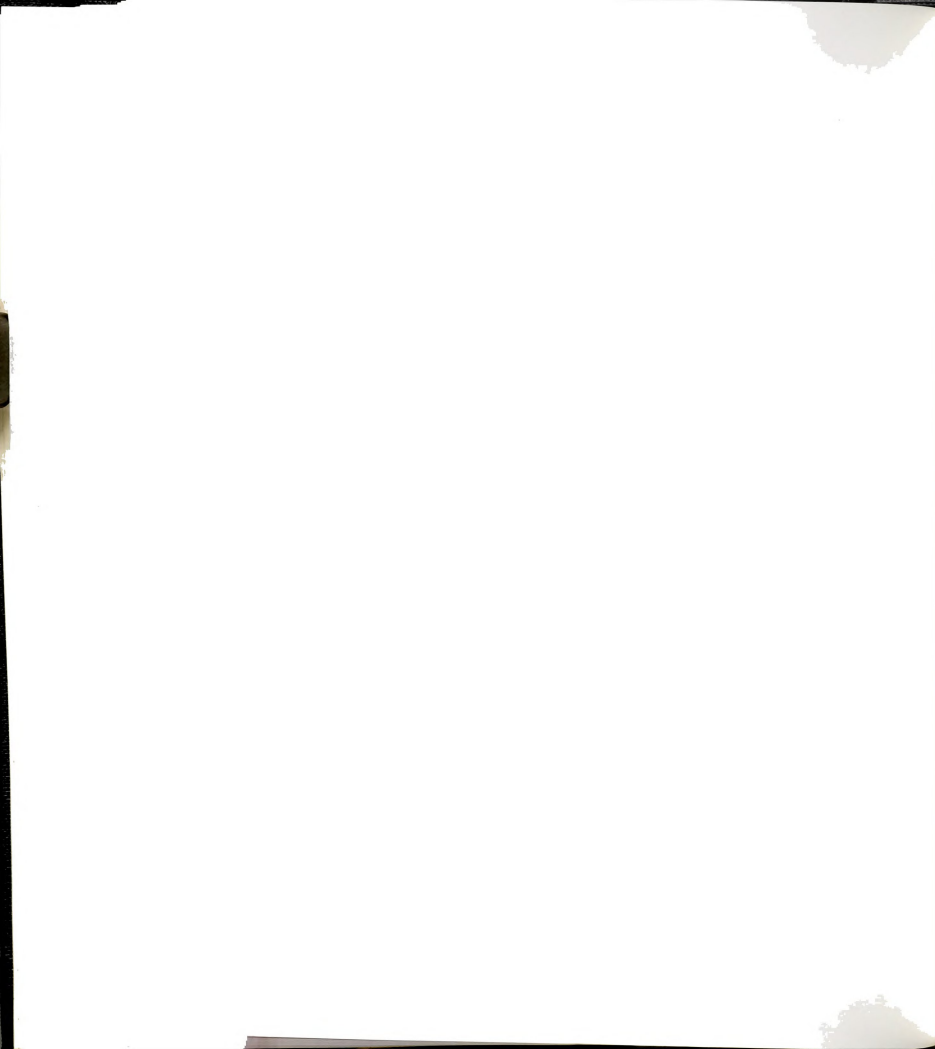
The dipolar shift, $(\Delta H/H)_{dip}$ arises from a through space interaction, and is non-zero only if the magnetic susceptibility tensor is anisotropic [32-36], i.e. $\chi_{11} - \chi_{\perp} \neq 0$. In the limit of axial symmetry the dipolar term is defined by:

$$\left(\frac{\Delta H}{H}\right)_{dip} = \frac{1}{3}N(\chi_{11} - \chi_{\perp}) \left(\frac{3\cos^2\theta - 1}{r^3}\right) \quad (2)$$

The $(3\cos^2\theta - 1)/r^3$ component is referred to as the geometric factor, and for a particular nucleus reflects the distance r from the metal center and the angle θ between the metal-nuclear vector and the primary axis.

Contact-shift contributions appear as a result of unpaired-spin delocalization through either σ or π molecular orbitals or both. For direct σ -spin delocalization, contact shifts are expected in a downfield direction and should attenuate with increasing atomic distance from the metal center. The contact-shift contribution is given by the conventional equation [32, 33] where A is the fermi coupling

$$\left(\frac{\Delta H}{H}\right)_{con} = -A \left(\frac{g\beta S(s+1)}{\gamma(2\pi)3\kappa T}\right) \quad (3)$$



constant which is proportional to the fraction of delocalized spin.

The dipolar and contact shift are very important contributors to the isotropic shift observed for the $C^{15}N$ iron (III) strapped porphyrins studied.

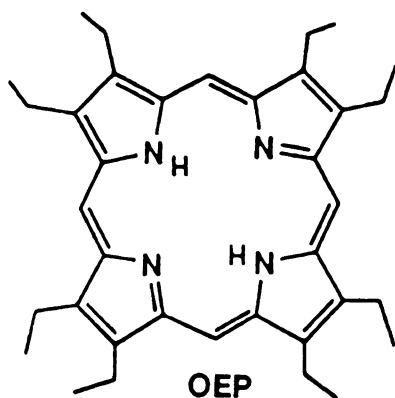
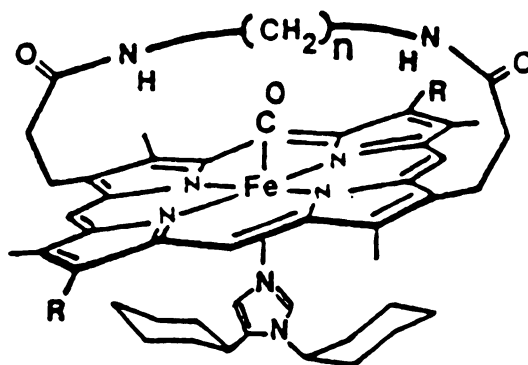
Results and Discussion

A. Dicyano Complex

The ^{15}N -NMR spectrum of a series of dicyano Fe(III) strapped porphyrins (Figure 4-3) was measured at 22° C in the presence of excess cyanide (Figure 4-4). Also the ^{15}N -NMR of dicyano complexes of Fe(III) octaethylporphyrin ($Fe^{III}OEP$) and Fe(III)-7,17-di(N-butyl)-3,8,13,18-tetramethyl-2,12-dipropanamide ($Fe(III)SP$) (Table 4-2) was measured. The NMR spectrum of $(C^{15}N^-)_2Fe^{III}OEP$ shows two peaks. One at -100 ppm (free $C^{15}N^-$) and the one that corresponds to the bound nitrile at 720 ppm. The NMR spectrum of $(C^{15}N^-)_2Fe^{III}SP$ also shows two peaks, one at -100 ppm (free $C^{15}N^-$) and the other at 743 ppm corresponding to the cyano complex. The difference of 23 ppm between $(C^{15}N^-)_2Fe^{III}OEP$ and $(C^{15}N^-)_2Fe^{III}SP$ is due to small differences in electronic effect between the two porphyrin rings.

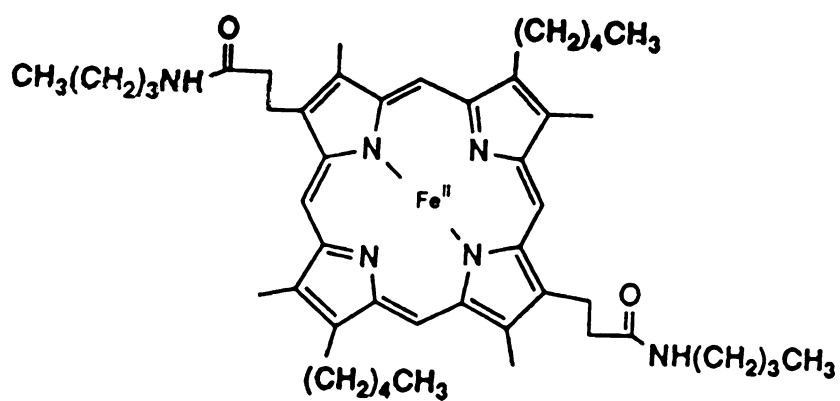
The NMR of the strapped porphyrin series typically exhibit three peaks (Figure 4-4). One corresponds to the free cyanide (-100 ppm) and the other two, correspond to the





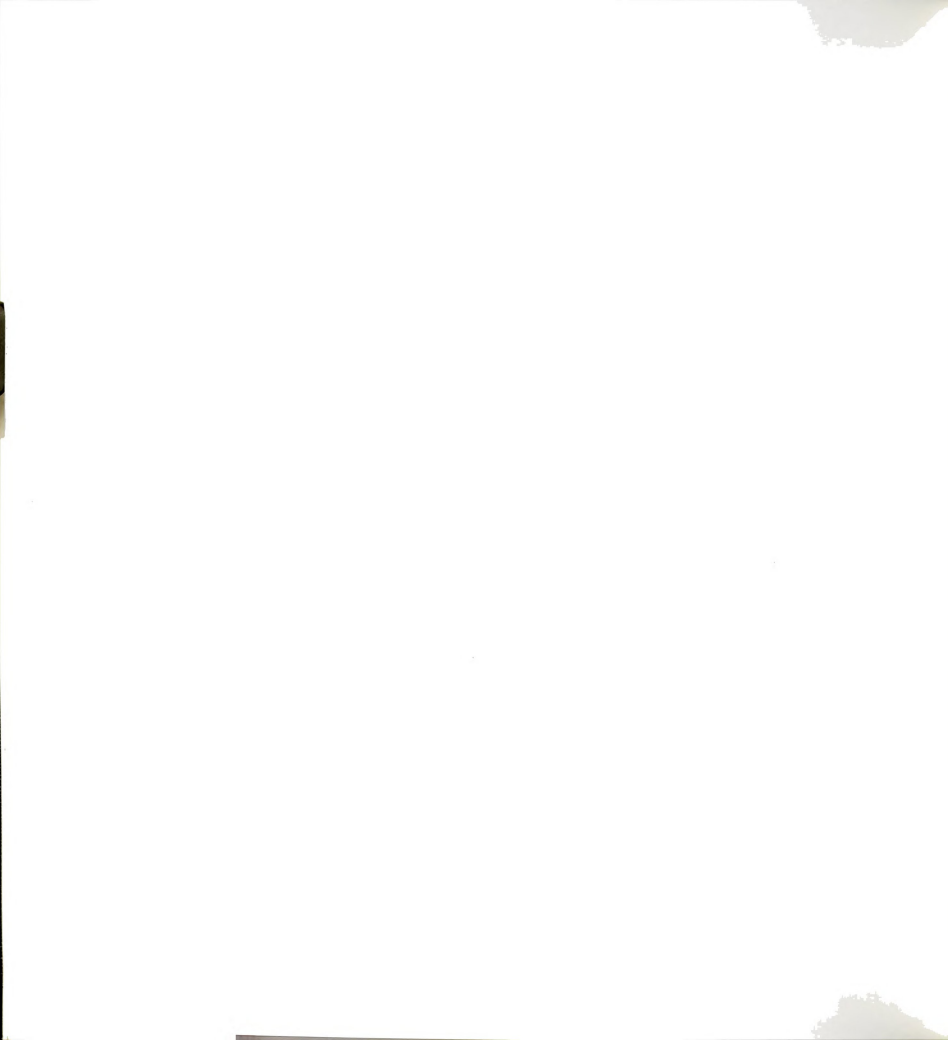
STRAPPED HEMES

FeSP-12	n=4
FeSP-13	n=5
FeSP-14	n=6
FeSp-15	n=7



FeSP

Figure 4-3. Chemical structure of OEP, FeSP and strapped hemes.



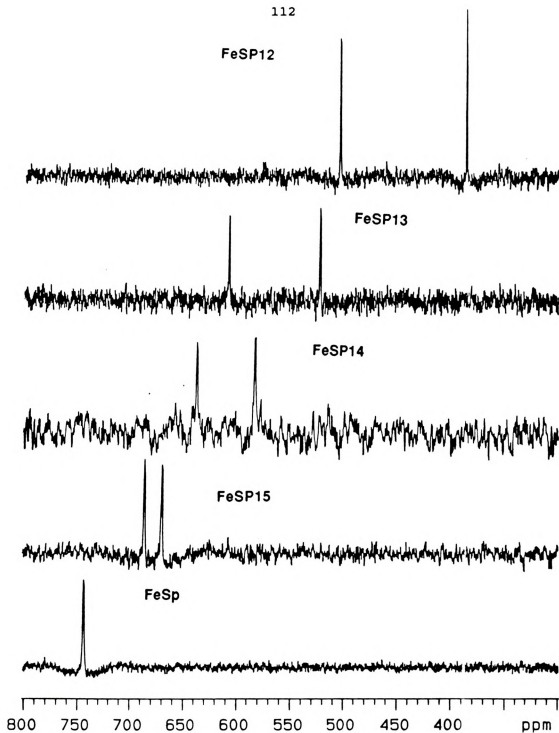


Figure 4-4. ^{15}N -NMR spectra of the dicyano unstrapped and strapped hemes.

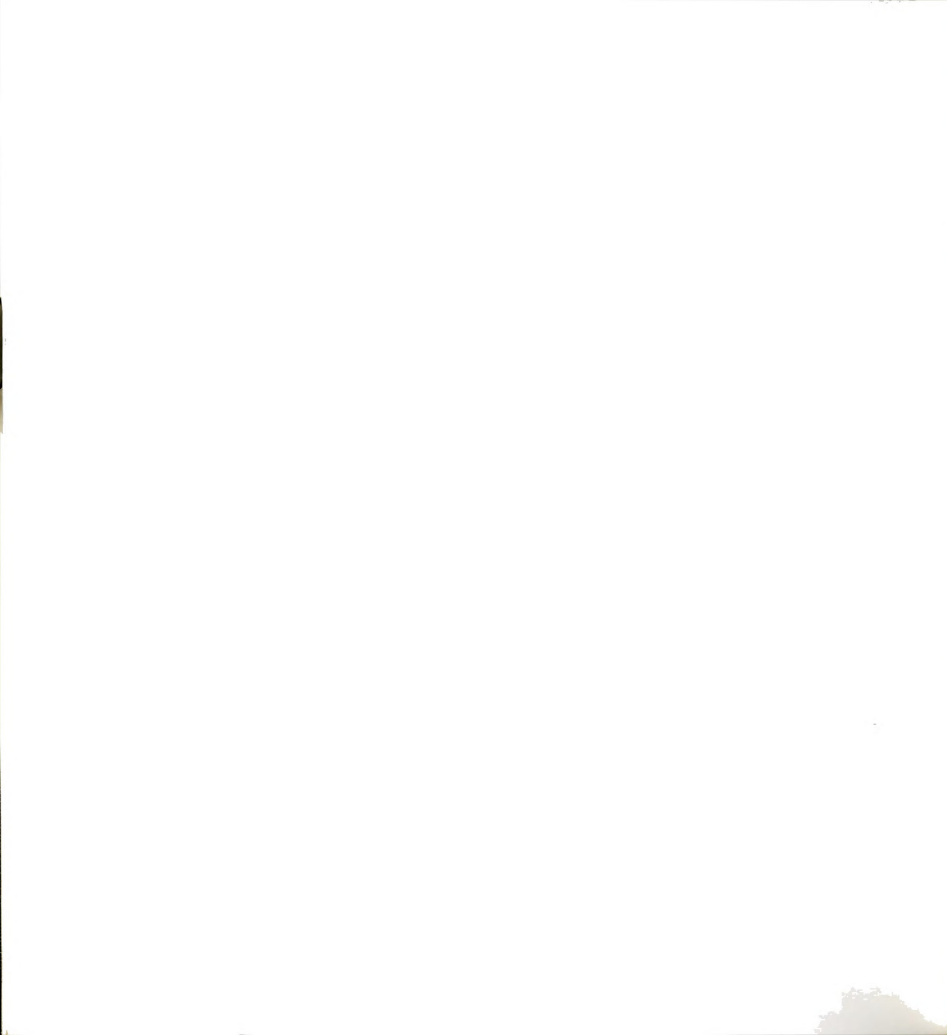
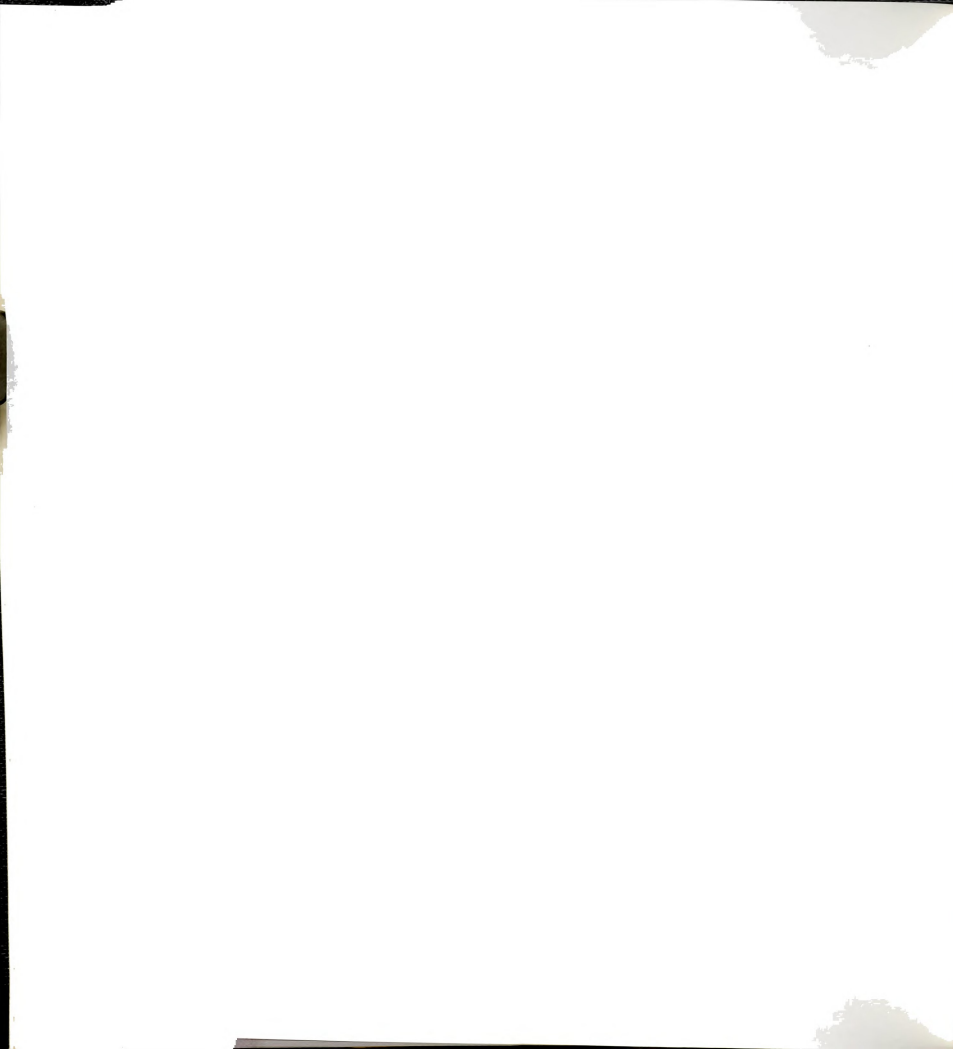


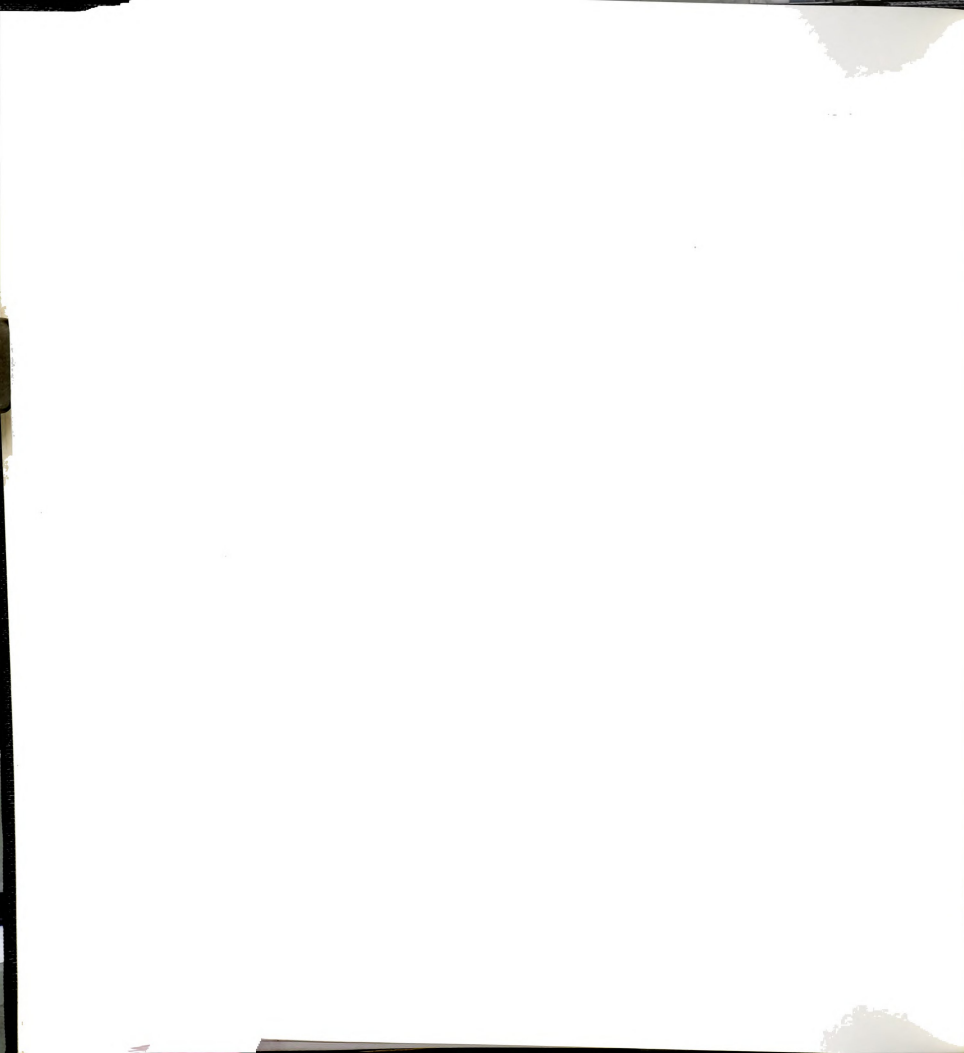
Table 4-2. ^{15}N Chemical Shift for Strapped Porphyrins

Porphyrin Complex	^{15}N Chemical Shift (ppm)
OEP	720
FeSP	743
FeSP15	686; 669.5
FeSP14	636.9; 582.9
FeSP13	607.2; 522.6
FeSP12	503.6; 386.3
FeSP(C ^{15}N χImid.)	984.5
FeSP15(C ^{15}N χImid.)	945
FeSP12(C ^{15}N χImid.)	834.4



two bound cyanide ligands. For the FeSP-15 porphyrin the two peaks appear at 686 and 669 ppm (Table 4-2). The peak at 669 ppm is assigned to the CN on the side of the strap (top) and the peak at 686 ppm is assumed to be the unhindered CN on the opposite side of the strap (bottom). By decreasing the number of atoms on the strap there is a consistent upfield shift for both cyanide peaks (Figure 4-4). The $(C^{15}N)_2FeSP12$ shows peaks at 503 and 386 ppm (Table 4-2). This is an upfield shift of 239 and 357 ppm with respect to the porphyrin with no strap. In addition, the difference in δ between the two peaks of a given strap porphyrin becomes larger as the strap becomes shorter (Figure 4-4). The FeSP11 did not form the hexacoordinate dicyano complex. As will be explained below, these changes in the ^{15}N isotropic shift for the different strap porphyrins are due to changes in the dipolar and contact contributions.

The cyanide ion is a strong-field ligand. This ensures the conversion of the iron (III) porphyrins to the low spin state. The orbital ground state configuration for low-spin iron (III) places d_{xz} , d_{yz} above d_{xy} with a spacing μ [37, 38]. As the strap becomes shorter, one of the cyanos is forced to bend, thus decreasing the interaction with the d orbitals of the iron. This decrease in interaction will lower d_{xz} , d_{yz} relative to d_{xy} , and hence decrease μ . Theoretical calculations presented by Loew [39], have shown that such a decrease in μ will decrease the magnetic

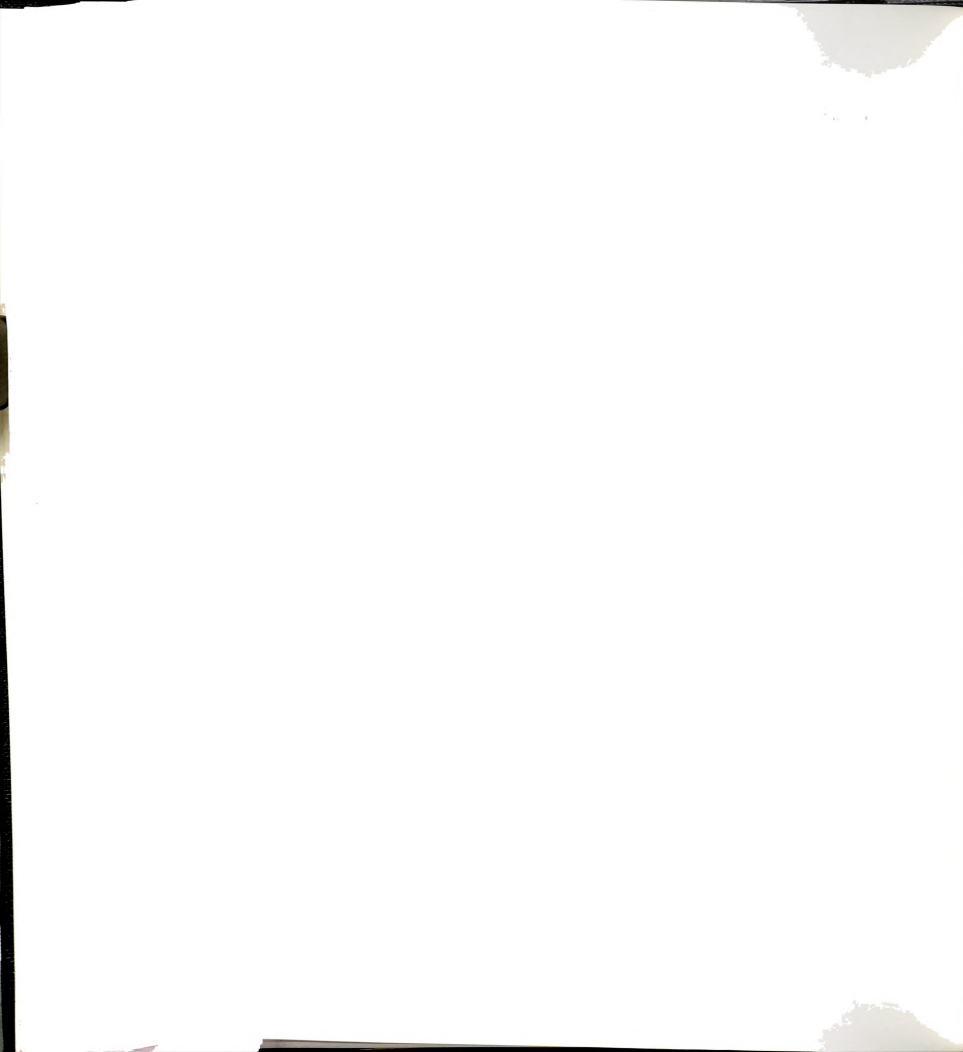


anisotropy. A decrease in the magnetic anisotropy will cause an upfield shift for both of the cyano nitrogens.

As mentioned earlier a larger upfield shift (357 ppm) is observed for the cyanide bound at the side of the strap. Bending of this cyano ligand weakens the Fe-CN bond and decrease the unpaired-spin delocalization. This causes additional upfield shift on the distorted cyanide.

B. Mixed Fe(III) Strap Complex

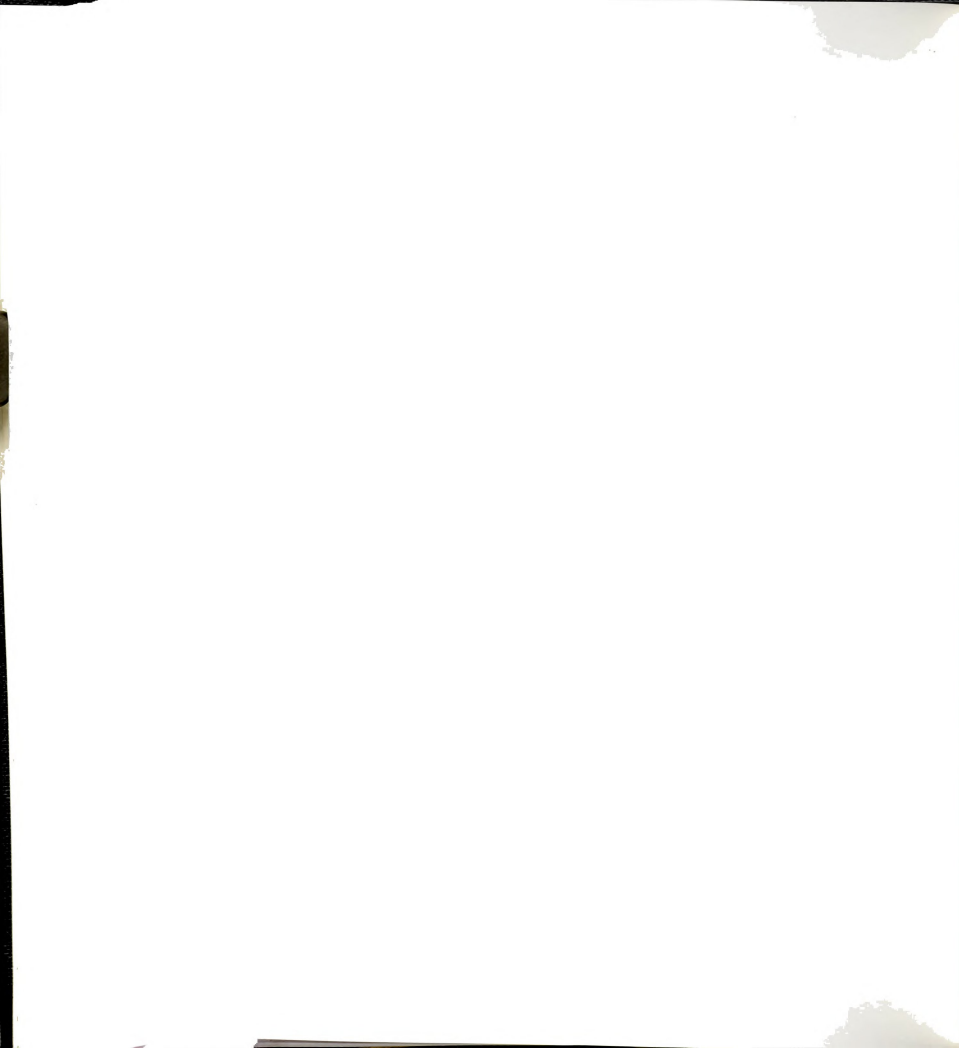
The ^{15}N -NMR of the mixed complex [1,3-diclohexyl-imidazole](C^{15}N) Fe^{III} for the FeSP, FeSP15 and FeSP12 was measured (Table 4-2). Their spectra exhibit only two peaks; the free cyanide (-100 ppm) and the one corresponding to the monocyano complex. Since the bulky imidazole is unable to form hexacoordinate complex with any of the strapped Fe(III) porphyrins, it is virtually certain that the cyanide is bound on the strapped side in these mixed complexes. A 150 ppm upfield shift was observed on going from the FeSP (no strap) to FeSP12 (shortest strap). While the magnitude of the shift is less drastic than the bis-cyanide series, the trend is unmistakably the same. In the previous model study [10] it was demonstrated that the trans ligand effect can be most prominent in dictating the cyano ^{15}N chemical shift of significant magnitude. The results presented above clearly establish that steric constraints imparted on the cyano ligand can likewise produce considerable shift on the ^{15}N signal.



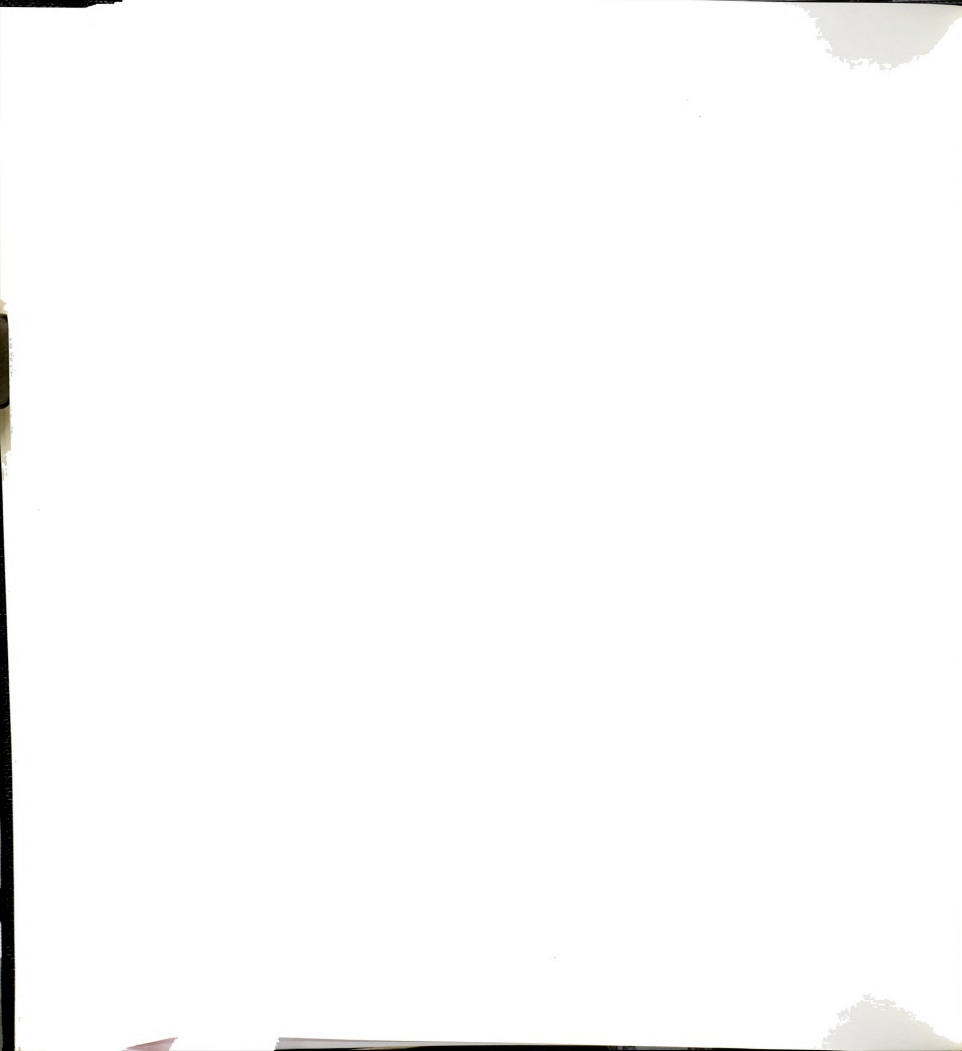
Biological Relevance

The difference in $C^{15}N$ resonance values of peroxidases compared to other hemoproteins is striking. This parallels functional diversity for the hemoproteins. Hemoglobin, myoglobin and cytochrome c have isotropic shifts between 1055 and 847 ppm (Table 4-1). Horseradish peroxidase, lactoperoxidase, chloroperoxidase and cytochrome P-450 have isotropic shift between 412 and 578 ppm (Table 4-1).

Among the factors that might induce an upfield shift for the peroxidases as compared with other hemoproteins are contributions from a basic charged trans ligand, hydrogen bonding at the distal axial cyanide ligand and, as we have demonstrated, steric constraints that enforce the Fe-CN linkage off axis from the normal heme. Both, trans ligand and hydrogen bonding are known to be relevant to the suggested mechanism for activation of the peroxide and dioxygen species in hemoproteins. For example, the presence of charged trans ligand such as the cysteinyl mercaptide ion is thought to be of importance for the scission of the O-O unit in cytochrome P-450 [40]. Likewise, the mercaptide ligand appears to be common to the chloroperoxidase enzyme [40], and this hemoprotein exhibits the ^{15}N signal with the greatest upfield bias. It has been suggested that the ^{15}N upfield shift observed for lactoperoxidase and horseradish peroxidase is due to an imidazole trans ligand with imidazolate character [10, 41]. Structural studies of cyanomethemoglobin have revealed a Fe-C-N bond angle of 150°

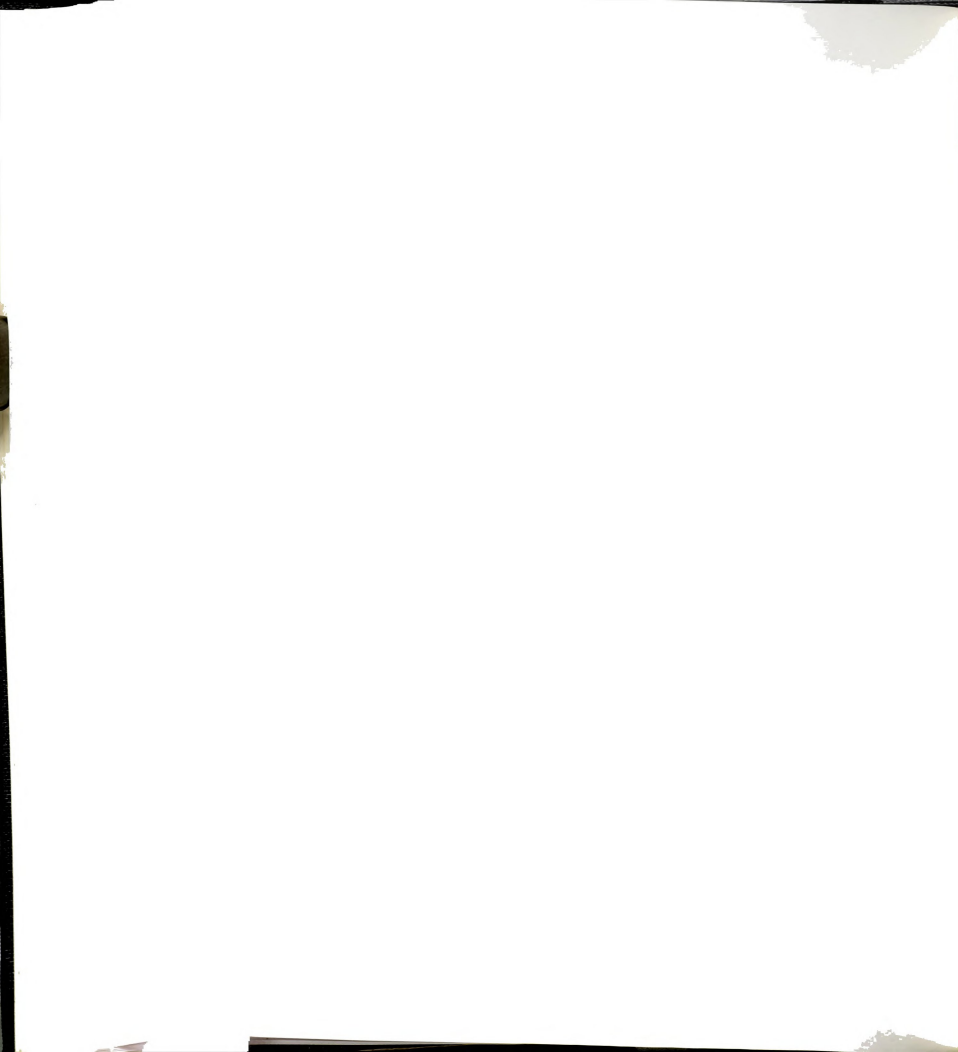


and 160° C [42]. This distal steric constraints may be greater in peroxidases. As clearly demonstrated in this paper, the ¹⁵N upfield shift observed for peroxidases may also be due to difference in the conformation of the proteins. The rather insignificant pH dependence of peroxidase C¹⁵N chemical shifts in the physiological range provide additional support for contributions from steric term as opposed to the hydrogen-bonding term.

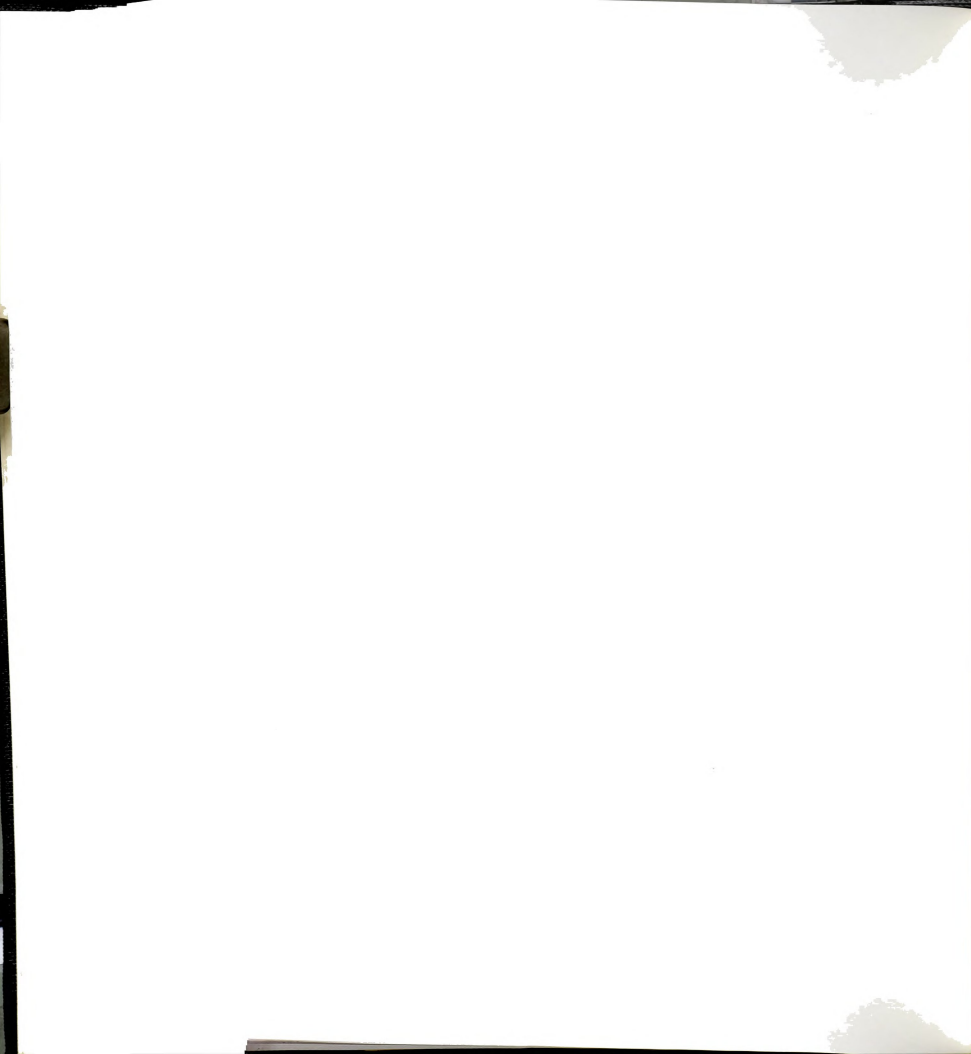


LIST OF REFERENCES

1. Roberts, J.D. Rice Univ. Stud. (1980) **66**, 147-178.
2. Kanamori, K. and Roberts, J.D. Acc. Chem Res. (1983) **16**, 35-41.
3. Mason, J. Chem. Rev. (1981) **81**, 205-227.
4. Goff, H.M. J. Am. Chem. Soc. (1977) **99**, 7723-7725.
5. Morishima, I.; Inubushi, T.; Neya, S.; Ogawa, S.; Yonezawa, T. Biochim. Biophys. Res. Commun. (1977) **78**, 739-746.
6. Morishima, I; Inubushi, T. FEBS Lett (1977) **81**, 57-60.
7. Morishima, I; Inubushi, T. J. Chem. Soc. Chem. Commun. (1977) 616-617.
8. Morishima I.; Inubushi, T. Biochem. Biophys. Res. Commun. (1978) **80**, 199-205.
9. Morishima, I; Inubushi, T. J. Am. Chem. Soc. (1978) **100**, 3568-3574.
10. Behere, D.V.; Gonzalez-Vergara, E; Goff, H.M. Biochim. Biophys. Acta (1985) **632**, 319-325.
11. Behere, D.V.; Ales, D.C. and Goff, H.M. Biochim. Biophys. Acta (1986) **871** 285-292.
12. Shiro, Y; Iizuka, T.; Makino, R.; Ishimura, Y.; Horishima, I. J. Am. Chem. Soc. (1989) **111**, 7707-7711.
13. Tanaka, T; Yu, N-T; Chang, C.K. Biophys. J. (1987) **52**, 801-805.
14. Huber, R.; Epp, O.; Formanek, H. J. Mol. Biol. (1970) **52**, 349.
15. Heidner, E.J.; Ladner, R.C.; Perutz, M.F: J. Mol. Biol. (1976) **104**, 707.



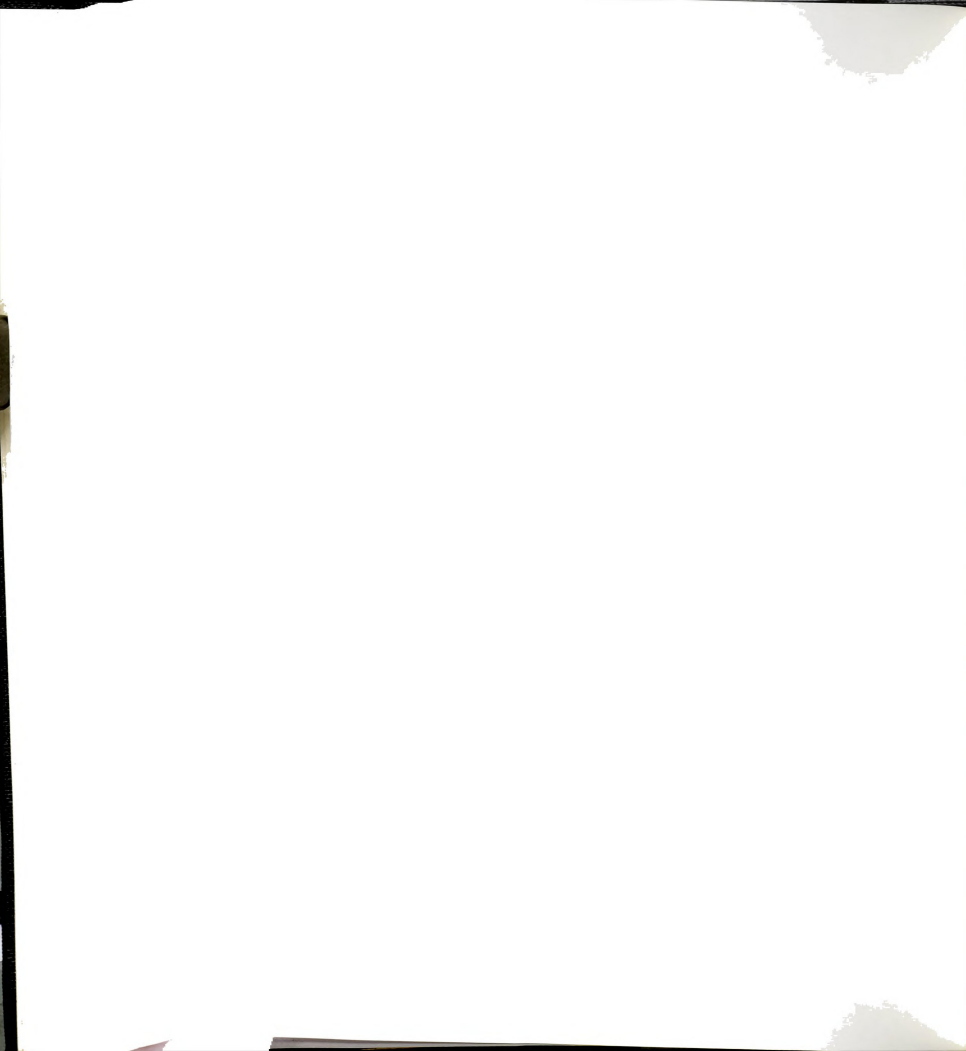
16. Norvell, J.C.; Nune, A.C.; Schoenborn, B.P. Science (Washington, D.C.) (1975) **190**, 568.
17. Steigemann, W.; Weber, E.J. J. Mol. Biol. (1979) **127**, 309.
18. Padlan, E.A.; Love, W.E. J. Mol. Biol. (1975) **249**, 4067.
19. Hoard, J.L., In Porphyrins and Metalloporphyrins, Smith, K.M., Ed.; Elsevier: New York, 1975; p. 351.
20. Peng S.M.; Ibers, J.A. J. Am. Chem. Soc. (1976) **98**, 8032.
21. Moffat, K.; Deatherage, J.F.; Seybert, D.W. Science (Washington, D.C.) (1979) **206**, 1035.
22. Perutz, M.F. Annu. Rev. Biochem. (1979) **48**, 327.
23. Caughey, W.S. Ann. N.Y. Acad. Sci. (1970) **174**, 148.
24. Perutz, M.F. Br. Med. Bull. (1976) **32**, 195.
25. Collman, J.P.; Brauman, J.I.; Halbert, T.R.; Suslick, K.S. Proc. Natl. Acad. Sci. U.S.A. (1976) **73**, 333.
26. Collman, J.P.; Brauman, J.I.; Doxsee, K.M. Proc. Natl. Acad. Sci. U.S.A. (1979) **76**, 6035.
27. Ward, B.; Wang, Ching-Bore; Chang, C.K. J. Am. Chem. Soc. (1981) **103**, 5236-5238.
28. Copper (II) porphyrins do not coordinate any ligand and cannot be reduced to Cu(I) state.
29. Yu, Nai-Teng; Kerr, E.A.; Ward, B.; Chang, C.K. Biochemistry (1983) **22**, 4534.
30. Wijesekera, T.P.; Pain III, J.B.; Dolphin, D.; Frederick, W.B.; Jones, T. J. Am. Chem. Soc. (1983) **105**, 6747-6749.
31. Chang, C.K.; DiNello, R.K.; Dolphin, D. Inorg. Synth. (1980) **20**, 147.
32. Goff, H.M. in Iron Porphyrins, Part I; Lever, A.B.P.; Gray; Harry, B., Eds.; Addison-Wesley: Massachusetts; (1983) pp. 237-281.
33. Jesson, J.P. in NMR of Paramagnetic Molecules; La Mar, G.N.; Horrocks, W.B., Jr.; and Holm, R.H., Eds.; Academic Press: New York; (1973) pp. 1-52.



34. Kurland, R.J. and McGarvey, B.R. J. Magn. Resonance (1970) **2**, pp. 286-290.
35. Frye, J.S.; La Mar, G.N. J. Am. Chem. Soc. (1975) **97**, 3561-3562.
36. La Mar, G.N.; Del Gaudio, J.; Frye, J.S. Biochim. Biophys. Acta (1977) **498**, 422-435.
37. Shulman, R.G.; Glarum, S.H. and Karplus, M. J. Mol. Biol. (1971) **57**, 93-115.
38. Zerner, M.; Gouterman, M. and Kobayashi, H. Theor. Chim. Acta (Berlin) (1966) **6**, 363-400.
39. Loew, G.M.H. Biophys. J. (1970) **10**, 196-212.
40. Hewson, W.D. and Hager, L.P. In The Porphyrins; Dolphin, D., Ed.; Vol. VII; Academic Press: New York; (1979) pp. 295-332.
41. LaMar, G.N., De Ropp, J.S.; Chacko, V.P.; Satterlee, J.D. and Erman, J.E. Biochim. Biophys. Acta. (1982) **708**, 317-325.
42. Thanabal, V.; De Ropp, J.S.; LaMar, G.N. J. Am. Chem. Soc. (1988) **110**, 3027-3035.



APPENDIX



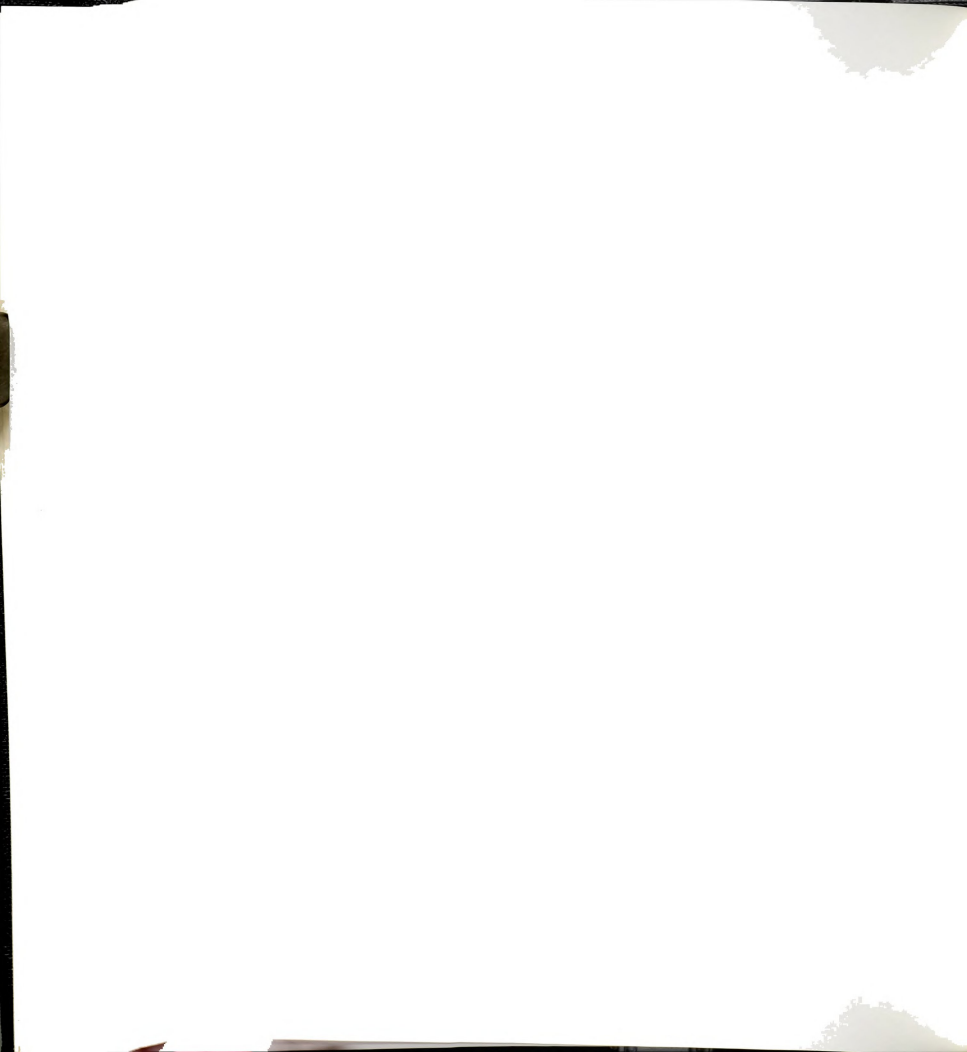
APPENDIX

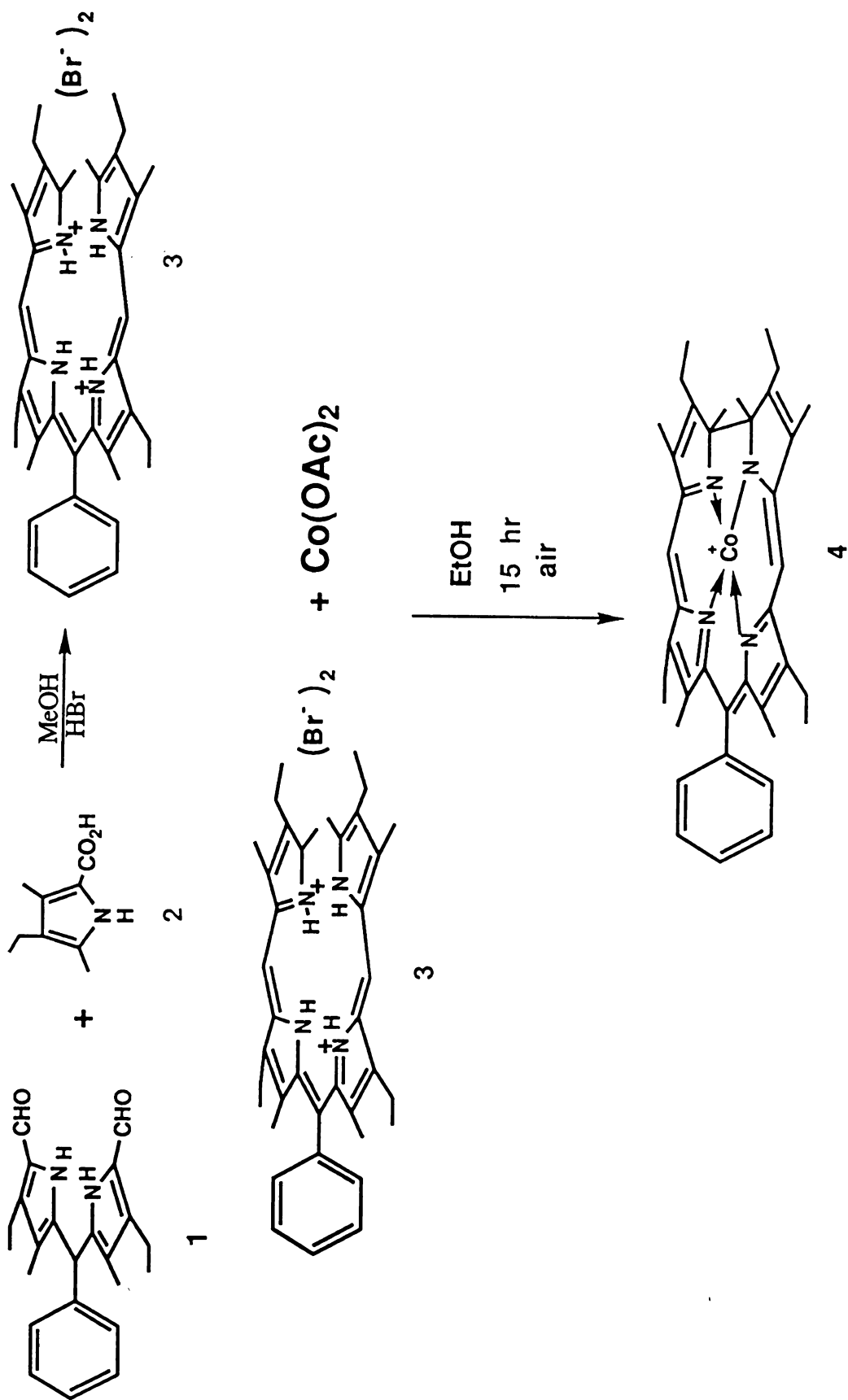
2,7,13,18-tetraethyl-1,3,8,12,17,19-hexamethyl-10-phenyltetrahydrocorrin cobalt (II) perchlorate (4)

(Scheme A1)

1.165g (3.2 mmol) of the phenyl diformyl dipyrromethane (1) and 1.075g (6.4 mmol) of the 2-carboxypyrrole (2) were added to 45 mL of methanol. The solution was then heated over a steam bath until both compounds were dissolved. To this hot solution 5 mL of HBr were added slowly. The MeOH and HBr were removed by heating over a steam bath and flushing the solution with Argon. Green crystal precipitated. This crystal was filtered, washed with ether (until solution almost clear) and air dried. The product was obtained in 97% yield and identified as the 1,19-dideoxybilidiene-ac dihydrobromide (3). NMR δ (Brucker 250 MHz): 1.01 (6H, t, Et), 1.17 (6H, t, Et), 1.92 (6H, s, Me), 2.26 (6H, s, Me), 2.38 (4H, q, Et), 2.56 (6H, s, Me), 2.66 (4H, q, Et), 3.88 (2H, s(broad), meso), 6.51 (2H, s, CH₂), 7.16-7.33 (5H, m, phenyl), 11.98 (2H, s, NH), 12.93 (2H, s(broad), NH).

1.58g (2.16 mmole) of the 1,19-dideoxybilidiene-ac dihydrobromide (3) was added to 125 mL of ethanol containing 1.3 g of Co(II)(OAc)₂. This solution was aerated while stirring for 15 hrs. After this period of time the solvent was evaporated to ~60 mL and water added (60 mL) to give a black precipitate which was filtered and treated with sodium





Scheme A1



perchlorate. The compound was purified by tlc plates (Silica-gel, 2% MeOH/CH₂Cl₂) to give 800 mg (52% yield) of the phenyl tetradehydrocorrins (4). UV-Vis λ_{\max} nm (rel. rat.): 563.0(1.0), 496.5(1.4), 359.0(2.9). MS(FAB): 628.1 (40, M⁺). See Figure A1 for MS and UV-Vis.

1,8-Bis[10-(2,7,13,18-tetraethyl-1,3,8,12,17,19-hexamethyl)-tetraelehydrocorrins] anthracene, cobalt(II) perchlorate. (7)
(Scheme A2)

0.4 g (0.54 mmol) of 5 and 0.358 g (2.1 mmol) of the pyrrole (2) were dissolved in 26 mL of methanol containing 5 drops of methylene chloride. To this solution 2 mL of HBr were added slowly. The solution was then heated on a steam bath while Argon was bubbled until dryness. The green solid obtained was washed with ether until solution was almost clear. The bilidiene (6) was obtained in 99% yield. 0.4 g (0.28 mmol) of the bilidiene (6) were added to 50 mL of absolute ethanol containing 0.61 g of cobaltous acetate. The solution was then aerated while stirring for 15 hrs. After this period the solvent was evaporated, the dark solid dissolved in methylene chloride, purified by tlc plates (Silica-gel, 5% MeOH/CH₂Cl₂) and treated with sodium perchlorate to give 159 mg (41%) of the anthracene ditetradehydrocorrins (7). MS(FAB): 1278.7(100, M⁺). (Figure A2).



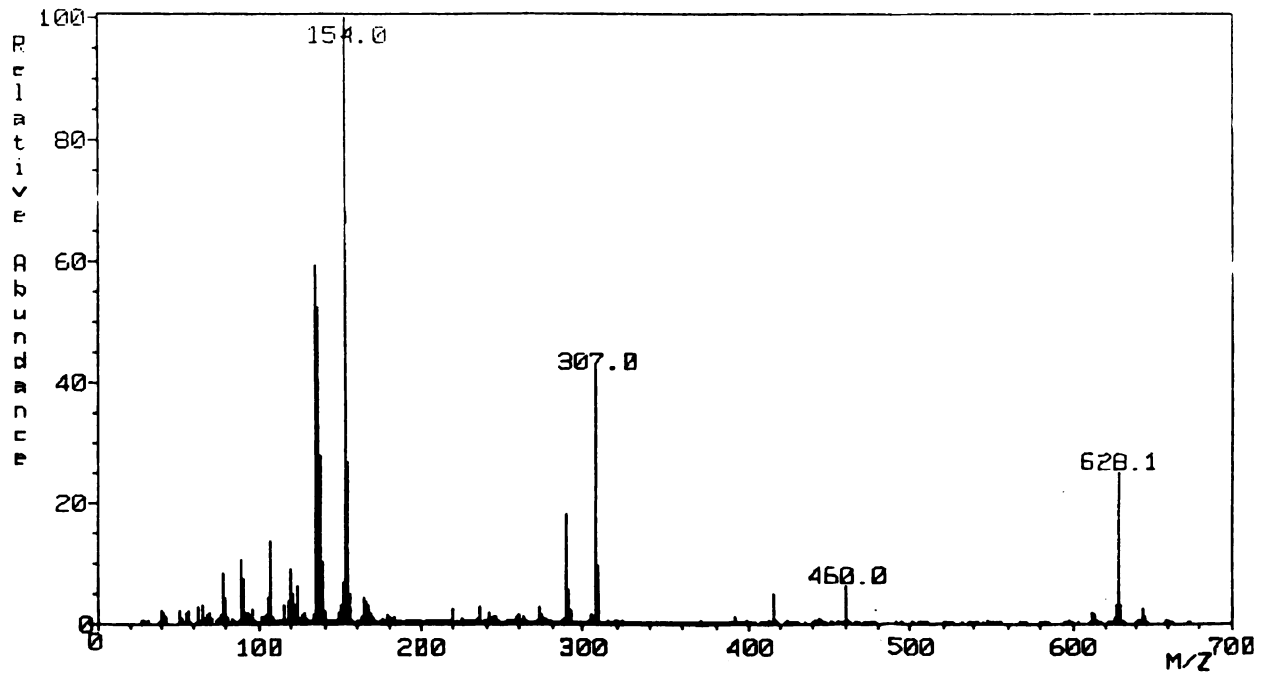
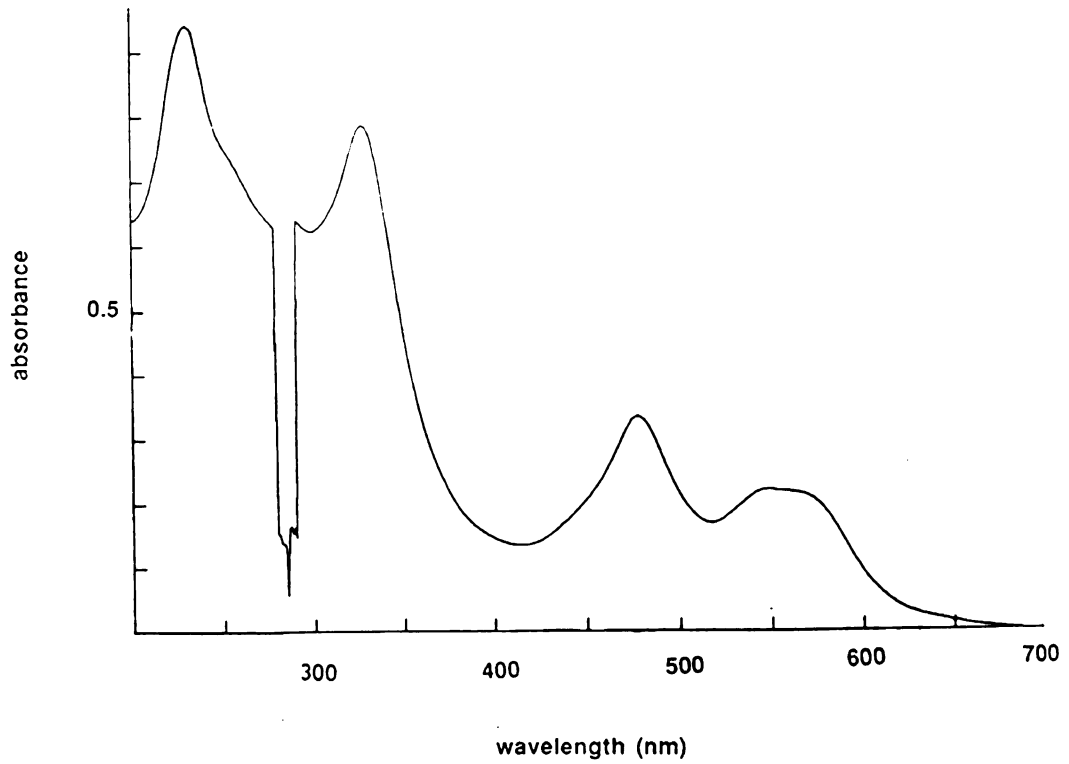
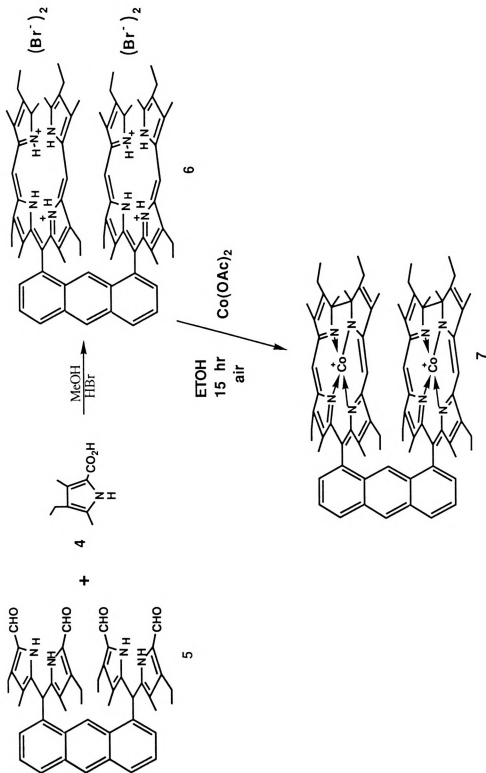


Figure A1. UV-Vis and MS of phenyl tetra-dehydrocorrins (4)





Scheme A2



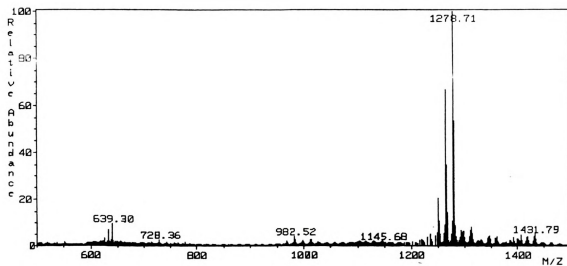
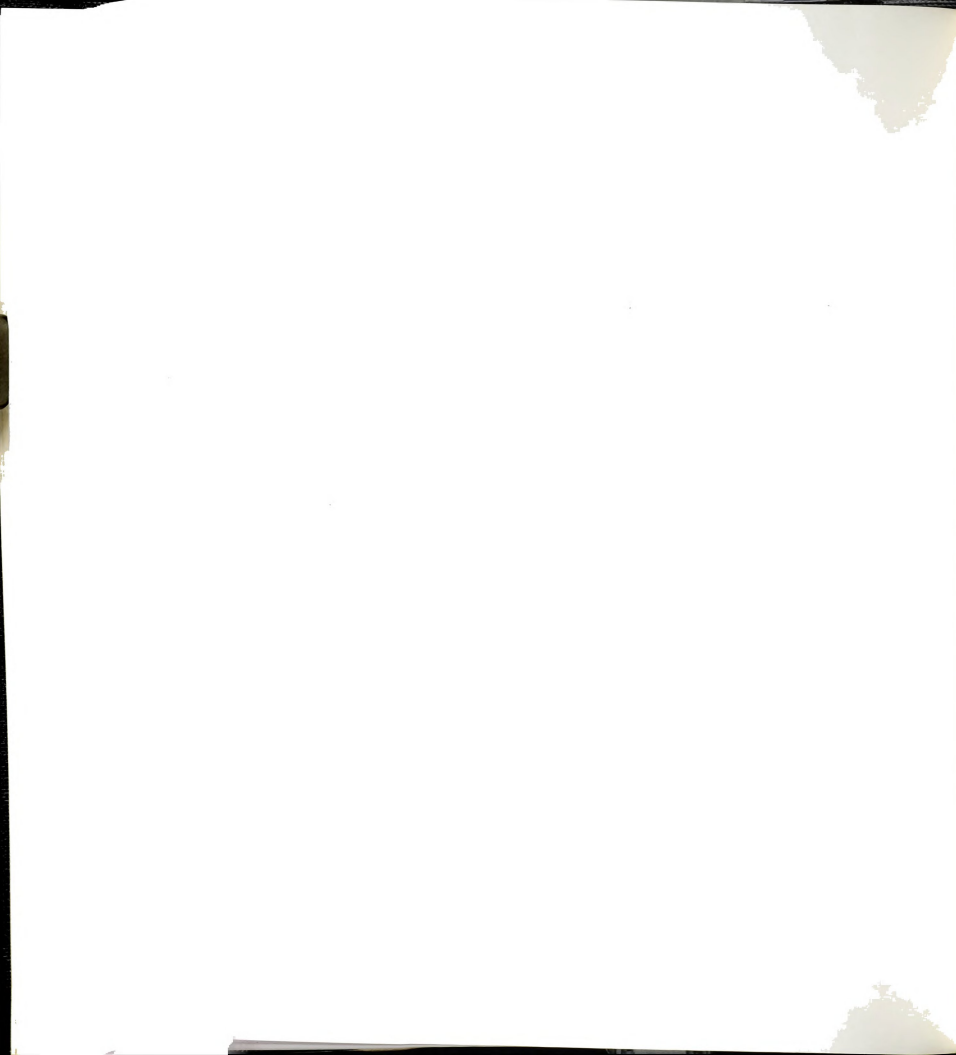


Figure A2. Mass spectra of anthracene ditetradehydrocorrin







MICHIGAN STATE UNIV. LIBRARIES



31293008963211